DOCTRIAL DISSERTATION

Sedimentation of Substitutional Solute Atoms in Some Binary System Alloys under Strong Gravitational Field

March 2003

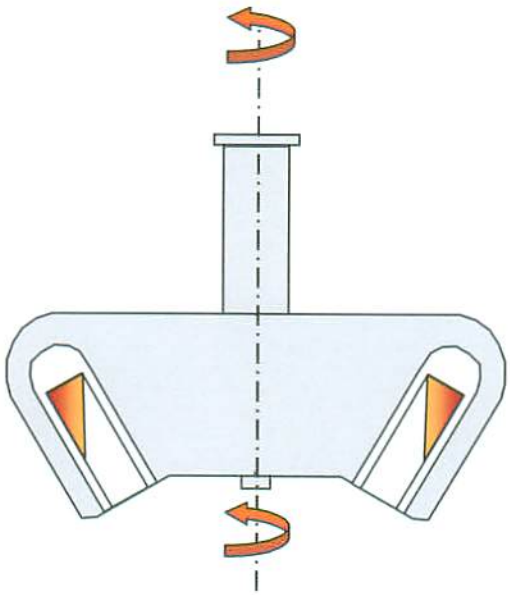

Masao Ono

Graduate School of Science and Technology
KUMAMOTO UNIVERSITY

CONTENTS

Title: Sedimentation of Substitutional Solute Atoms in Some Binary System Alloys under Strong Gravitational Field

CHPTER 1
Preface

1-1. Introduction

While micro gravity field ($10^{-6} \sim g$) has been used in many fields, the materials science under a strong gravitational field (mega-gravity field: ~ 10^6 g) is remained unexplored. Under strong gravitational field, one-dimensional body force displaces each atom, and as a result, a unique molecular-crystal state is realized. If the relative body forces based on differences in atomic weight and volume overcome the chemical potential, the sedimentation occurs in condensed matter of liquid state or even in bulk body. The phenomenon can be used to control the concentration of elements in condensed matter even isotopes. Strong gravitational field is very useful for material science. However, no experimental result for the sedimentation of elemental atoms in condensed matter had been reported until our work. The main reason was that there had been no general ultracentrifuge having enough performance for realizing the sedimentation of atoms in condensed matter. Also, the reason was that the previous theories for sedimentation were for sedimentation in macro scale and it can not be forecasted sedimentation phenomena of elemental atoms.

To study the sedimentation of atoms or crystal-chemical instability in solids under a strong gravitational field, Mashimo *et al.* developed an ultracentrifuge in 1996[1] on the basis of self-consistent theory for the sedimentation of atoms in condensed system presented in 1988 and in 1994[2, 3]. This apparatus can generate an acceleration of over $1x10^6 g$ for long time duration at elevated temperature around 100 to 250 ℃. And, for the first time, Mashimo *et al.* realized the sedimentation of substitutional solute atoms on a binary system alloy of the Bi-Sb system using this apparatus [4,5].

After the experiment for Bi-Sb system, another ultracentrifuge experiments and machine testing have been performed on many alloys searching the best experimental conditions improving the ultracentrifuge mainly in attachments of rotor, capsules, turbine motor, thermal instruments, lubricants etc.. Also, the production of the new ultracentrifuge was started in 1999 at Japan Atomic Energy Research Institute (*JAERI*), which could generate strong gravitational field up to over $1.0x10^6$g in a wide temperature range up to over 500℃ with

high stability controls, to expand the investigation variety in materials and phenomena.

In this study, we studied the sedimentation of atoms and the interaction with the phase equilibrium mainly in binary alloys under strong gravitational field using the ultracentrifuge of Kumamoto University and of *JAERI*. And, in some of alloys, the sedimentation process was mostly cleared by investigating in the centrifuged sample and comparing the experimental results with simulation ones, although the mechanism was not cleared. We are going to arrange and discuss the new experimental results of ultracentrifuge experiment for miscible systems on Bi-Sb, Se-Te and In-Pb alloy. The Bi-Sb and Se-Te alloy are the all-proportional miscible system. The In-Pb alloy is miscible system that has several phases according to the composition rate. Especially, the experimental discussion was devoted to the In-Pb system because Mashimo *et al.* already presented the well-worked experimental study for Bi-Sb system. For the Bi-Sb and Se-Te system, we mainly discuss the sedimentation process and mechanism comparing with simulation result and using the phase diagram having introduction of new experimental result. Also we are going to arrange and discuss the experimental results of ultracentrifuge experiment on intermetallic compound of Bi_3Pb_7. The experiment was aimed to cause decomposition by sedimentation of atoms and also aimed to realize the atomic-scale graded structures in the intermetallic compound. And, we are going to have a introduction for developing of the new ultracentrifuge at *JAERI*.

1-2. Strong-gravitational field for material science

Strong gravitational field (Ultra-centrifugal field) realize the sedimentation of atoms in condensed matter or create a unique one-dimensional crystal strain state based on differences in atomic weight and volume. So, the phenomenon can be used to control the concentration of elements or even isotopes, and to change the crystal structures. Also it can be used to form non-equilibrium composite structures such as graded structure on the atomic scale, non-stoichiometric structure, metastable solution structure, etc. in solids. Such nanocomposite materials are expected to show unique electric and optical properties. However, the sedimentation of atoms is very difficult to realize in solids or liquids, because the chemical potential of the atoms is usually much greater than the mechanical energy. So,

sedimentation phenomenon had been just used for biochemistry[6,7] or casting for industrial use of sedimentation of macro-particles in liquids.

1-3. Previous studies

1-3-1. Theoretical studies

Almost all sedimentation phenomena of both macroscopic solutes and atoms or molecules have been analyzed using the Lamm(1929) sedimentation equation[8] or similar equations (Miller 1956[9], Brenner and Condiff 1972[10]), which were formulated for axially symmetric macroscopic particles on the basis of macroscopic mechanics and thermodynamics. In these theories, the self-interaction effects between macroscopic solutes caused by centrifugal fields are not considered and, therefore, the driving force is not expressed as a function of solute concentration. In previous studies on liquid solvents (Archibald 1947[11], Van Holde and Baldwin 1958[12], Block et al. 1977[13]), the density was either assumed to be constant or else experimentally determined. The sedimentation phenomena of atoms in solids have been similarly analyzed (Barr and Smith 1969[14], Anthony 1970[15], Rushbrook and Barr 1978[16]). However, when the constituting particles are atoms or molecules, the density of the mixture solvent changes with concentration, especially at higher solute concentrations. Therefore Lamm's theory is not strictly applicable to such sedimentations.

Prof. Mashimo has proposed self-consistent equations for the sedimentation of atoms in a multi-component condensed system in 1988 and in 1994[2, 3]. We would like to introduce the self-consistent equation *in Chapter 2*. The theory was constructed on the basis of the mean-field approximation, the linear phenomenological matrix law with an expression for the atom fluxes and the Nernst-Einstein relation. Accordingly, the effects of self-interaction between the solutes, density changes and chemical activities, etc., were consistently taken into account. Steady-state solutions of the sedimentation of atoms were obtained under centrifugal field in two- and three-component systems under several atomic and chemical conditions in the infinite energy region. By using this theory, we can simulate the sedimentation process without additional assumptions or experimental data, even for finite regions. We would like to introduce the simulation procedure *in Chapter 2*.

1-3-2. Experimental studies

Previous experiments on sedimentation of atoms in solids except for ours are summarized in table 1-1.

Table 1-1 Ultracenrifuge experiments for sedimentation in solids.

Reference	Conditions	Material	year
Barr and Smith [14]	40,000 rpm (1.6x105g: about 18 cm in dia.), at 17℃, 3 days	198Au in K (interstitial solute, impurity level)	1969
Anthony [15]	25,000 rpm (1.05x105 g : about 30 cm in dia.), at 40℃, 3 days	195Au in In (interstitial solute, impurity level)	1970
Rushbrook and Barr [16]	40,000 rpm (1.4x105 g: about 19 cm in dia.), at 307℃*, 4 days	198Au in Pb (interstitial solute, impurity level)	1978

*heated by cold emission electron plasma in a low pressure helium atmosphere.

There is no sedimentation of component atoms in a solid (alloy or compound). There have been a few experiments (Barr and Smith 1969[14], Anthony 1970[15], Rushbrook and Barr 1978[16]) investigating the sedimentation of just Au atoms in elemental metals with low melting temperatures (K, In and Pb) under maximum acceleration fields of (1-2)x10^5 g. In these studies, the concentrations of an Au isotope were at an impurity level, and the concentration changes achieved were small, while the interstitial solutes acted in these systems (ultrafast diffusion).

1-3-3. Experimental study on Bi-Sb system in our laboratory

To study the sedimentation of atoms or crystal chemical instability in solids under a strong acceleration field, Mashimo *et al.* developed an ultracentrifuge apparatus in 1996 [1]. The apparatus can generate an acceleration field of over 10^6 g for long time duration at high temperatures. The specifications of the ultracentrifuge are introduced in the Introduction of the *Chapter 3*. Using this apparatus, they recently formed atomic-scale graded structures by the sedimentation of component of atoms in an all-proportional miscible system of the 70 mol% Bi- 30 mol% Sb alloy bulk body in 1997[4, 5]. The experimental conditions were summarized in the Table 1-2.

Table 1-2. Experimental conditions of the previous study for Bi-Sb alloy.

Stating sample	Rotation rate (rev. min^{-1})	Maximum acceleration (g)	Temperature (℃)	Time (h)
Bi:Sb=70:30at%, (Rhombohedral A7)	195,000-215,000	(0.79-0.96) x10^6	220-240	85

Continuous composition gradients of Sb (about 20-0 wt%) and Bi (about 80-100 wt%) were observed in the centrifuged sample (Figure 1-1-a). Also, the continuous changes in the lattice constants were observed by XRD method. These result shows that an atomic-scale graded structure was formed by the sedimentation of atoms in all-proportional miscible alloy under strong gravitational field of 1 million g in maximum acceleration at high temperature. It must be noted that the substitutional solutes with component level rate acted in the sedimentation of this system, while interstitial solutes (Au) at an impurity level rate acted in some elemental metals with low melting temperature in the previous studies[14, 15, 16]. And, in addition, crystal growth in the direction of acceleration field was also observed (Figure 1-1-b). It is expected that the sedimentation of substitutional atoms can be used to control the compositions and structure of alloys or compounds. The diffusion mechanism of substitutional solutes in a Bi-Sb alloy is, however, unknown.

1-4. Purpose of the present study

In this study, we studied the sedimentation of atoms and the interaction with the phase equilibrium mainly in binary alloys under strong gravitational field using the ultracentrifuge of Kumamoto University and of *JAERI*. And, in some of alloys, the sedimentation process was mostly cleared by investigating the centrifuged sample and comparing the experimental results with simulation ones, although the mechanism was not cleared. We are going to arrange and discuss the new experimental results of ultracentrifuge experiment for miscible systems on Bi-Sb, Se-Te and In-Pb alloy. The Bi-Sb and Se-Te alloy are the all-proportional miscible system. The In-Pb alloy is miscible system that has several phases according to the composition ratio. For the Bi-Sb system, Mashimo *et al.* already presented a well-worked

study under strong gravitational field using the ultracentrifuge of Kumamoto University one in 1997[4, 5]. This previous experimental result is summarized in this *Chapter 1, section 1-3-3)*. This work revealed the phenomenon that an atomic-scale graded structure was formed by the sedimentation of atoms in all-proportional miscible alloy under strong gravitational field. So, in this study, we just have composition analysis on the centrifuged sample of the Bi-Sb and Se-Te system that was performed using new ultracentrifuge of *JAERI* one, and discuss the sedimentation process and mechanism comparing with simulation and using the phase diagram, as these systems are the all-proportional miscible system, and it is convenient to examine the sedimentation process and mechanism comparing with the simulation. Also we are going to arrange and discuss the experimental results of ultracentrifuge experiment on intermetallic compound of Bi_3Pb_7. The experiment was aimed to cause decomposition by sedimentation of atoms and also aimed to realize the atomic-scale graded structures in the intermetallic compound. And, we are going to have a introduction for developing of the new ultracentrifuge at *JAERI*.

1-5. Summary of the present study

In this *Chapter 1*, we introduced ultra-centrifugal field and the expected effect on materials.

In the *Chapter 2*, we introduce the self-consistent equations for the sedimentation of atoms in a multi-component condensed system and simulation procedure of the sedimentation process for atoms, and we performed the simulation for Bi-Sb alloy.

In the *Chapter 3*, we introduce the development of the new ultracentrifuge and arrange the specification of the two different type ultracentrifuge used for the experiment.

We have been studied the sedimentation of atoms and the interaction with the phase equilibrium in binary alloys under strong gravitational field for several years. And, up to now, the sedimentation of atoms is confirmed in some alloys. So, we arrange these experimental results and have discussions in *Chapter 4* to *6*. In the *Chapter 4-5*, we arrange and discuss the experimental results of ultracentrifuge experiment on miscible systems; Bi-Sb, Se-Te and In-Pb alloy. The Bi-Sb and Se-Te alloy are the all-proportional

miscible system. The In-Pb alloy is miscible system that has several phases according to the composition rate. We would like to arrange and discuss the experimental result in classifying into "the all-proportional miscible system (*Chapter 4*)" and "miscible system in case that has several phases according to the composition rate (*Chapter 5*)".

In the *chapter 6*, we arrange and discuss the experimental results of ultracentrifuge experiment on intermetallic compound of Bi_3Pb_7. The experiment was aimed to cause decomposition by sedimentation of atoms and also aimed to realize the atomic-scale graded structures in the intermetallic compound.

REFERENCES

[1] T. Mashimo: Phys. Rev. A**38** (1988) 4149-4154.

[2] T. Mashimo: Philos. Mag. A**70** (1994) 739-760.

[3] T. Mashimo, S. Okazaki, S. Shibazaki: Rev. Sci. Instr. **67** (1996) 3170-3174.

[4] T. Mashimo, S. Okazaki, S. Tashiro: Jpn. J. Appl. Phys. **36** (1997) 498-500.

[5] T. Mashimo, H. Ikeda, I. Minato: J. Appl. Phys. **90** (2001) 741-744.

[6] S. Svedberg: Nature **139**(1937)1051.

[7] J. W. Beams: Rev. mod. Phys. **10** (1938) 245.

[8] O. Lamm: Ark. Mat. Astron. Fys, B, 21, No. 1(1929).

[9] D. G. Miller: Am J. Phys. **18** (1956) 362.

[10] H. Brenner and D. W. Condiff: J. Colloid Interface Sci. **41** (1972) 228.

[11] W. J. Archibald: J. appl. Phys. **18** (1947) 362.

[12] K. E. Van Holde and R. L. Baldwin: J. appl. Phys. **62** (1958) 734.

[13] T. E. Block, , E. Dickinson, C. M. Knobler, V. M. Schumaker and R. L. Scott: J. chem.. phys. **66** (1977) 3786.

[14] L. W. Barr, and F.A. Smith: Phil. Mag. **20** (1969) 1293-1294.

[15] T. R. Anthony: Act. Met. **18** (1970) 877-880.

[16] S. J. C. Rushbrook and L. W. Barr: J. Nucl. Materials **68/78** (1978) 556-558.

(a)

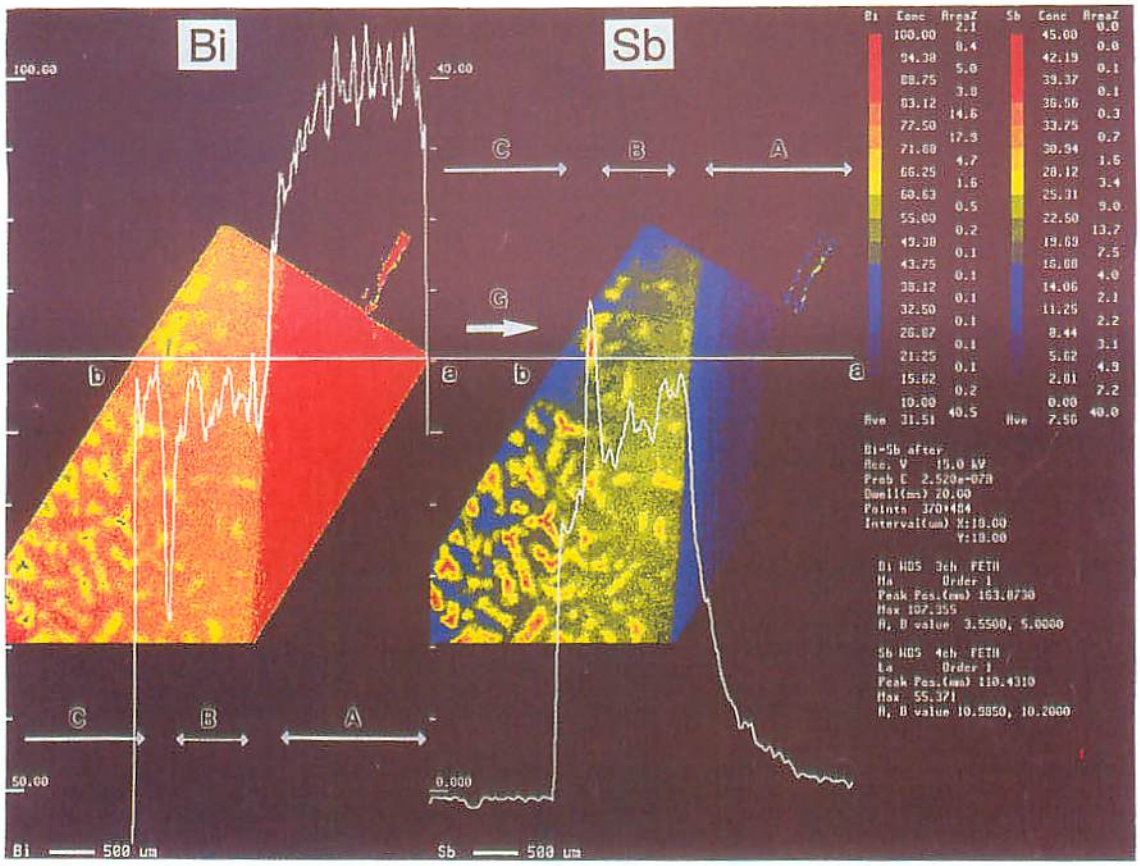

(b)

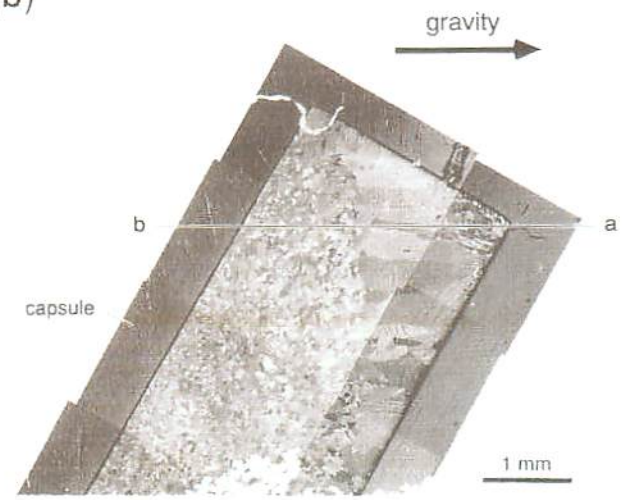

Starting material : Bi:Sb=70:30 at.% (80:20 wt.%)

Experiment condition :

Rotation rate:	195,000 ~ 215,000 rpm
Acceleration :	79,1000 ~ 96,2000 g
Temperature :	220 ~ 240 °C
Time :	85hours

Fig1-1. Experimental result of Bi-Sb system (70:30 at.%).[5]

CHAPTER 2
Simulation of sedimentation process for atoms.

2-1. Introduction

Strong acceleration field (mega-gravity field) realizes the sedimentation of atoms in condensed matter. We have realized the atomic-scale graded structures in a Bi-Sb (70:30 in mol %) system alloy by the sedimentation of component atoms under the mega-gravity field in 1997[1, 2]. This phenomenon can be analyzed by the self-consistent theory presented by one of the authors[3, 4].

In this *Chapter-2*, we are going to introduce the summary of self-consistent theory of diffusion in centrifugal force and going to explain the simulation procedure and discuss the result of the sedimentation process for atoms in the binary system simulating for Bi-Sb system comparing with the experimental result[1, 2]. Newly experimented study for this system will be discussed in the *Chapter-4*.

In the beginning, we made the simulation program based on the self-consistent theory and simulated it in the infinite energy range, and verified the validity of the simulation. After that, we performed the simulation in the finite energy range to discuss the experimental result.

2-2. Summary of self-consistent theory for sedimentation of atoms in condensed matter[3, 4]

T. Mashimo has proposed self-consistent equations for the sedimentation of atoms in a multi-component condensed system [3, 4]. The equation (16) written in bellow is the self-consistent equations for the sedimentation of atoms in a multi-component condensed system. The equation number is the same number in the *ref.3*.

$$\frac{\partial C_i}{\partial t} = \sum_l^s \left(D'_{il1} \frac{\partial^2 C_l}{\partial r^2} \right) + \sum_l^s \left(D'_{il1} \frac{1}{r} \frac{\partial C_l}{\partial r} \right) + \sum_l^s \sum_n^s \left(\frac{\partial D'_{il1}}{\partial C_n} \frac{\partial C_n}{\partial r} \frac{\partial C_l}{\partial r} \right)$$

$$- \frac{r\omega^2}{RT} \left[\sum_j^s D'_{ij2} \left(M_j - M_j^* \right) \right] \frac{\partial C_i}{\partial r}$$

$$- \frac{r\omega^2}{RT} \left\{ \sum_j^s \left[\sum_n^s \left(\frac{\partial D'_{ij2}}{\partial C_n} \frac{\partial C_n}{\partial r} \left(M_j - M_j^* \right) \right) - D'_{ij2} \frac{\partial M_j^*}{\partial r} + \frac{2}{r} D'_{ij2} \left(M_j - M_j^* \right) \right] \right\} C_i \qquad (16)$$

C : concentration of elements	r : radius from the center of rotation
R : gas constant	T : temperature
M : atomic weight	M^* : effective mass

Here D'_{il} and D'_{ij2} are the diffusion coefficients for the internal chemical potential (intrinsic coefficient of diffusion) and sedimentation, respectively. The theory was constructed on the basis of the mean-field approximation, the linear phenomenological matrix law with an expression for the atom fluxes and *the Nernst-Einstein relation.* Accordingly, the effects of self-interaction between the solutes, density changes and chemical activities, etc., were consistently taken into account.

In this section, we introduce the formula for multi-component system referring *ref.1*and *ref. 2*, and finally, we lead the formula of two-component system to use for the simulation of sedimentation in binary system.

a) The mean-field approximation, Effective mass, Density:

The external force acting on one atom j in the element F_j by a mean-field approximation and the effective mass of the surrounding mixture solvent is represented as follows, respectively:

$$m_j^* = \left(\sum_l^s \alpha_{jl} C_l m_l\right) / \left(\sum_j^s C_l\right) \tag{3}$$

$$F = g_r\left(m_j - m_j^*\right) \tag{2}$$

The density can be expressed as

$$\rho = \sum_l^s C_l m_l \tag{5}$$

Here, The density of the mixture solvent varies in proportional to the effective mass. So, the density ignoring the vacancy increase is written as follows:

$$\rho = \rho_0 \cdot \frac{m_j^*}{m_{j0}^*} \tag{6}$$

Converting the equation (6), the effective mass of the surrounding mixture solvent considering the density change with concentration

$$m_j^* = \frac{\rho}{\rho_0} \cdot m_{j0}^* \tag{6'}$$

b) The restrictions on the fluxes, The basic diffusion equation in a multi-component system in the external force field, which corresponds to the Fick's first law:

According to the linear phenomenological matrix law of diffusion, the atom flux of an atom j in s-component system in thermal equilibrium is represented as follows:

$$J = \sum_{j}^{s} L_{ij} X_j \tag{7}$$

Where L_{ij} and X_j are the phenomenological coefficients and the thermodynamic forces respectively. If we use the coordinate relative to the fixed parts of the lattice, the fluxes relative to the fixed parts of the lattice J'_i are written as follows from eqn. (7):

$$J' = \sum_{j}^{s} L'_{ij} X_j \tag{8}$$

Here the phenomenological coefficients L'_{ij} is

$$L'_{ij} = L_{ij} - C_i \sum_{l}^{s} L_{lj} / \sum_{l}^{s} C_l \tag{9}$$

And, the thermodynamic force X_j consists of a chemical potential term and an external force term is as follows:

$$X_j = -\nabla_{T,P} \mu_j + F_j$$

$$= -\sum_{l}^{s} \left(\frac{\partial \mu_j}{\partial C_l} \nabla C_l \right) + g\left(m_j - m_j^*\right) \tag{11}$$

Thermodynamic force = Chemical potential term + External force term

Here, as the flax is relative to the fixed parts of the lattice, we have the following restriction on the fluxes:

$$\sum_{l}^{s} J'_i = 0 \quad \text{(restriction on the flaxes)} \tag{10}$$

And, since the temperature is uniform, there is a following restriction on the flaxes, too:

$$\sum_{j}^{s} C_j X_j = 0 \quad \textit{(Gibbs-Duhem's} \text{ equation)} \tag{15}$$

As a result, the basic diffusion equation J'_i in a multi-component system in the external force field, which corresponds to *the Fick's first law*, is represented as follows:

$$J'_i = -\sum_{l}^{s} \sum_{j}^{s} \left(L'_{ij} \frac{\partial \mu}{\partial C_l} \nabla C_l \right) + \sum_{j}^{s} L'_{ij} g\left(m_j - m_j^*\right) \tag{12}$$

c) The diffusion equation in a multi-component system under a centrifuge field, which corresponds to the Fick's first law:

In the equation (12), supposing that *the Nernst-Einstein relation* holds for the whole range of concentrations in a multi-component system. Thus the equation can be rewritten as follows:

$$J_i' = -\sum_l^s \left(D_{il1}' \nabla C_l\right) + \sum_j^s \frac{D_{il2}'}{RT} g\left(M_j - M_j^*\right) C_i \qquad (13)$$

where

$$D_{il1}' = \sum_l^s \left(L_{ij}' \frac{\partial \mu}{\partial C_l}\right), \quad D_{il2}' = L_{ij}' \frac{kT}{C_i} \qquad (14)$$

D'_{il1} and D'_{ij2} are called the chemical potential diffusion coefficients and the external force field diffusion coefficient respectively in this study.

d) The diffusion equation in a multi-component system under a centrifuge field, which corresponds to the Fick's second law:

For a multi-component (s) sysytem in a centrifugal field, the diffusion equation for the atom i can be derived from *Fick's second law* in a cylindrical-coordinate representation, and from eqn. (13)

$$\frac{\partial C_i}{\partial t} = \sum_l^s \left(D_{il1}' \frac{\partial^2 C_l}{\partial r^2}\right) + \sum_l^s \left(D_{il1}' \frac{1}{r} \frac{\partial C_l}{\partial r}\right) + \sum_l^s \sum_n^s \left(\frac{\partial D_{il1}'}{\partial C_n} \frac{\partial C_n}{\partial r} \frac{\partial C_l}{\partial r}\right)$$

$$- \frac{r\omega^2}{RT} \left[\sum_j^s D_{ij2}' \left(M_j - M_j^*\right)\right] \frac{\partial C_i}{\partial r}$$

$$- \frac{r\omega^2}{RT} \left\{\sum_j^s \left[\sum_n^s \left(\frac{\partial D_{ij2}'}{\partial C_n} \frac{\partial C_n}{\partial r} \left(M_j - M_j^*\right)\right) - D_{ij2}' \frac{\partial M_j^*}{\partial r} + \frac{2}{r} D_{ij2}' \left(M_j - M_j^*\right)\right]\right\} C_i \qquad (16)$$

This is the equation that is introduced in the beginning of this section. We can analyze the equilibrium state and process in a multi-component condensed system by solving numerically s-simultaneous differential equations of eqn. (13) and eqn.(16) respectively. These equations are complicated to solve as each one involves s-external force terms in addition to s-chemical potential terms. However, in the case of two- and three-component systems, these equations can be rewritten in simple useful forms using

eqn. (10) and eqn. (15) by reducing the external force terms to one, as follows:

$$\frac{\partial C_i}{\partial t} = \sum_l^s \left(D_{il1}^{'} \frac{\partial^2 C_l}{\partial r^2} \right) + \sum_l^s \left(D_{il1}^{'} \frac{1}{r} \frac{\partial C_l}{\partial r} \right) + \sum_l^s \sum_n^s \left(\frac{\partial D_{il1}^{'}}{\partial C_n} \frac{\partial C_n}{\partial r} \frac{\partial C_l}{\partial r} \right)$$

$$- \frac{r\omega^2}{RT} \left[D_{ii2}^{'} \left(M_i - M_i^{\bullet} \right) \right] \frac{\partial C_i}{\partial r}$$

$$- \frac{r\omega^2}{RT} \left[\sum_n^s \left(\frac{\partial D_{ii2}^{'}}{\partial C_n} \frac{\partial C_n}{\partial r} \left(M_i - M_i^{\bullet} \right) \right) - D_{ii2}^{'} \frac{\partial M_j^{\bullet}}{\partial r} + \frac{2}{r} D_{ii2}^{'} \left(M_i - M_i^{\bullet} \right) \right] C_i \tag{31}$$

e) The diffusion equation in a two-component system (binary system) under a centrifugal field:

The diffusion equation in a two-component system is written as follows, applying s=2 in eqn. (31).

$$\frac{\partial C}{\partial t} = D_1 \frac{\partial^2 C}{\partial r^2} + \left(\frac{D_1}{r} + \frac{\partial D_1}{\partial C} \cdot \frac{\partial C}{\partial r} - \frac{r\omega^2}{RT} \left[D_2 \left(M - M^{\bullet} \right) + \left(M - M^{\bullet} \right) C \cdot \frac{\partial D_2}{\partial C} - D_2 C \cdot \frac{\partial M^{\bullet}}{\partial C} \right] \right) \frac{\partial C}{\partial r}$$

$$- \frac{2\omega^2}{RT} D_2 \left(M - M^{\bullet} \right) C$$

Here, D_1 and D_2 are the diffusion coefficients for the internal chemical potential (intrinsic coefficient of diffusion) and sedimentation, respectively.

f) The diffusion equation for the simulation:

In the upper equation, there is no previous data for explain the relationship of the both diffusion coefficients D_1 and D_2. So we put $Q=D_1/D_2=1+ \ (ln\gamma)/ \ (ln\, c)$ by using the following chemical potential representation: $\mu = \mu_0(T)+kTln(\gamma c)$, where γ is the activity coefficient. In addition, we assumed that the diffusion coefficients for the two elements were equal. We do not mean $D_1=D_2$. This means that the D_1 for the element a is equal to D_1 for the element b, and D_2 for the element a is equal to D_2 for the element b, when we choose the elements as a and b. With upper considerations, the diffusion equation in the two-component system can be written in simple form as follows:

$$\frac{1}{D} \cdot \frac{\partial C}{\partial t} = \frac{\partial^2 C}{\partial r^2} + \left(\frac{1}{r} - \frac{r\omega^2}{QRT} \left[\left(M - M^{\bullet} \right) - C \cdot \frac{\partial M^{\bullet}}{\partial C} \right] \right) \frac{\partial C}{\partial r} - \frac{2\omega^2}{QRT} \left(M - M^{\bullet} \right) C$$

We are going to perform the simulation with the equation.

2-3. Simulation procedure

In this *section*, we are going to explain the simulation procedure for the sedimentation process of atoms in the binary system computing with finite-difference method. At first, we will explain the simulation in the case of the infinite energy range to verify the validity of the simulation. For the second, we will explain the simulation in the finite energy range to discuss the experimental result.

Before those explanations, we are going to summarize the derivation of the finite-difference equation and the coordinate transformation for compiling the simulation program.

2-3-1. Derivation of Finite-difference diffusion equation for binary system

a) Finite-difference diffusion equation

The diffusion equation that was applied for the simulation is written in simple form as we explained in the section 2-2. (f):

$$\frac{1}{D}\cdot\frac{\partial C}{\partial t}=\frac{\partial^2 C}{\partial r^2}+\left(\frac{1}{r}-\frac{r\omega^2}{QRT}\left[\left(M-M^*\right)-C\cdot\frac{\partial M^*}{\partial C}\right]\right)\frac{\partial C}{\partial r}-\frac{2\omega^2}{QRT}\left(M-M^*\right)C$$

The numerical calculation can not be performed in this equation form as it expresses the variation of continuous quantity of state. So we have to derive the finite-difference equation to simulate the concentration change depending on time passing by the finite-difference method. The finite-difference equation is expressed with *the Taylor's series expansion* as follows:

$$\frac{1}{D}\cdot\frac{C_i^{j+1}-C_i^j}{\tau}=\frac{C_{i-1}^j-2C_i^j-C_{i+1}^j}{h^2}+\left(\frac{1}{r}-\frac{r\omega^2}{QRT}\left[\left(M-M^*\right)-C_i^j\frac{M_{i+1}^*-M_{i-1}^*}{C_{i+1}^j-C_{i-1}^j}\right]\right)\frac{C_{i+1}^j-C_{i-1}^j}{2h}$$

$$-\frac{2\omega^2}{QRT}\left(M-M^*\right)C_i^j$$

Here, the time interval τ of computation is expressed as $\tau=h^2/DF$, so

$$C_i^{j+1}=C_i^j+\left(\frac{1}{F}\right)\left(C_{i-1}^j-2C_i^j-C_{i+1}^j\right)+\left(\frac{h}{F}\right)\left(\frac{1}{r}-\frac{r\omega^2}{QRT}\left[\left(M-M^*\right)-C_i^j\frac{M_{i+1}^*-M_{i-1}^*}{C_{i+1}^j-C_{i-1}^j}\right]\right)\frac{C_{i+1}^j-C_{i-1}^j}{2}$$

$$-\left(\frac{h^2}{F}\right)\frac{2\omega^2}{QRT}\left(M-M^*\right)C_i^j$$

And, also using the relationship $E=Ar^2$ and $A=(M_a-M_b)\omega^2/2RT$,

$$C_i^{j+1} = C_i^j + \left(\frac{1}{F}\right)\left(C_{i-1}^j - 2C_i^j - C_{i+1}^j\right) + \left(\frac{h}{F}\right)\left(\frac{1}{r} - \frac{2rA}{Q(M_a - M_b)}\left[\left(M - M^*\right) - C_i^j \frac{M_{i+1}^* - M_{i-1}^*}{C_{i+1}^j - C_{i-1}^j}\right]\right)\frac{C_{i+1}^j - C_{i-1}^j}{2}$$
$$-\left(\frac{h^2}{F}\right)\frac{4A}{Q(M_a - M_b)}\left(M - M^*\right)C_i^j$$

b) The coordinate transformation to Lagrangian

Just using the equation derived in a), the total sum of atoms in unit volume vary with the concentration change if the element *a* and *b* have different atomic volume. It is necessary for the computation to keep the total sum of the atoms in unit volume constant, so the correction of the volume was considered using the relation ship that the cubic root of the volume calculated from the concentrations shows the changing rate of radius. *The Lagrangian coordinate systems* are used for the simulation.

If the atomic-volume is constant independent from concentration change, the volume is written as follows:

$$V^* = \frac{C_a V_a + C_b V_b}{C_a + C_b}$$

And the volume used as a standard volume is:

$$V_0^* = \frac{C_{a0} V_a + C_{b0} V_b}{C_{a0} + C_{b0}}$$

So, the coefficient f_c for correcting volume is written as follows:

$$f_c = \left(\frac{r}{r_0}\right) = \left(\frac{V^*}{V_0^*}\right)^{1/3} = \sqrt[3]{\frac{C_a V_a + C_b V_b}{C_a + C_b} \cdot \frac{C_{a0} + C_{b0}}{C_{a0} V_a + C_{b0} V_b}}$$

The equation below is the diffusion equation that is just converting to the finite-difference equation.

$$\frac{1}{D}\cdot\frac{\partial C}{\partial t} = \frac{\partial^2 C}{\partial r^2} + \left(\frac{1}{r} - \frac{r\omega^2}{QRT}\left[\left(M - M^*\right) - C\cdot\frac{\partial M^*}{\partial C}\right]\right)\frac{\partial C}{\partial r} - \frac{2\omega^2}{QRT}\left(M - M^*\right)C$$

In the equation, the concentration change is described by concentration C and radius r. The coordination r is to be transforming into the coordination Z using the coefficient f_c for correcting volume.

The relationship between the coordinate r and the coordinate Z is written as follows:

$$dZ = f_c dr$$

so, the coordination Z is,

$$Z = \int f_c dr$$

And, the coordination r is,

$$r = \int \frac{1}{f_c} dZ$$

$$\frac{\partial C}{\partial r} = \frac{\partial C}{\partial Z} \cdot \frac{\partial Z}{\partial r} = f_c \cdot \frac{\partial C}{\partial Z}$$

$$\frac{\partial^2 C}{\partial r^2} = \frac{\partial}{\partial r}\left(\frac{\partial C}{\partial r}\right) = \frac{\partial}{\partial r}\left(f_c \cdot \frac{\partial C}{\partial Z}\right) = \frac{\partial C}{\partial Z} \cdot \frac{\partial}{\partial r}(f_c) + f_c \cdot \frac{\partial}{\partial r}\left(\frac{\partial C}{\partial Z}\right)$$

$$= \left\{\frac{\partial Z}{\partial r} \cdot \frac{\partial}{\partial Z}(f_c)\right\} \cdot \frac{\partial C}{\partial Z} + f_c \cdot \frac{\partial Z}{\partial r} \cdot \frac{\partial}{\partial Z}\left(\frac{\partial C}{\partial Z}\right)$$

$$= \left\{f_c \cdot \frac{\partial}{\partial Z}(f_c)\right\} \frac{\partial C}{\partial Z} + f_c^{\,2} \cdot \frac{\partial^2 C}{\partial Z^2}$$

Using upper relations, the diffusion equation can be converted the coordinate r to Z as follows:

$$\frac{1}{D} \cdot \frac{\partial C}{\partial t} = f_c^2 \cdot \frac{\partial^2 C}{\partial Z^2} + \left(f_c \frac{\partial f_c}{\partial Z}\right) \cdot \frac{\partial C}{\partial Z} + \left\{\frac{1}{\int \frac{1}{f_c} dZ} - \frac{r\omega^2}{QRT}\left[\left(M - M^*\right) - C \cdot \frac{\partial M^*}{\partial C}\right]\right\} \cdot f_c \cdot \frac{\partial C}{\partial Z}$$

$$- \frac{2\omega^2}{QRT}\left(M - M^*\right)C$$

And, next equation is the finite-difference diffusion equation of upper equation that was derived same method as we explained in section a).

$$C_i^{j+1} = C_i^j + \frac{\left(f_{ci}^{\,j}\right)^2}{F} \cdot \left(C_{i-1}^j - 2C_i^j - C_{i+1}^j\right)$$

$$+ \frac{h \cdot f_{ci}^{\,j}}{F} \cdot \left(\frac{f_{ci}^{\,j} - f_{ci-1}^{\,j}}{r_i^j - r_{i-1}^j} + \frac{1}{r_i^j} - \frac{2rA}{Q(M_a - M_b)}\left[\left(M - M^*\right) - C_i^j \cdot \frac{M_{i+1}^* - M_{i-1}^*}{C_{i+1}^j - C_{i-1}^j}\right]\right) \cdot \frac{C_{i+1}^j - C_{i-1}^j}{2}$$

$$- \frac{h^2}{F} \cdot \frac{4\omega^2}{Q(M_a - M_b)}\left(M - M^*\right) \cdot C_i^j$$

c) Relationship between Effective mass and Density

Using equation (3), the effective mass for two-component system is written as follows:

$$M_a^* = \frac{\alpha_{aa} C_a M_a + \alpha_{ab} C_b M_b}{C_a + C_b} = \frac{C_a}{C_a + C_b} M_a + \frac{C_b}{C_a + C_b} M_b \alpha$$

$$M_b^* = \frac{\alpha_{bb} C_b M_b + \alpha_{ba} C_a M_a}{C_a + C_b} = \frac{C_a}{C_a + C_b} M_a \frac{1}{\alpha} + \frac{C_b}{C_a + C_b} M_b = \frac{M_a^*}{\alpha}$$

Here, $\alpha = V_a/V_b$ is the ratio of the atomic volume between the element *a* and *b*. If we use the upper formula of the effective mass in the simulation just as it is, the computation can not converge to the steady state because of no consideration the relationship between effective mass and density. The relationship between effective mass and density is equation (6) as we explained in section 2-a):

$$m_j^* = \frac{\rho}{\rho_0} \cdot m_{j0}^* \tag{6}$$

From equation (5), the density ρ is written as follows:

$$\rho = C_a m_a + C_b m_b = \frac{C_a M_a + C_b M_b}{N}$$

And, the density ρ_0 used as a standard density is:

$$\rho_0 = C_{a0} m_a + C_{b0} m_b = \frac{C_{a0} M_a + C_{b0} M_b}{N}$$

Here, the C_0 is a standard concentration. We can set the standard state as you like, for example, as the starting concentration, as the concentration of center of rotation at the end of the computation, etc..

Also, the effective mass M^*_0 used as a standard effective mass is written from equation (6) as follows:

$$M_{a0}^* = \frac{C_{a0}}{C_{a0} + C_{b0}} M_a + \frac{C_{b0}}{C_{a0} + C_{b0}} M_b \alpha$$

$$M_{b0}^* = \frac{C_{a0}}{C_{a0} + C_{b0}} M_a \frac{1}{\alpha} + \frac{C_{b0}}{C_{a0} + C_{b0}} M_b = \frac{M_{a0}^*}{\alpha}$$

So, the relationship between effective mass and density for the simulation is as follows:

$$M_a^* = \left(\frac{C_{a0}}{C_{a0} + C_{b0}} M_a + \frac{C_{b0}}{C_{a0} + C_{b0}} M_b \alpha \right) \cdot \left(\frac{C_a M_a + C_b M_b}{C_{a0} M_a + C_{b0} M_b} \right)$$

$$M_b^* = \frac{M_a^*}{\alpha}$$

d) About the simulation using this Finite-difference method

In the simulation by the finite-difference method with the procedure explained in this section, the concentration $C^{j+1}{}_i$ at the time is expressed with the concentration $C^j{}_i$ and $C^{j-1}{}_i$ value of just on step time separation τ before. So, the

In the simulation, it should be noticed that we put the diffusion coefficients for the internal chemical potential and sedimentation always constant.

2-3-2. Simulation procedure in the case of the infinite energy range (infinite radius)

The theoretical solution of the sedimentation equation for two-component system at the steady state was analyzed in the paper of *ref. 3* and *4*. The numerical analysis was performed by *the Runge-Kutta method*, using FORTRAN program. So, we planed to simulated the sedimentation process from the starting state to steady state. In the beginning, we made the simulation program and simulated it in the infinite energy range to verify the validity of the simulation by confirming if the concentration change converge to the steady state of theoretical solution from the starting state of average concentration of steady state of the theoretical solution or not.

a) Reduction of parameter's dimension

It is convenient for the sedimentation equation for flaxes of atoms to express in non-dimensional parameters, because the state is discussed in energy field. So, the main calculation parameters of the theoretical solution in *ref. 3* or *4* were reduced to no-dimensional parameters. And, we have to simulate the sedimentation with reduced parameter to use the theoretical solution for the starting state of average concentration of steady state.

The reduced concentration X was expressed as $X=C/C_0$, in which the standard concentration C_0 was defined as the concentration at the center of rotation in steady state for converging the computation to value 1.0 at the center of the rotation. The coordinate transformed diffusion equation for sedimentation that was explained in section 2-3-1 was described by using $X=C/C_0$ to next form of just substituted C to X.

$$X_i^{j+1} = X_i^j + \frac{\left(f_{ci}^{\ j}\right)^2}{F}\cdot\left(X_{i-1}^j - 2X_i^j - X_{i+1}^j\right)$$

$$+\frac{h\cdot f_{ci}^{\ j}}{F}\cdot\left(\frac{f_{ci}^{\ j} - f_{ci-1}^{\ j}}{r_i^j - r_{i-1}^j} + \frac{1}{r_i^j} - \frac{2rA}{Q(M_a - M_b)}\left[\left(M - M^*\right) - X_i^j\cdot\frac{M_{i+1}^* - M_{i-1}^*}{X_{i+1}^j - X_{i-1}^j}\right]\right)\cdot\frac{X_{i+1}^j - X_{i-1}^j}{2}$$

$$-\frac{h^2}{F}\cdot\frac{4\omega^2}{Q(M_a-M_b)}(M-M^*)\cdot X_i^j$$

The effective mass m^* is rewritten as following form by using $X=C/C_0$ and $\beta = C_{a0}/C_{b0}$.

$$M_a^* = \left(\frac{C_{a0}}{C_{a0}+C_{b0}}M_a + \frac{C_{b0}}{C_{a0}+C_{b0}}M_b\alpha\right)\cdot\left(\frac{C_aM_a+C_bM_b}{C_{a0}M_a+C_{b0}M_b}\right)$$

$$= \frac{(\beta M_a+\alpha M_b)(\beta X_aM_a+X_bM_b)}{(1+\beta)(\beta M_a+M_b)}$$

$$M_b^* = \frac{M_a^*}{\alpha}$$

Here, the β is the ratio of concentration of steady state for two elements at the center of rotation.

The coefficient f_c for correcting volume is rewritten as follows:

$$f_c = \left(\frac{r}{r_0}\right) = \left(\frac{V^*}{V_0^*}\right)^{1/3} = \sqrt[3]{\frac{C_aV_a+C_bV_b}{C_a+C_b}\cdot\frac{C_{a0}+C_{b0}}{C_{a0}V_a+C_{b0}V_b}}$$

$$= \sqrt[3]{\frac{(\beta X_a+\alpha X_b)(1+\beta)}{(\beta X_a+X_b)(\beta+\alpha)}}$$

b) Starting concentrations

The simulation needs starting concentrations. In the starting sample, the distributions of both elements are uniform. So, the starting concentrations are determined as average concentration of steady state of the theoretical solution.

The Runge-Kutta method is used for calculating the concentrations of the theoretical solution.

$$\frac{dX_i^{\infty}}{dz} = \left(X_i^{\infty}, z\right)$$

$$z = \log_{10}E = \log_{10}100r^2 \qquad (55)$$

$$N = \int_0^r X_i^{\infty}\cdot 2\pi r dr$$

The N is the total sum of the no-dimensional concentrations. From the equation (55),

$$\frac{dN}{dr} = X_i^* \cdot 2\pi r$$

$$\frac{dX_i^*}{dr} = \frac{dX_i^*}{dz} \cdot \frac{dz}{dr} = \frac{dX_i^*}{dz} \cdot \frac{2}{r \log 10} = n\left(X_i^*, \log_{10} 100r^2\right) \qquad (56)$$

The N and X are calculated using the coalition differential equation (56). So, the starting concentrations $X(r, 0)$ is determined as following:

$$X_i^0 = \frac{N}{\pi r^2} \qquad (57)$$

c) First conditions

The parameters of first conditions for the simulation of sedimentation in case infinite radius is defined as following:

$0<E<100$: the calculation range in energy scale ($E=100r^2$, $0<r<1$).

m: the division number of partition for the radius of the sample.

h: h(cm)$=r/m$.

τ (s): time interval of computation.

n: last statement number to be executed in the loop. (the data sampling was done every 2000 times)

M_a(g): the atomic mass of element a

R_a(Å): the atomic radius of element a

M_b(g): the atomic mass of element b

r_b(Å): the atomic radius of element b

$M_a>M_b$: we have to put the element that has large atomic mass for a.

T(K): experiment temperature.

Q=1.0 : the ratio of diffusion coefficient, $Q=D_1/D_2==1+\ (ln\gamma)/\ (ln c)$.
(γ : activity coefficient)

β : the ratio of concentration of steady state for two elements at the center of rotation, $\beta = C_{a0}/C_{b0}$.

α : the ratio of atomic volume of two elements, $\alpha = V_a/V_b$

d) Boundary conditions

The theoretical solutions are calculated as the relationship between the energy and concentrations of both elements. Figure 2-1-a is the image of the gravitational field of in finite energy range at steady state. The state can be considered as the state in case

that the angular speed is constant and the sample has infinite radius. The computation can not be performed in case the object has infinite calculation area, so we approximate the infinite radius to finite radius of r=1(cm) by setting the enough high angular speed that can elevate the energy at r=1(cm) to E=100. With enough high angular speed, the energy at r=1(cm) can be considered as infinite energy because the convergence of concentration by self-interaction can be seen over E=10. The boundary conditions for the simulation in case infinite radius are as following:

At the center of rotation:

If we put the concentration $X(r=0)$ as X_1^2, the X_1^2 is expressed as following:

$$X_1^2 = X_1^1 + \frac{4\left(f_{c(1)}\right)^2}{F}\left(X_2^1 - X_1^1\right) - \frac{4h^2\varepsilon}{F\left(M_a - M_b\right)}\left(M - M_{(1)}^*\right)X_1^1$$

This is the boundary condition at the center of rotation.

At the maximum radius:

① When the specific weight for element a > The specific weight for element b.

$M_a^* = M_a$, $X_a = X_a max$, $X_b = X_b max = 0$.

From the relationship between effective mass and density,

$$M_{a_x}^* = \frac{(\beta M_a + \alpha M_b)\beta X_{a_{max}} M_a}{(1+\beta)(\beta M_a + M_b)} = M_a$$

So, the boundary conditions at the maximum radius is

$$X_{a_{max}} = \frac{(1+\beta)(\beta M_a + M_b)}{\beta(\beta M_a + \alpha M_b)}$$

$$X_{b_{max}} = 0$$

② When the specific weight for element a < The specific weight for element b.

Same as ①, $M_b^* = M_b$, $X_a = X_a max = 0$, $X_b = X_b max$.

The boundary conditions at the maximum radius is

$$X_{a_{max}} = 0、 \quad X_{a_{max}} = \frac{(1+\beta)(\beta M_a + M_b)\alpha}{(\beta M_a + \alpha M_b)}$$

2-3-3. Simulation procedure in the case of the finite energy range (finite radius)

The simulation in the infinite energy range that we explained in the section 2-3-2 is convenient to explain the theory of sedimentation. But in the experiment, the sample has finite radius, the accomplishable energy is limited to around E=2 or so. So, it is important for us to simulate in case finite radius and compare it with experimental results. Figure 2-1-b is the image of the gravitational field of finite energy range.

a) About the simulation program in case of the finite radius

The simulation in the infinite energy range was performed using non-dimensional parameters. The starting concentrations were got from theoretical solutions of diffusion equation. So, it was convenient to explain the theory of sedimentation.

In case finite energy range, we are going to perform the simulation with dimension parameters. And, the starting compositions can decide as you like for example element *a* to element *b* equals to 50:50. So, it is convenient for comparing with the experimental results.

b) Starting composition rate

The starting concentrations for both elements (*a, b*) are defined from the total mass of atoms per 1 cm^3. The maximum concentrations each are expressed as following:

$$C_{a_{max}} = N \cdot d_a / M_a$$

$$C_{b_{max}} = N \cdot d_b / M_b = A \cdot C_{a_{max}}$$

Here, the α is the ratio of atomic volume of two elements that was expressed as $\alpha = V_a/V_b = (M_a/d_a N)/(M_b/d_b N)$. As the both concentration proportional to α, the starting concentrations can express as following form:

$$C_{as} = 0 + C_{a_{max}} \cdot x$$

$$C_{bs} = \left(C_{a_{max}} - C_{as}\right) \cdot A = C_{b_{max}} - C_{b_{max}} \cdot x = C_{b_{max}} \cdot (1 - x)$$

Here, the molar ratio of both element was put element *a* to element *b* as $x:\alpha(1\text{-}x)$ $(0<x<1)$

c) First conditions

The parameters of first conditions for the simulation of sedimentation in case finite

radius is defined as following:

r(cm): the calculation range in radius ($r_0<r<r_{max}$).

m: the division number of partition for the radius of the sample.

h: h(cm)=$(r_1-r_0)/m$.

τ (s): time interval of computation.

n: last statement number to be executed in the loop. (the data sampling was done every 2000 times)

W_a(g): the atomic mass M_a of element a

$Dens_a$(g/cm^3): the density of element a

W_b(g): the atomic mass M_b of element b

$Dens_b$(g/cm^3): the density of element b

$W_a>W_b$: we have to put the element that has large atomic mass for a.

T(K): experiment temperature.

Q=1.0 : the ratio of diffusion coefficient, $Q=D_1/D_2==1+\ (ln\gamma)/\ (ln c)$.

(γ : activity coefficient)

$\alpha=(W_a/Dens_a)/(W_b/Dens_b)$: the ratio of atomic volume of two elements, $\alpha=V_a/V_b$

C_{as}, C_{bs}: the starting concentrations

d) Boundary conditions

The boundary conditions for the simulation in case infinite radius are as following:

At the minimum radius:

①*When we put the minimum radius of r_0 to the center of the rotation:*

We can set the boundary condition taking advantage of symmetry with respect to the axis of rotation. Putting the concentration at the center of the rotation (r=0) as C_1^2, the C_1^2 is expressed as following:

$$C_1^2 = C_1^1 + \frac{4\left(f_{c(1)}\right)^2}{F}\left(C_2^1 - C_1^1\right) - \frac{4h^2\varepsilon}{F\left(M_a - M_b\right)}\left(M - M_{(1)}^*\right)C_1^1$$

②*When the radius r is not 0 ($0<r_0<r_{max}$):*

The minimum radius of the sample in the experiment is not 0 value because the specimen is filled in the capsule of sample holder usually. In this case, the boundary is the capsule wall, and we can set the boundary condition that the fluxes

of atoms are zero at the edge of the sample, as following:

$$C_1^1 = C_3^1 - \frac{4hf_{c(1)}\varepsilon r}{M_a - M_b} \cdot \left(M - M_1^*\right) C_2^1$$

At the maximum radius:

Also, the boundary at the maximum radius is the capsule wall, and we can set the boundary condition that the fluxes of atoms are zero at the edge of the sample, too:

$$C_{m+1}^1 = C_{m-1}^1 + \frac{4hf_{c(m)}\varepsilon r}{M_a - M_b} \cdot \left(M - M_m^*\right) C_m^1$$

2-4. Result of the simulation

2-4-1. In the case of the infinite energy range (infinite radius)

Figure 2-2 shows the simulation result of sedimentation in the 70mol% Bi-30mol%Sb system in the infinite energy range for an ideal reference system (γ =1, i.e. Q=1). Here, C/C_0 on the horizontal axis is the difference between the reduced potential energies of the Bi and Sb atoms, where C_0 is the concentration at the center of rotation (r=0), and M_{Bi} and M_{Sb} are the atomic masses of Bi and Sb equal to 209.0 and 121.8 respectively. The starting concentration profiles were uniform with a Bi:Sb ratio of 70:30 (mol%), and the ratio of atomic volumes ($\alpha = V_{Bi}/V_{Sb}$) was 1.44. In the case of an infinite radius, the body force or potential energy difference greatly increases up to infinity. Even for this calculation we simulated using the same boundary conditions from $E=10^{-4}$ to E=100. However, $E=10^{-4}$ is small enough to be treated as zero energy and E=100 is large enough to be treated as infinity energy in this calculation. In fact, the simulation result shows good agreement with the theoretical solutions of steady state in an infinite energy range (Mashimo 1994).

The calculated concentration profiles changed gradually with time. Heavy Bi atoms moved in the direction of gravity, and light Sb atoms moved in the opposite direction. The change in concentration was notable beyond E=1, where the external field energy per unit mole counterbalanced the thermal energy for one degree of concentration of Sb appeared at around E=1, which might be caused by stagnation of Sb atoms due to the slow diffusion velocity in the small gravitational region. Below E=1, the concentrations are more influenced by the internal chemical potential than by the gravity field; therefore, the concentration changes were small. Sb atoms diffuse from the strong gravitational region and accumulate at around E=1; thus the concentration of

Sb around E=1 higher than that under the E=1 area at an early stage. The concentrations at the starting state were uniform values, which were derived by integrating the concentrations at steady state. The concentrations in the low-gravitation decrease to 1, where the concentrations were equal to that at r=0 at steady state. This change was caused by the internal chemical potentials acting as a force driving towards uniform concentrations. The concentration profiles finally converged to their respective steady-state solutions (Mashimo 1994), which showed that the simulation was successful.

2-4-2. The case of a finite radius

Figure 2-3(a), (b) and (c) show the simulation results of sedimentation in the 70 mol%Bi – 30 mol% Sb system in the finite energy range (r=15.2-18.6mm) at Q=1, 1/10 and 1/20 respectively. Here, the starting composition profiles were uniform in the ratio of 70:30 (mol%), the ratio of the atomic volume was 1.44, the rotation rate N was 205000 rev.min^{-1} and the temperature T was 503K (230°C). Those conditions were almost all the same as the average of experimental value (Mashimo et al. 1997, 2001), which was introduced in the *Chapter 1*, section 1-3-3). The difference E between the reduced potential energy of the Bi and Sb atoms at the maximum radius (18.2mm) was 1.75, which was larger than the thermal energy. The time interval of each of the composition profiles depends on the diffusion coefficient of the system. Thus the calculated composition profiles changed gradually with time, and that of Sb increased in the opposite direction. Both composition profiles converged to their respective steady states.

At Q_{ii}=1, the change in composition was very small. It increased with the decrease in Q, and the values at Q=1/20 was notable. Near the right edge of the sample (high-gravity region), the concentration changes of both elements were very large, where atoms could not move any longer, and Bi atoms gradually accumulated there in the boundary condition that the flux of atoms was zero at the edge.

2-5. Discussion

The experimental results of composition profiles of 70 at.% Bi-30at.% Sb alloy measured by the electron probe micro analysis (EPMA) and X-ray diffraction (XRD) methods (experimental conditions: rotation rate, 195000-215000 rev·min^{-1}; temperature, 493-513K; duration, 85h) are shown in figure 2-4 or figure 1-1 in the *Chapter 1*. Near

the right edge of the sample, the concentration of Bi approached almost 100 mol% and, opposite to it, that of Sb approached almost 0 mol% where the lattice space was mostly occupied by Bi atoms. The final concentration distribution of the simulation result at Q=1/20 (figure 2-3(c)) was reasonably compare with the experimental result (Mashimo et al. 1997, 2001, figure 2-4), as shown in figure 2-5. Q_{ii}=1/20 indicates that the diffusion coefficients for sedimentation were twenty fold lager than the conventional values. More than two concentration data sets (two experiments) are needed to calculate the real Q value. We obtained Q=1/20, when the experimental data were assumed to be mostly at steady state. However, as it might take more time to reach a steady state than the experimental value, the real Q value would be smaller (the sedimentation coefficient become larger), that is, the diffusion coefficients for sedimentation would be greater than the conventional value by more than 20 times. It can be concluded that the diffusion rates for sedimentation are much faster than conventional value, even though substitutional solutes act in this system.

In the small-radius region (low-gravity field), the observed composition changes were smaller than the calculated values. Sb atoms accumulated in the middle part of the specimen as shown in figure 2-4 or figure 1-1 in the *Chapter 1*. This difference was caused by the simulation conditions that the diffusion coefficients for the two components were always equal. The velocity of diffusing atoms is proportional to the acceleration field and, in addition, the diffusion coefficients in the low-gravity region are assumed to be small in this system. The diffusion coefficients are influenced by the composition, melting temperature, etc. It was assumed that the diffusion coefficient of Sb atoms with small atomic volumes in the Bi-rich region (low-gravity region) is smaller than that of Bi atoms with large atomic volumes in the Sb-region (Moore 1965).

The experiments on sedimentation of atoms in solids are summarized in table 1-1 in the *Chapter 1*. In previous studies, the concentrations of Au atoms were at an impurity level in K, In or Pb solvent, and the concentration changes achieved were small, while interstitial solutes acted in these systems (ultra fast diffusion systems). For sedimentation in the Bi-Sb system, substitutional solutes with component level rates should act. The present simulation results suggested that the diffusion coefficient for sedimentation was remarkably larger than for the internal chemical potential. As a result, it is suggested that the diffusion mechanism for sedimentation was different from the vacancy mechanism. Under a strong gravitational field of over 10^6 g at maximum acceleration, each atom is forced in a gravity field direction by a very large body force, which corresponds to a 0.1-1 GPa level in pressure, even though the body force is

essentially different form pressure. It is assumed that the substitutional solutes can push open the lattices and act as an interstitial solute under such a strong gravitational field. We recently observed the strained crystal state in large crystal grains with large concentration gradients by the Laue X-ray method, which might be related to this assumption.

REFERENCES

[1] T. Mashimo, S. Okazaki, S. Tashiro: Jpn. J. Appl. Phys. **36** (1997) 498-500.

[2] T. Mashimo, H. Ikeda, I. Minato: J. Appl. Phys. **90** (2001) 741-744.

[3] T. Mashimo: Phys. Rev. A**38** (1988) 4149-4154.

[4] T. Mashimo: Philos. Mag. A**70** (1994) 739-760.

a) In the case of infinite energy range (infinite radius)

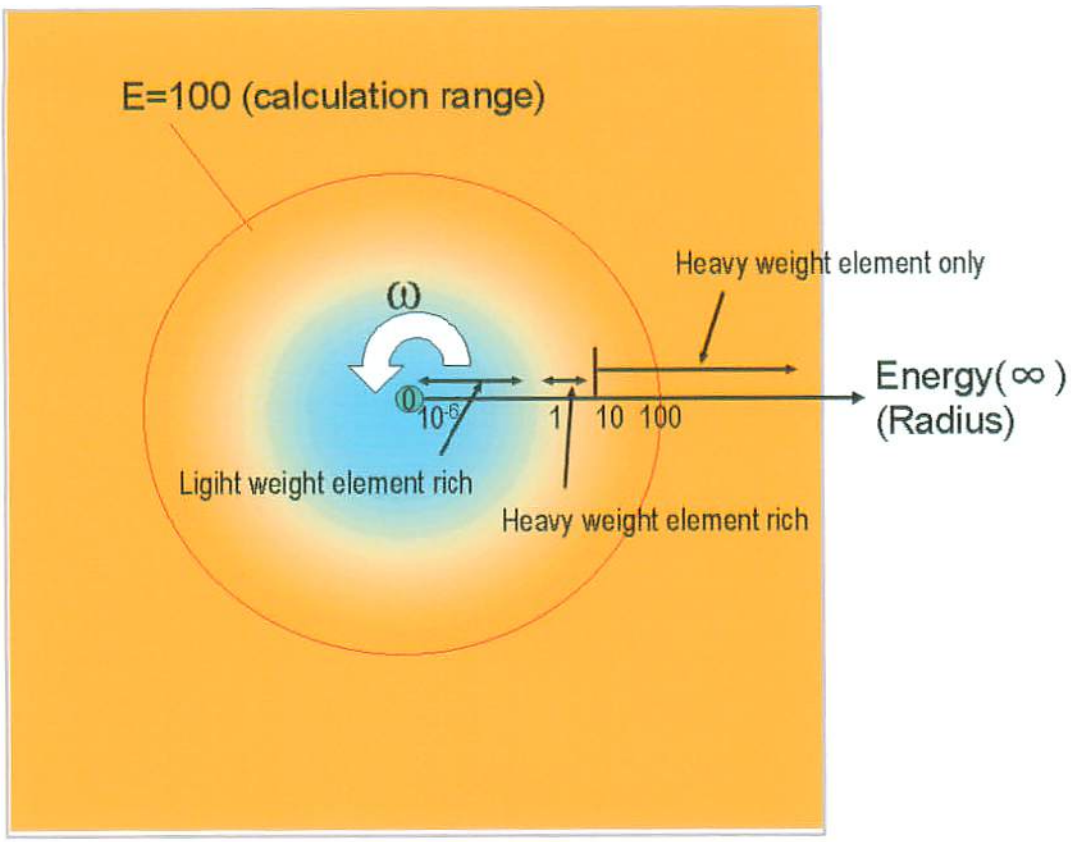

b) In the case of finite radius

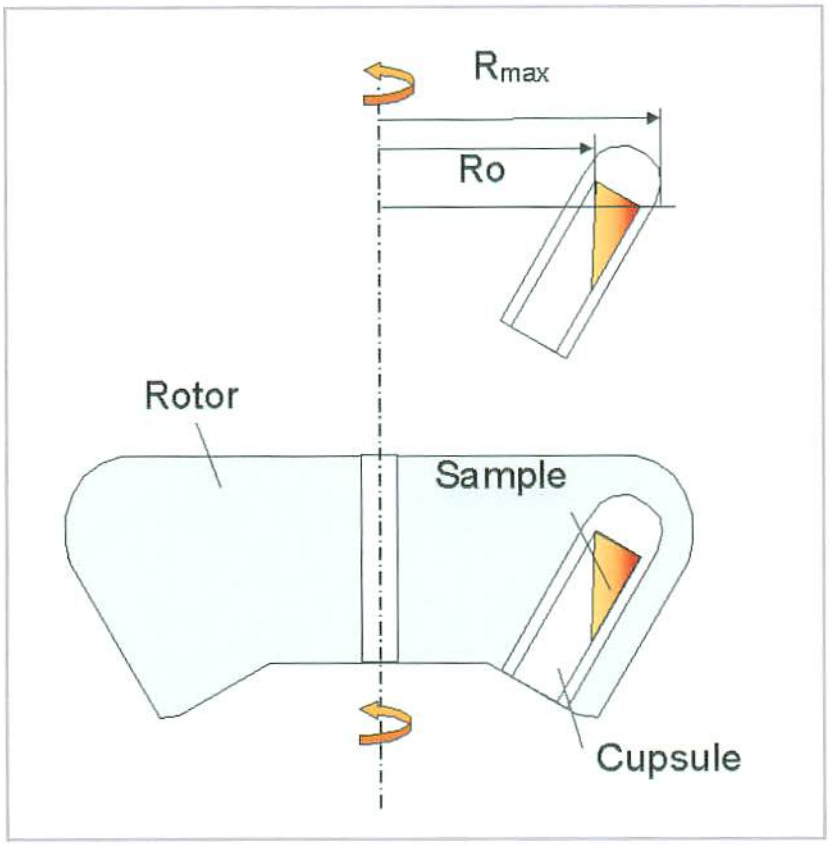

Fig. 2-1 Image of grvitational field for the simulation

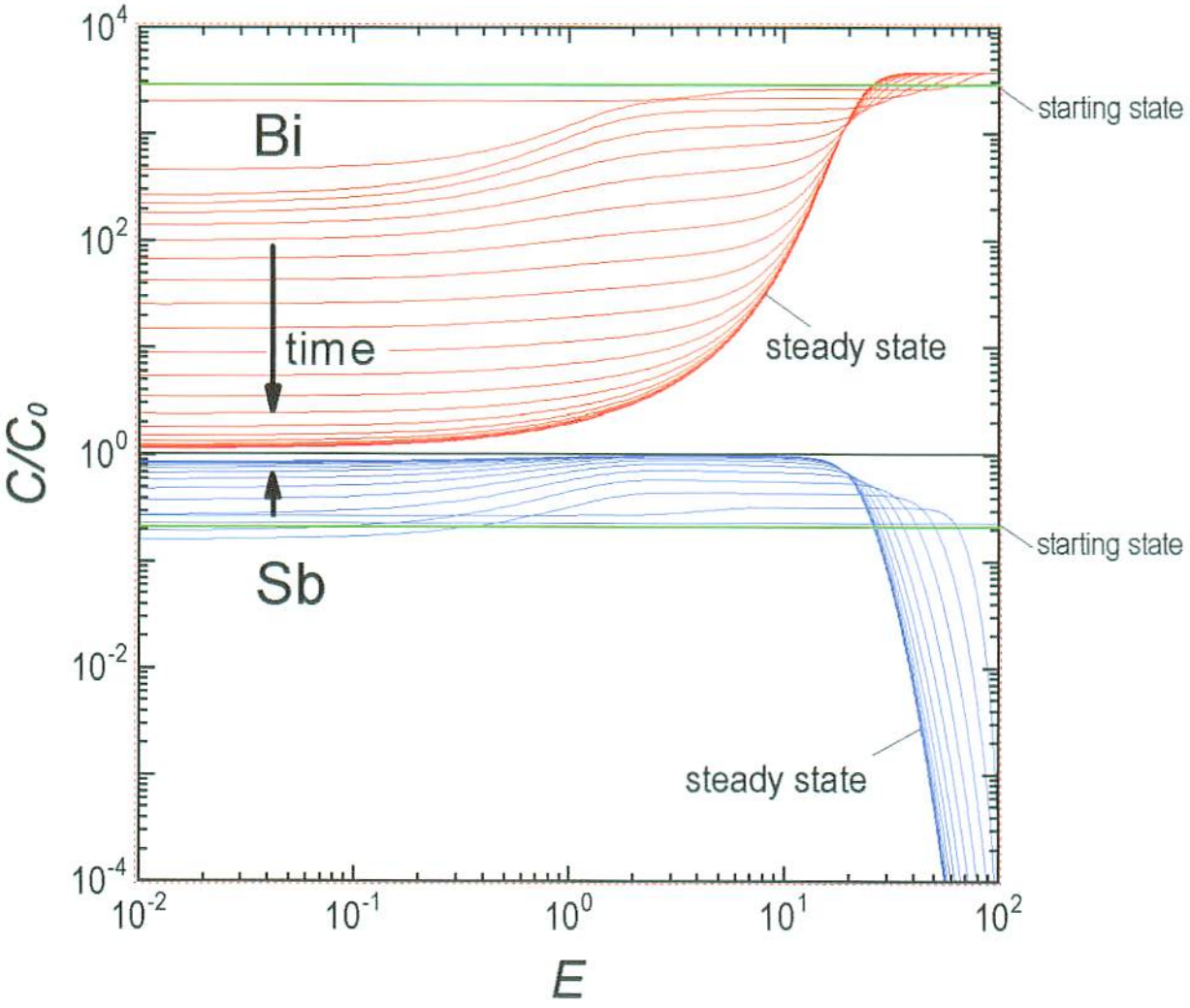

Fig.2-2 Result of the simulation of sedimentation process for atoms in Bi-Sb system. (infinite energy range)

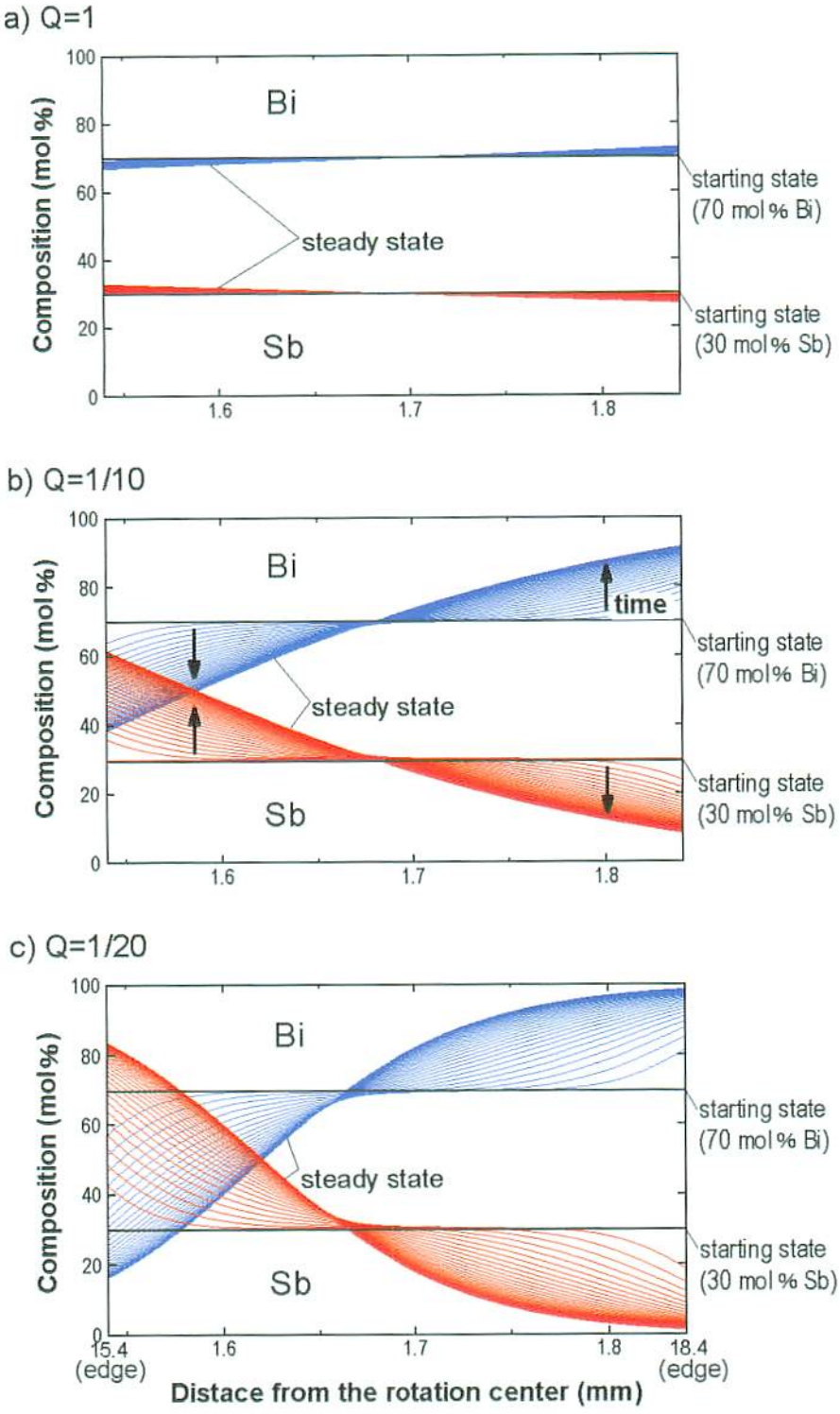

Fig. 2-3 Results of the simulations in the finite energy range (Bi:Sb=70:30mol%)

Simulation conditions;

Rotational speed: 215,000 rpm

Temperature: 230 ℃

Radius: 1.54-1.84 cm

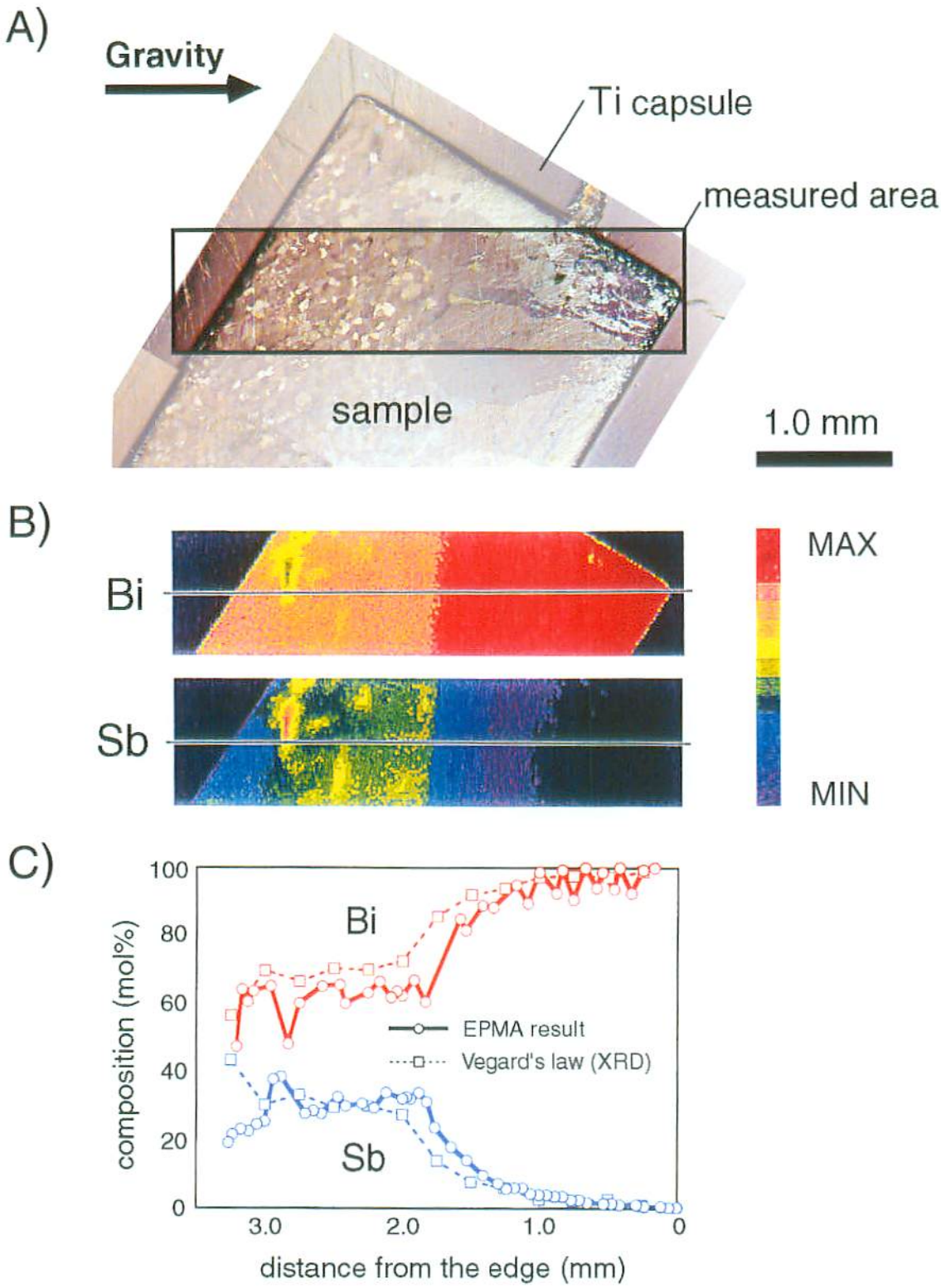

Starting material : Bi:Sb=70:30 at.% (80:20 wt.%)

Experiment condition :

Rotation rate:	195,000 ~ 215,000 rpm
Acceleration :	79,1000 ~ 96,2000 g
Temperature :	220 ~ 240 °C
Time :	85hours

Fig. 2-4 Experimental result of Bi-Sb system (70:30 at.%).

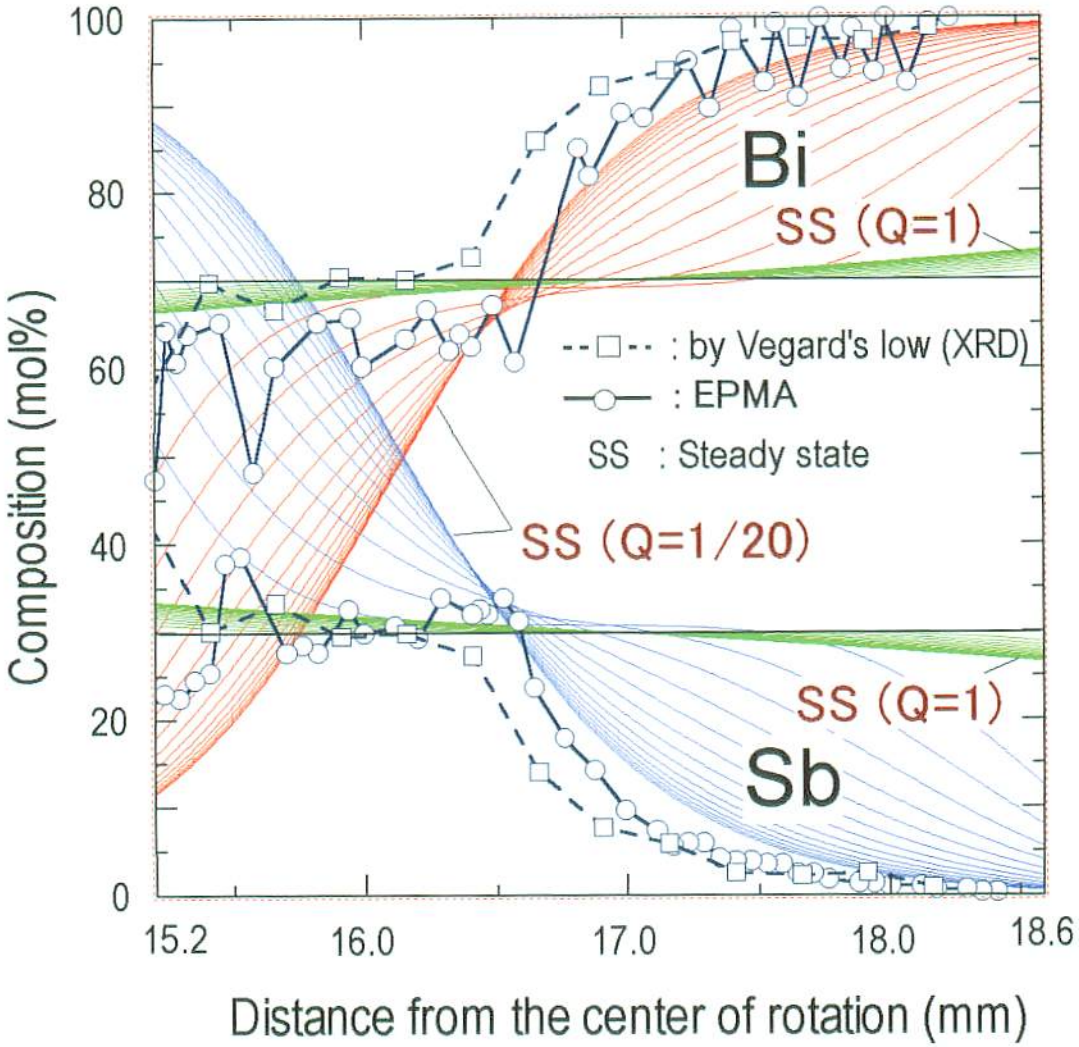

Fig.2-5 Result of the simulation of sedimentation process for atoms in Bi-Sb system together with the experimental result. (finite energy range)

CHAPTER 3

Production of the advanced high-temperature ultracentrifuge.

3-1. Introduction

To study the sedimentation of atoms or crystal chemical instability in solids under a strong acceleration field, Mashimo *et al.* developed an ultracentrifuge apparatus in Kumamoto University in 1996 [1]. The apparatus can generate an acceleration field of over 10^6 g for long time duration at high temperatures. Figure 3-1 is the photograph of the ultracentrifuge and the specifications. Figure 3-2-a is the photograph of the rotors that has outer diameter of 46 mm and the capsules for the experiment. They are made of Ti alloy and the maximum radius of the sample is 18.6mm with the capsule that has an inner diameter of 3 mm and a depth of 13.5 mm. The image of the rotation is shown in figure 3-2-b. Mega gravity of 10^6 g on the sample is to be accomplished in the rotational speed of 219,200 rev.min^{-1} with the rotor and capsule. The maximum rotational speed of the rotor have ever been recorded is 240,000 rev.min^{-1}(1,200,000g very short time). 225,000 rev.min^{-1}(1,005,000g) is the maximum rotational speed for performing the experiment in safely for long time duration.

However, the gravitational field, energy range and sample scale achieved by this apparatus were very limited, because the small rotor (46 mm in outer diameter) with center bore was used in air atmosphere by a hot air turbine motor. The temperature of sample was also limited to about 300℃ due to the hot air heating method on this apparatus. In addition, the stabilities in rotational speed and temperature were not so good with the ripples of about 5 % and 5 degrees, respectively.

In this study, we newly produced an ultracentrifuge apparatus in Japan Atomic Energy Research Institute (*JAERI*), which could generate strong gravitational field up to over 1,000,000 g in a wide temperature range up to over 500℃ with high stability controls, to expand the investigation variety in materials and phenomena.

3-2. Apparatus

The schematic layout of the ultracentrifuge apparatus is shown in figure 3-3. The setup mainly consists of an air turbine motor, a sample rotor, a vacuum chamber and a controller. The air turbine motor of the model 2100 provided by *Maruwa Electronic Inc.* consists of two 32 mm-diam turbine wheels made of aluminum alloy, a spindle made of stainless steel, and two ceramic ball bearings (P/N 1119C). Two turbine wheels are driven by compressed air (up to 4 kg/cm^2) supplied by a screw compressor through an electromagnetic air control valve (1800-N-P) allowing the air flow to be precisely controlled. By changing the torques for two turbine wheels which can be driven at opposite direction each other, the rotational speed can be precisely controlled. The dumper section is set at the down side of the turbine wheels to suppress the vibration of rotor for high stability. Figure 3-4 shows a schematic around the dumper section and rotor. The dumper section consists of two dumper bushings (upper and lower bushings). The upper one is constructed by the inner (1) and outer (2) bushings (double structure) made of different kinds of metals to decrease the friction velocities of the bushing with the spindle and dumper for the further high speed rotation, as shown in figure 3-4. The rotor chamber is vacuumed by a rotary pump to less than 10^{-2} torr. The turbine motor and the rotor are connected by a 4.77mm-diam spindle, and are separated by an oil seal (NO. 3114) made of rubber (Viton), which support vacuum in the chamber. The rotational speed and the vibration are measured by an electromagnetic pickup. The motor is capable of rotating the rotor with a diameter up to 160 mm to a rotational speed up to 200,000 rpm in a vacuum, but, the rotational speed is limited mainly by the strength of the rotor. The present apparatus is equipped with safety circuits.

Figure 3-5 shows a photograph of the rotor with an outer diameter of 70 mm and sample capsules. The rotor has not a center bore, but has a shallow hole for setting at the spindle by using screws. We can raise the maximum rotational speed or the scale of rotor, because the ultracentrifuge-induced stresses generated in non-bored rotor are remarkably smaller than those in bored rotor. The rotor is made of titanium alloy (Ti-6Al-4V) or iron-nickel alloy (Inconel 718) for the experiments at temperature of up to or higher than about 400°C, respectively. Six sample capsules with an inner diameter of 5 mm and a depth of about 20 mm inserted at 30° from the spindle axis at

two symmetrical sides of the rotor. The dynamic balancing of the rotor is carefully set up within a residual unbalance value of 0.4g·mm.

The rotor can be heated by a radiant heating in a vacuum. The radiation plate made of pure aluminum or carbon graphite with an inner diameter of 180 mm is heated by joule heating or radio-frequency heating to achieve the final rotor temperature of up to about 250℃ or >500℃, respectively. The rotor temperature is measured by infrared radiation thermometers through a ZnS window, and is controlled by the PID control. Figure 3-6 shows an example of the temperature control data (temperatures of the sample, and rotor together with one of the pure aluminum radiation plate), when the rotor was stopped, and the final setting temperature of the rotor was 200℃. The radiation plate was heated to a maximum of about 460℃ at about 1.8 hours by the joule heating. The temperatures of the rotor and further the sample followed it, and the one of the sample finally reached to the setting temperature (200℃) at about 3 hour. We confirmed that the rotor could be heated to >500℃ using a carbon graphite radiation plate combined with radio-frequency heating, as shown in figure 3-7. Figure 3-8 shows the photographs of the main part, and the heater unit and dummy rotor of the present apparatus.

3-3. Procedure and Performance

Ultracentrifuge experiments were performed to determine the performance of the present apparatus by using a 70 mm-diameter rotor made of titanium alloy. Figure 3-9 shows the typical rotation data (rotational speed, rotor temperature and vibration) of a long-time and high-temperature ultracentrifuge experiment (155,000 rpm, 150°C, 100 hours), where the maximum gravitational field at sample was 820,000 G at 30.5 mm in radius. The vibration value of the rotor was within 23 μm for 100 hours. The rotational speed and the sample temperature were remarkably stable with the ripples of <0.05 % and <1 degree, respectively, for 100 hours.

The ultracentrifuge experiments are summarized in Table 3-1.

Table 3-1 Summary of the ultracentrifuge experiments

No	Rotor material	Rotor Diameter (mm)	Rotational speed[a] (rev. min^{-1})	Maximum vibration (μm)	Maximum acceleration(radious) (g)	Sample temperature[b] (°C)	Potential energy[c]	Time Duration (h)
1	Ti-6Al-4V	70	170,000	16	986,300 (30.5 mm)	room temp.	1.6	24
2	Ti-6Al-4V	70	190,000	20	1,232,100 (30.5 mm)	room temp.	2.0	very short
3	Ti-6Al-4V	70	150,000	11	767,900 (30.5 mm)	room temp.	1.3	very short
4	Ti-6Al-4V	70	155,000	23	820,000 (30.5 mm)	150	1.3	100
5	Ti-6Al-4V	70	170,000	37	986,300 (30.5 mm)	130	1.6	100
6	Ti-6Al-4V	80	170,000	50	1,152,900 (35.8 mm)	room temp.	2.2	very short
7	Ti-6Al-4V	80	155,000	16	957,100 (35.8 mm)	75	1.8	24
8	Ti-6Al-4V	80	160,000	20	1,026,100 (35.8 mm)	220	2.0	100
9	Ti-6Al-4V	80	160,000	20	1,026,100 (35.8 mm)	260	2.0	100

[a] ripple: <0.05 %

[b] ripple: <1 degree

[c] The potential energies are represented by the competitive rates with that of the Kumamoto University one as a standard (Rotation condition: rotational speed=220,000 rpm, radius=18.6 mm)

The maximum rotational speed of 190,000 rpm was recorded despite for a short time, where the maximum gravitational field at sample was over 1,200,000 G. The high-temperature and long-time ultracentrifuge experiments by using the 70 and 80 mm-diameter rotors made of titanium alloys (170,000rpm - 130°C - 100 hours, and 160,000rpm - 220°C - 100 hours, respectively), where the maximum acceleration field were 986,300 and 1,026,100g, respectively, were also successfully performed as shown in Table 3-1. It is important to raise sample temperature for the expansion of investigated variety of materials and phenomena. We confirmed the rotation of

150,000 rpm using the Inconel 718 rotor, which will be used for the further high-temperature experiments of >400°C. In order to realize large composition change of element or isotope by sedimentation of atoms in solids or liquids, we necessitate a large value of potential energy rather than gravitational field. The final composition profiles are represented as a function of the difference in potential energy between atoms ($\triangle E = \triangle M r^2 \omega^2 / 2RT$ ($\triangle M$, R, T, ω and r are the difference in atomic weight, the gas constant, absolute temperature, angular rate, and radius, respectively) according to the self-consistent theory of the sedimentation of atoms in condensed matter[2, 3]. The maximum potential energy achieved by the present apparatus increased by a factor of even >2 compared with that of the Kumamoto University one[1]. The sample volume also increased by a factor of >4 compared with the Kumamoto University one. The comparison of the performance between the apparatuses of Kumamoto University and the present one (*JAERI*) is summarized in Table 3-2.

Table 3-2 Comparison of the performance between the ultracentrifuge apparatuses of Kumamoto University and JAERI (present one).

Apparatus	Diameter of rotor (mm)	Sample size (mm)	Maximum Rotational speed[a] (rev. min^{-1})	Maximum Acceleration (g)	Sample temperature[b] (°C)	Potential energy[c]
Kumamoto Univ.	46	3ϕ10L	220,000	1,000,000	80~300	1
JAERI (present one)	70-160	>5ϕ15L	200,000	>1,200,000	-50~500	>2

[a] The potential energy of the Kumamoto University one is set by 1 as a standard (Rotation condition: rotational speed=220,000 rpm, radius=18.6 mm).

The maximum gravitational field can be increased more by improvement of the design and material of rotor, etc. The sample temperature can be increased to >500°C by a radiant heat combined with the radio-frequency heating. The potential energy and sample volume can be also increased by the factors of larger than 3 and 10, respectively, compared with those of the Kumamoto University one by using the rotor with a diameter of >80 mm. We are now adding a cooling system by a radiant cooling method and gas cooling method (using He gas) with this apparatus. It is expected that the investigation materials and phenomena under an ultra-strong gravitational field will be expanded much by using the present apparatus.

REFERENCES

[1] T. Mashimo, S. Okazaki, S. Shibasaki, Rev. Sci. Instr. 67, 3170 (1996).

[2] T. Mashimo, Phys. Rev. A 38, 4149 (1988).

[3] T. Mashimo, Phil. Mag. A 70, 739 (1994).

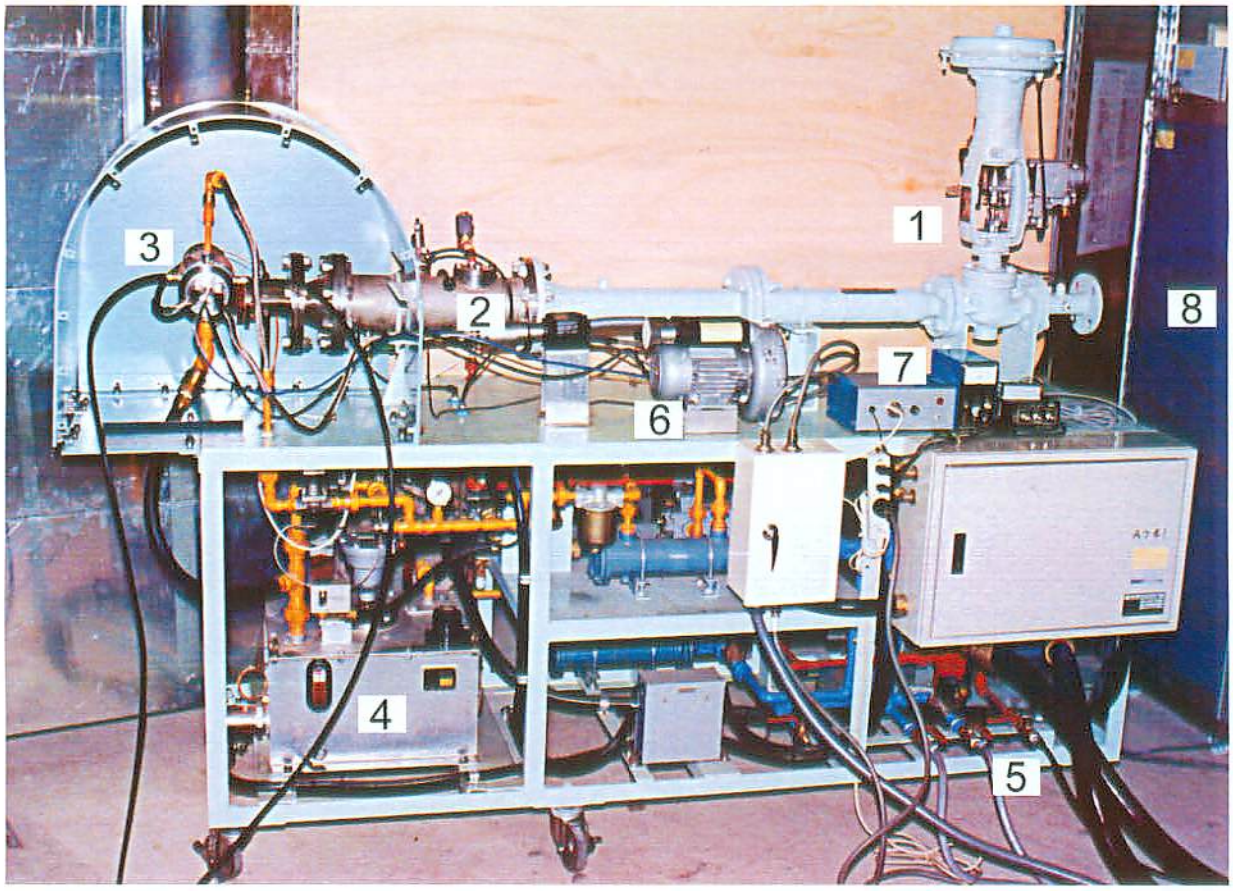

1. air control valve
2. combustion tube
3. turbine motor
4. oil tank
5. fuel (kerosene)
6. air heater
7. laser rotation sensor
8. air compressor

specifications;

rotor diameter:	46 mm
rotation rate:	>220,000 rpm
acceleration:	>1,000,000 g
temperature:	>250 °C

stabirity;

rotation ripple:	5 %
temperature ripple:	5 degrees

Fig. 3-1 Photograph of the main part of the ultracentrifuge [1]

a) Ti alloy rotor, cupsules and centrifuged sample

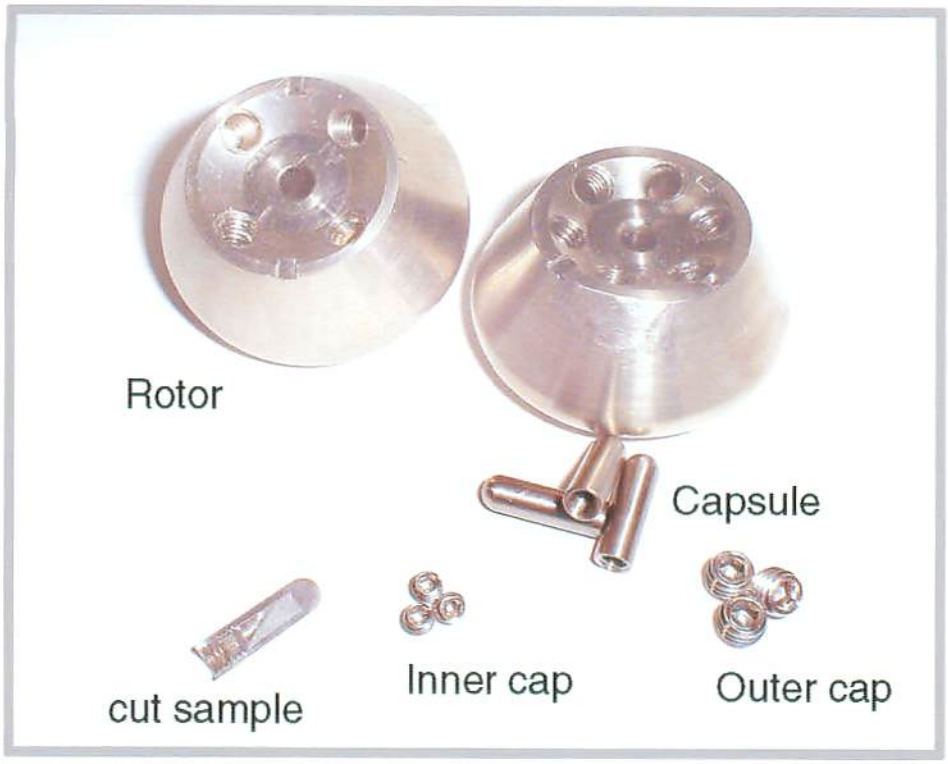

b) Image of the centrifugation

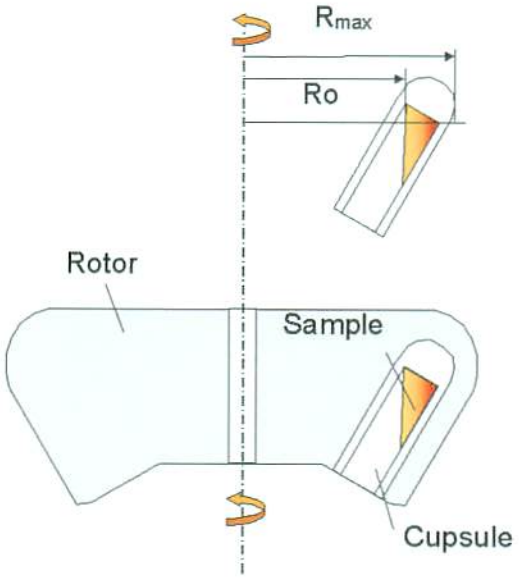

Fig3-2. Rotors and capsules for the ultracentrifuge of Kumamoto-Univ. one.

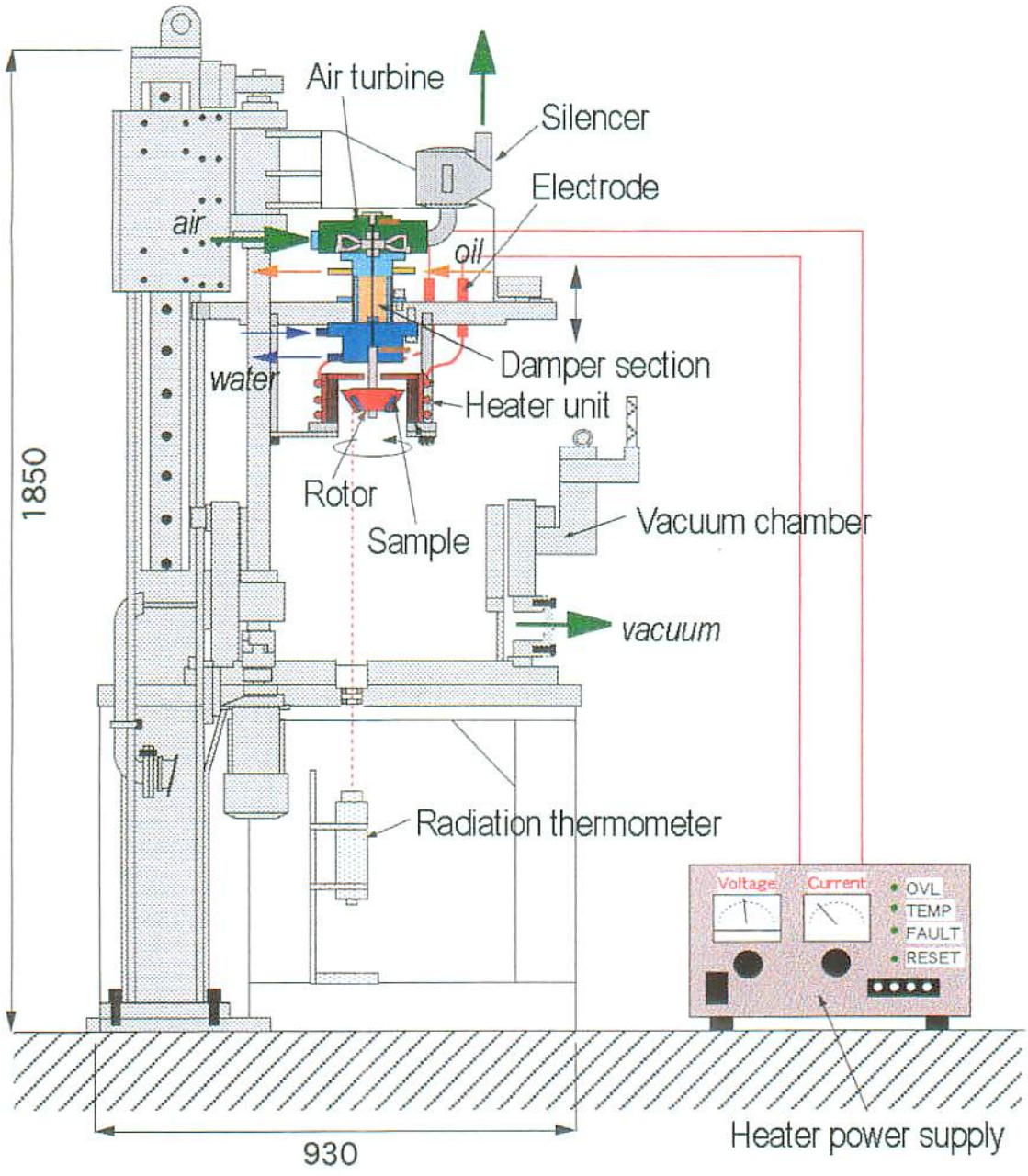

Fig. 3-3 Schematic layout of the ultracentrifuge

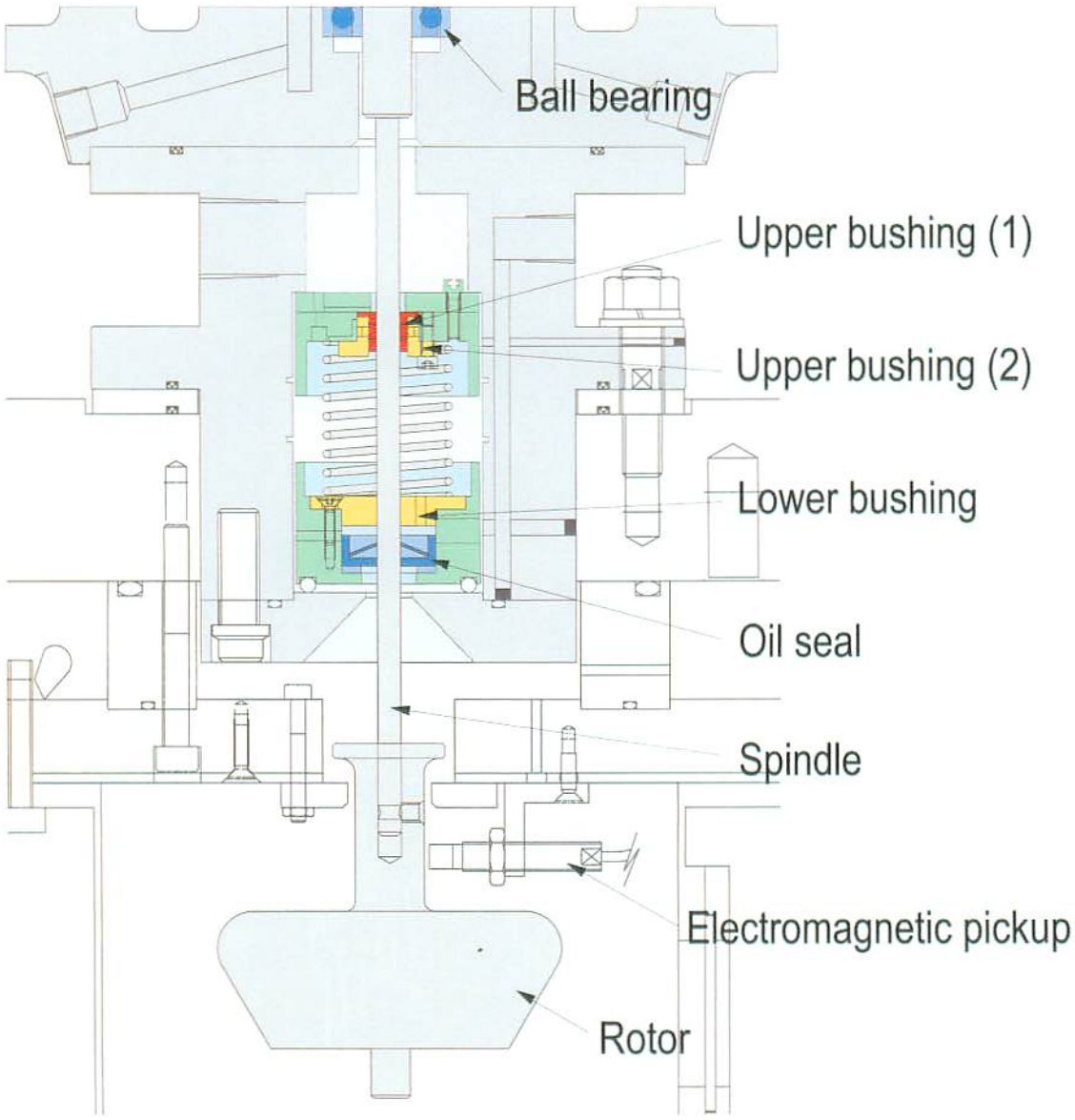

Fig. 3-4 Schematic around the dumper section and rotor

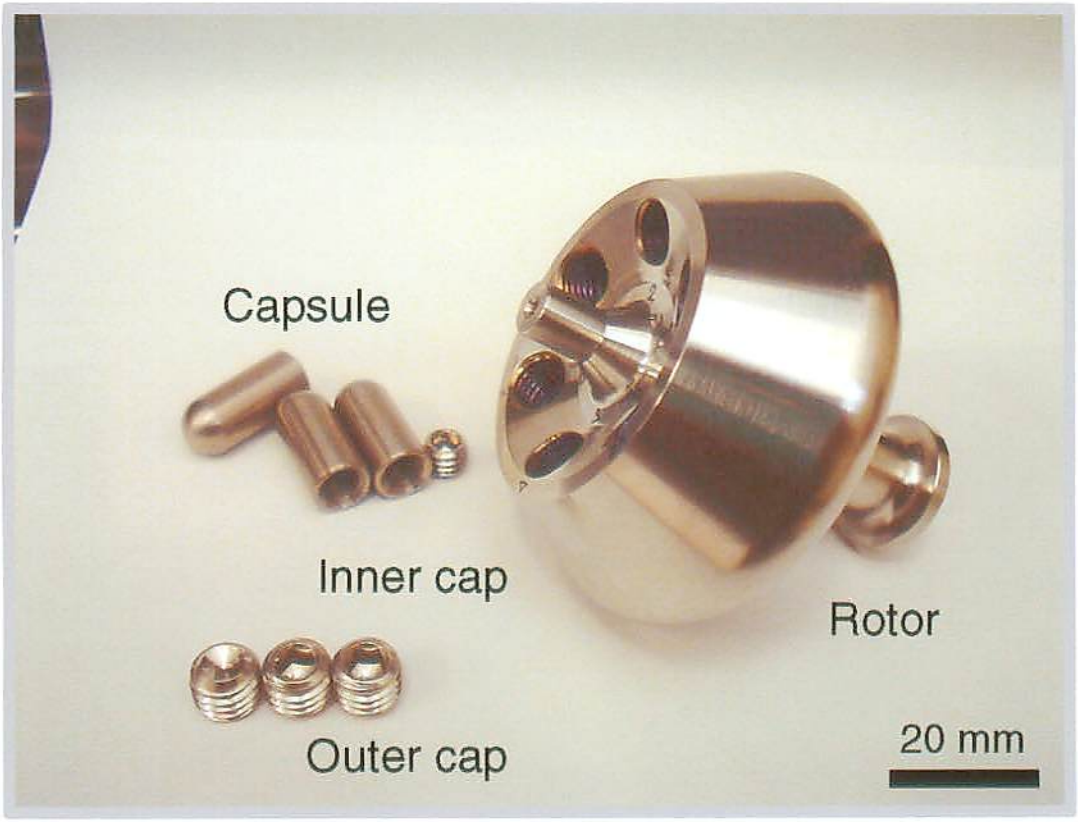

Fig. 3-5 Photograph of the titanium alloy rotor (70 mm in outer diameter) and sample capsules.

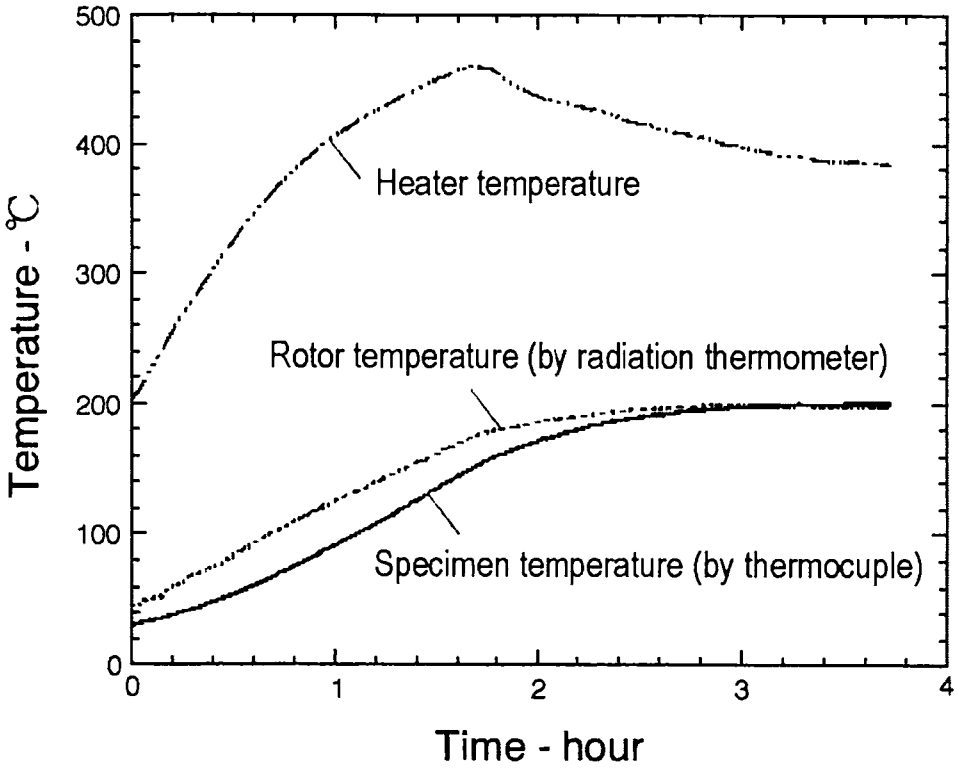

Fig. 3-6 Temperature control data of the rotor measured by a radiation thermometer and of sample measured by a thermocouple, together with that of a pure aluminum radiationplate heated by the joule heating, when the final setting temperature of sample was 200 ℃ .

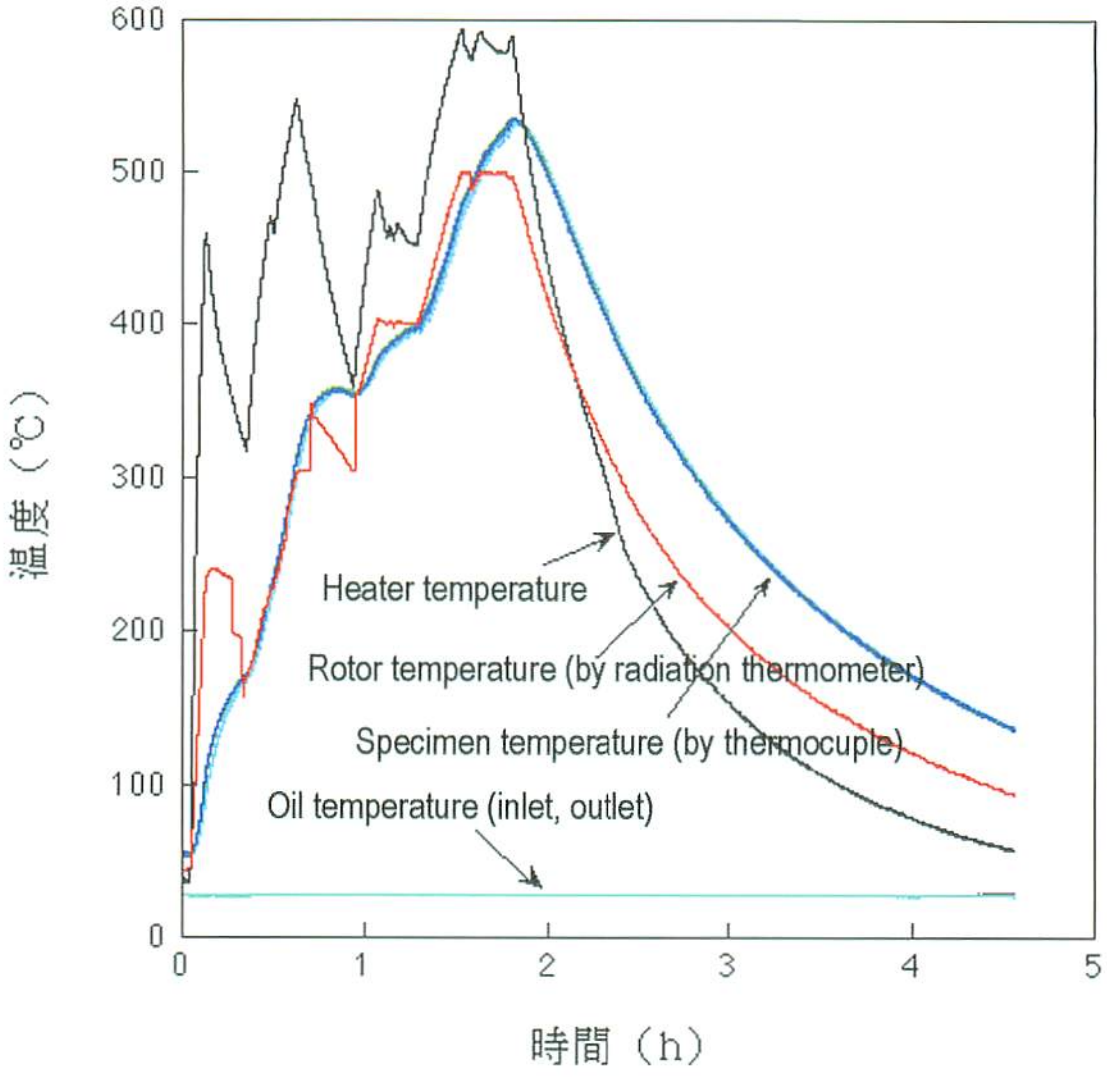

Fig. 3-7 Temperature records of sample measured by a thermocouple, together with the that of a carbon graphite radiation plate heated by the radio-frequency heating, when the maximum temperature of sample was >500℃.

a) Main part

b) Heater unit and dummy rotor

Fig. 3-8 Photographs of the main part (a), and the heater unit and dummy rotor (b)

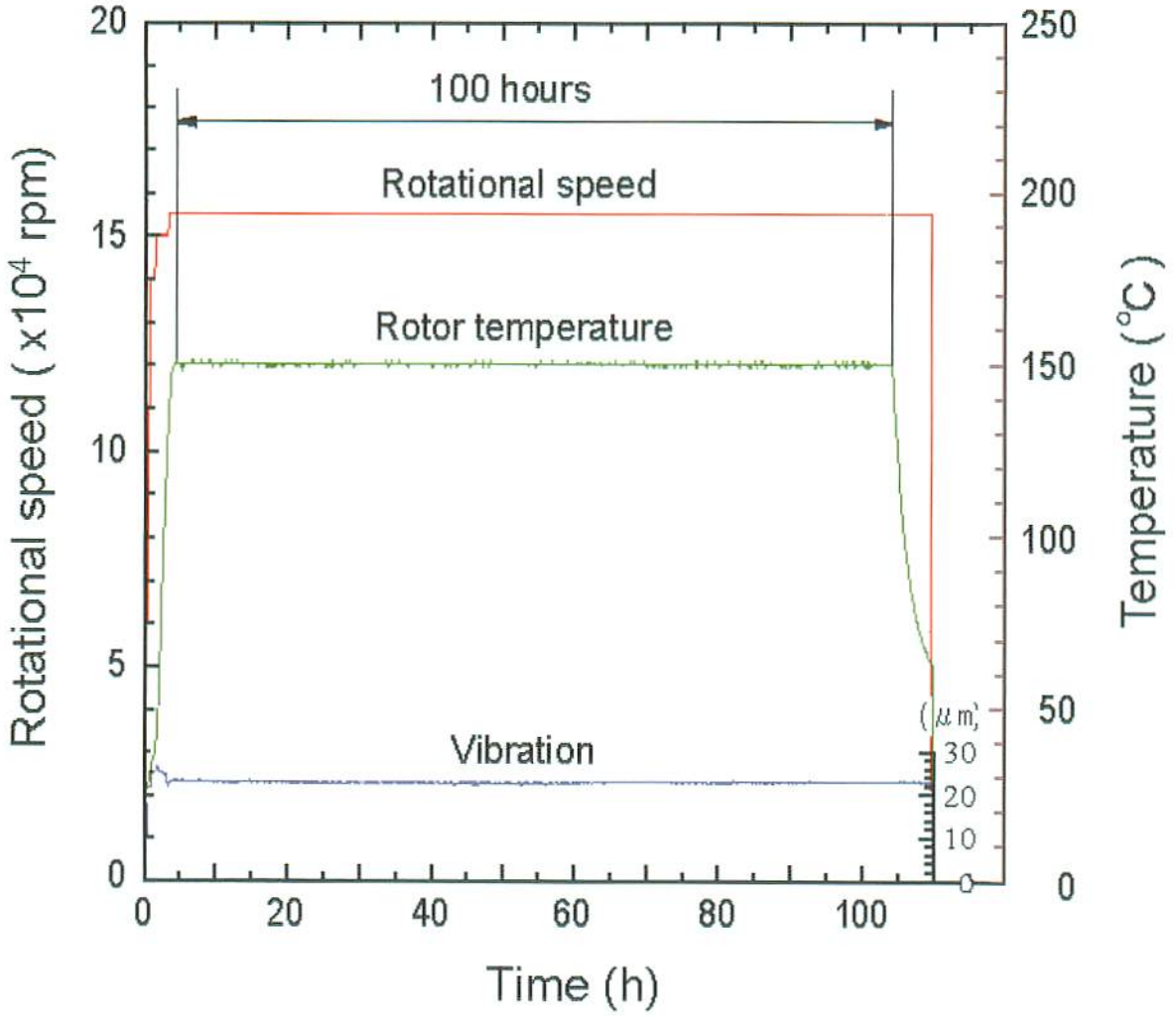

Fig. 3-9 Driving data of the long-time and high-temperature ultracentrifuge experiment (155,000 rpm, 150 °C , 100 hours)

CHAPTER 4

Sedimentation of atoms in all-proportional miscible alloy under strong gravitational field.

4-1. Introduction

In the *Chapter 4*, we arrange and discuss the experimental results of ultracentrifuge experiment on all-proportional miscible system. The Bi-Sb alloy and Se-Te alloy was chosen for ultracentrifuge experiment because they are all-proportional miscible system and their melting temperature satisfy the performance of maximum-temperature limit for the apparatus. For the Bi-Sb system, Mashimo *et al.* already presented a well-worked study under strong gravitational field using the ultracentrifuge of Kumamoto University one in 1997[1, 2]. This previous experimental result is summarized in this *Chapter 1, section 1-3-3)*. This work revealed the phenomenon that an atomic-scale graded structure was formed by the sedimentation of atoms in all-proportional miscible alloy under strong gravitational field. So, in this study, we just have composition analysis on the centrifuged sample of the Bi-Sb and Se-Te system that was performed using new ultracentrifuge of *JAERI* one, and discuss the sedimentation process and mechanism comparing with simulation and using the phase diagram, as these systems are the all-proportional miscible system, and it is convenient to examine the sedimentation process and mechanism comparing with the simulation.

4-2. About the Bi-Sb system and Se-Te system:

Bi-Sb system[3]:

Bi-Sb system is the all-proportional miscible system. Though the uniform solid solution had not ever been gotten even in slowly cooled alloys or annealed alloy because of the wide solidification interval caused by the strong coring. The property that the system forms the continuous series of solid solution was confirmed by the founding the property that the lattice parameters vary linearly with composition rate.

The crystal structure is Trigonal/Rhombohedral A7 (A7: type As, $D_{3d}^5 - R\bar{3}m$). The phase diagram is shown in figure 4-1.

Se-Te system[4]:

Se-Te system is also the all-proportional miscible system. It was confirmed by thermal investigation and XRD analysis that two elements form uninterrupted series of solid solutions. As the solidification interval is very small, about 10℃ or less, it is easy to form the uniform state. The crystal structure is Hexagonal A8 (A8: type Se, $D_3^4 - P3_121$). The phase diagram is shown in figure 4-2.

4-3. Experimental Procedures

a) Stating sample:

Bi-Sb system:

The Bi-Sb (70:30 in mol%, ≒80:20 in wt. %) system alloy lump was prepared by melting 16.0g-Sb and 4.0g-Bi shots in the Pyrex test tube at 639℃ above the melting temperature of both elements (Bi:271.4℃, Sb:630.7℃) for 30 minutes under a vacuum atmosphere. The purity values of Bi and Sb shots were both 5N. The lump shaped sample was cut into column shaped pieces with a diameter of 4.5 mm and height of 5.5 mm, and was set into Ti alloy capsules with an inner diameter of 5 mm. The Bi-Sb alloy is comparatively fragile at room temperature, and it is considered that the sample may be break just starting centrifugation ought to the clearance between capsule and the sample. So, to avoid sample crush into small pieces in starting centrifugation at room temperature, the clearance between capsule and the sample was taken away by the following method. The sample temperature was elevated to 260 ℃ of experimental temperature (The melting temperature of the starting sample is 300 ℃) and kept for 15 minutes. After that, the sample was pressed to fit the capsule with SUS 304 rod using hand press tool. These processes were done under an Ar atmosphere. The starting sample consisted of Sb-rich and Bi-rich dendrite-shaped clusters the sizes of which were several tens to several hundreds of μm, and which were randomly dispersed.

Se-Te system:

The Se-Te (70:30 in mol%, ≒59:41 in wt.%) system alloy lump was prepared by melting 5.9g-Se and 4.1g-Te shots in the Pyrex test tube at 639℃ above the melting temperature of both elements (Se:220.2℃, Te: 449.8℃) for 30 minutes under an Ar atmosphere. The purity values of Se and Te shots were both 4N. The uniformity of the sample was confirmed by the EPMA analysis. The lump was crushed into powder and was again melted at about 430℃under vacuum in the hollow grass rod with inner diameter of just 4.0 mm to get the sample with the diameter for several minutes till melt the sample. The sample was cut into column shaped pieces height of 5.0 mm, and was set into SUS 304 capsules with an inner diameter of 4 mm. The clearance between capsule and the sample was small enough to avoid sample crush into small pieces in starting centrifugation at room temperature.

b) Equipments for the experiments:

The Ultracentrifuge experiment for both samples was simultaneously performed using the ultracentrifuge of *JAERI* one. The specification of the apparatus was introduced in *Chapter 3.* A rotor that has outer diameter of 80 mm was used for the experiment. It was made of Ti alloy and the maximum radius of the sample is 35.82mm with the Ti alloy capsule.

c) Analysis and Observation:

The composition analysis was carried out using Electron Probe Micro Analyzer (EPMA, JXA-8900R, JEOL Ltd., Tokyo, Japan).

4-4. Ultracentrifuge experiment

4-4-1. Experimental conditions:

The ultracentrifuge experiment was performed under the condition that was shown in Table 4-2.

Table 4-2 Experimental conditions.

Stating sample	Rotation rate (rev. min^{-1})	Maximum acceleration (g)	Temperature (℃)	Time (h)
Bi:Sb=70:30at%, (Rhombohedral A7) Se:Te=70:30at%, (Hexagonal A8)	160,0000	1.02×10^6	260	100

It took 5 hours to reach aiming experimental conditions (temperature, rotation rate), and also it took 10 hour to cool down the sample temperature to 70 ℃ before release the gravity. These times were not counted in the experiment. Figure 4-3 is the operating records of the ultracentrifuge.

4-4-2. Experimental results and discussions of Bi-Sb system:

Figure 4-4 shows the microscope photograph at the polished surface cut at a plane containing the rotation axis of the centrifuged sample. The surface was finished with 1/4 μm diamond paste. In the strong gravitational field region, large and long crystals oriented in the direction of gravity can be seen. The sizes of the crystal grains were several mm length and several hundreds of μm width. This crystal growth might be related to a strong gravitational field.

Figure 4-5-a) shows the EPMA mapping photographs of the sample. The composition profiles were obtained along a straight line between h-h'. The Bi content continuously increased in the direction of gravity (arrow direction in the figure) from about 60 to 100 wt.%, and conversely, the Sb content greatly decreased from about 45 to almost 0 wt.%, even in crystal grains. The large composition gradients observed even

in single-crystal particles (refer Fig.4-4). This showed that the graded structure was continuous in atomic scale. Figure 4-5-b) is the peaks of the micro area XRD patterns for every measurement points. The peaks sift gradually to high angle with the Sb content become higher. This showed the lattice constants change to small value with the Sb content sifts higher. This tendency was the other proof that the graded structure was continuous in atomic scale and the graded structure was formed by the sedimentation of atoms.

4-4-3. Experimental results and discussions of Se-Te system:

Figure 4-6 shows the microscope photograph at the polished surface cut at a plane containing the rotation axis of the centrifuged sample. The surface was finished with 1/4 μm diamond paste. But, the surface was very fragile to polish and many holes can be seen in the right hand of the sample were created in the polishing process. The crystal growth was seen in the counter side of strong gravitational field region. In this region, the crystal grains were several mm length and several hundreds of μm width. This crystal growth might be related to a strong gravitational field.

Figure 4-7-a) shows the EPMA mapping photographs of the sample. The composition profiles were obtained along a straight line between h-h'. The Te content continuously increased in the direction of gravity (arrow direction in the figure) from almost 0 to 70 wt.% through the maximal of 75 wt.%, and conversely, the Se content greatly decreased from almost 100 to about 35 wt.% also having minimal of 30 wt.%. These smooth and large composition gradients observed even in single-crystal particles (refer Fig. 4-6). This showed that the graded structure was continuous in atomic scale. Figure 4-7-b) is the peaks of the micro area XRD patterns for every measurement points. The peaks sift gradually to high angle with the Se content become higher. This showed the lattice constants change to small value with the Se content sifts higher. The tendency was the other proof that the graded structure was continuous in atomic scale and the graded structure was formed by the sedimentation of atoms.

4-5. Simulation of sedimentation process for atoms

The simulation of sedimentation process for atoms in Bi-Sb system and Se-Te system were performed using self-consistent theory to discuss the sedimentation mechanism[5,6]. The simulation procedures were presented in *Chapter 2*. Performing the simulation program, we can simulate the change of the composition rate from starting state to steady state for binary system under gravitational field, and also we can estimate the ratio of diffusion coefficient for sedimentation to that for usual diffusion by the internal chemical potential.

a) Bi-Sb system:

The simulation conditions were summarized in Table 4-3.

Table 4-3 Simulation conditions.

Stating state	Rotation rate (rev. min^{-1})	Maximum acceleration (g)	Temperature (°C)	Q ($Q=D_1/D_2$)
Bi:Sb=70:30at% (uniform)	160,000	$1.02x10^6$	260	1
Bi:Sb=70:30at% (uniform)	160,000	$1.02 x10^6$	260	1/20
Bi:Sb=70:30at% (uniform)	160,000	$1.02 x10^6$	260	1/30

These conditions were almost the same as the experimental ones. Here, Q was the ratio of the diffusion coefficient for sedimentation (D_2) to that for usual diffusion by the internal chemical potential (D_1), and it was described as $Q=D_1/D_2=1+ln\ (\gamma)/\ ln(c)$ by using the following chemical potential representation: $\mu=\mu_0(T)+kTln(\gamma c)$, where γ was the activity coefficient[6, 7]. In addition, we assumed that the diffusion coefficients for the two components were equal and constant as the simulation parameter did not measured.

Figure 4-8 shows the simulation results of the Bi-Sb (70:30 at%) system together

with the experimental result. Here, the plot in vertical axis was the composition rate, and the plot in horizontal axis was the distance from the center of rotation. The starting composition profiles were uniform in the ratio Bi:Sb=70:30 (at%). In the simulations, the calculated composition profiles gradually changed with time as shown by the slight lines in the figure, and the content of Bi increased gradually in the direction of centrifugal force, and that of Sb increased to the opposite direction. This showed that the heavy Bi atoms moved in the direction of gravity, and the light Sb atoms moved to the opposite direction with time. The composition change of both elements was notable near edges of the sample, where atoms could not move more, and gradually accumulated there by the boundary condition that fluxes of atoms were zero at edges of the sample. Finally, the changes in composition profiles converged to the respective steady states. If we assumed that the experimental data was almost at steady state (100h), the simulation at Q=1/30 was rather comparable to the experimental result. It means that the diffusion coefficient for sedimentation was at least 30 times larger than that of usual diffusion.

It was found that the diffusion coefficient for sedimentation in the Bi-Sb system was much larger than that for usual diffusion. Under the strong gravitational field, the Bi-Sb alloy sample was also exposed to high pressure of around 0.4GPa. Under high-pressure field, the number of vacancy decrease and the diffusion coefficient become small. So, it was suggested that the diffusion mechanism of the sedimentation in this system was different from the vacancy mechanism.

b) Se-Te system:

The simulation conditions were summarized in Table 4-4.

Table 4-4 Simulation conditions.

Stating state	Rotation rate (rev. min^{-1})	Maximum acceleration (g)	Temperature (°C)	Q ($Q=D_1/D_2$)
Se:Te=70:30at%	160,000	1.02×10^6	260	1

(uniform) Se:Te=70:30at% (uniform)	160,000	1.02×10^6	260	1/10
Se:Te=70:30at% (uniform)	160,000	1.02×10^6	260	1/20

These conditions were almost the same as the experimental ones. Here, Q was the ratio of the diffusion coefficient for sedimentation (D_2) to that for usual diffusion by the internal chemical potential (D_1), and it was described as $Q=D_1/D_2=1+ln\ (\gamma)/\ ln(c)$ by using the following chemical potential representation: $\mu=\mu_0(T)+kTln(\gamma c)$, where γ was the activity coefficient[6, 7]. In addition, we assumed that the diffusion coefficients for the two components were equal and constant as the simulation parameter did not measured.

Figure 4-9 shows the simulation results of the Se-Te (70:30 at%) system together with the experimental result. Here, the plot in vertical axis was the composition rate, and the plot in horizontal axis was the distance from the center of rotation. The starting composition profiles were uniform in the ratio Se:Te=70:30 (at%). In the simulations, the calculated composition profiles gradually changed with time as shown by the slight lines in the figure, and the content of Te increased gradually in the direction of centrifugal force, and that of Se increased to the opposite direction. This showed that the heavy Te atoms moved in the direction of gravity, and the light Se atoms moved to the opposite direction with time. The composition change of both elements was notable near edges of the sample, where atoms could not move more, and gradually accumulated there by the boundary condition that fluxes of atoms were zero at edges of the sample. Finally, the changes in composition profiles converged to the respective steady states. By the way, the simulation result was not fit on the experimental result. But the Q value was at least under Q=1 because the remarkable concentration change cannot be explained by Q=1. The Q value is estimated as around Q=1/10. It means that the diffusion coefficient for sedimentation was at least 10 times larger than that of usual diffusion.

It was found that the diffusion coefficient for sedimentation in the Se-Te system was much larger than that for usual diffusion. Under the strong gravitational field, the Se-Te alloy sample was also exposed to high pressure of around 0.1GPa. Under high-pressure field, the number of vacancy decrease and the diffusion coefficient become small. So, it was suggested that the diffusion mechanism of the sedimentation in this system was different from the vacancy mechanism.

4-6. Conclusions

In this study, we performed the ultracentrifuge experiment on the Bi-Sb and Se-Te system alloy using new ultracentrifuge of *JAERI* one. We just have composition analysis on the both centrifuged sample, and discuss the sedimentation process and mechanism comparing with simulation, as it is convenient to examine the sedimentation process and mechanism comparing with the simulation on the all-proportional miscible system.

In the centrifuged Bi-Sb alloy, the Bi content continuously increased in the direction of gravity (arrow direction in the figure) from about 60 to 100 wt.%, and conversely, the Sb content greatly decreased from about 45 to almost 0 wt.%, even in crystal grains.

In the centrifuged Se-Te alloy, the Te content continuously increased in the direction of gravity (arrow direction in the figure) from almost 0 to 70 wt.% through the maximal of 75 wt.%, and conversely, the Se content greatly decreased from almost 100 to about 35 wt.% also having minimal of 30 wt.%. In the both alloys, the large composition gradients observed even in single-crystal particles. This showed that the graded structure was continuous in atomic scale in both alloys and the obtained graded structures were formed by the sedimentation of substitutional solute atoms.

Also it was found that the diffusion coefficients for sedimentation in the two alloys (Bi-Sb, Se-Te alloy) were much larger than that for usual diffusion by simulations.

This simulation results indicated that the diffusion mechanism of the sedimentation in this system was different from the vacancy mechanism.

REFERENCES

[1] T. Mashimo, S. Okazaki, S. Tashiro: Jpn. J. Appl. Phys. 36 (1997) 498-500.

[2] T. Mashimo, H. Ikeda, I. Minato: J. Appl. Phys. 90 (2001) 741-744.

[3] M. Hansen and K. Anderko: *Constitution of Binary Alloys*, 2nd ed., (Genium Publishing corporation, New York, 1991) p.332-334.

[4] M. Hansen and K. Anderko: *Constitution of Binary Alloys*, 2nd ed., (Genium Publishing corporation, New York, 1991) p.1188-1189.

[5] T. Mashimo: Phys. Rev. A38 (1988) 4149-4154.

[6] T. Mashimo: Philos. Mag. A70 (1994) 739-760.

[7] M. Ono, T. Mashimo: Philos. Mag. A82 (2002) 591-600.

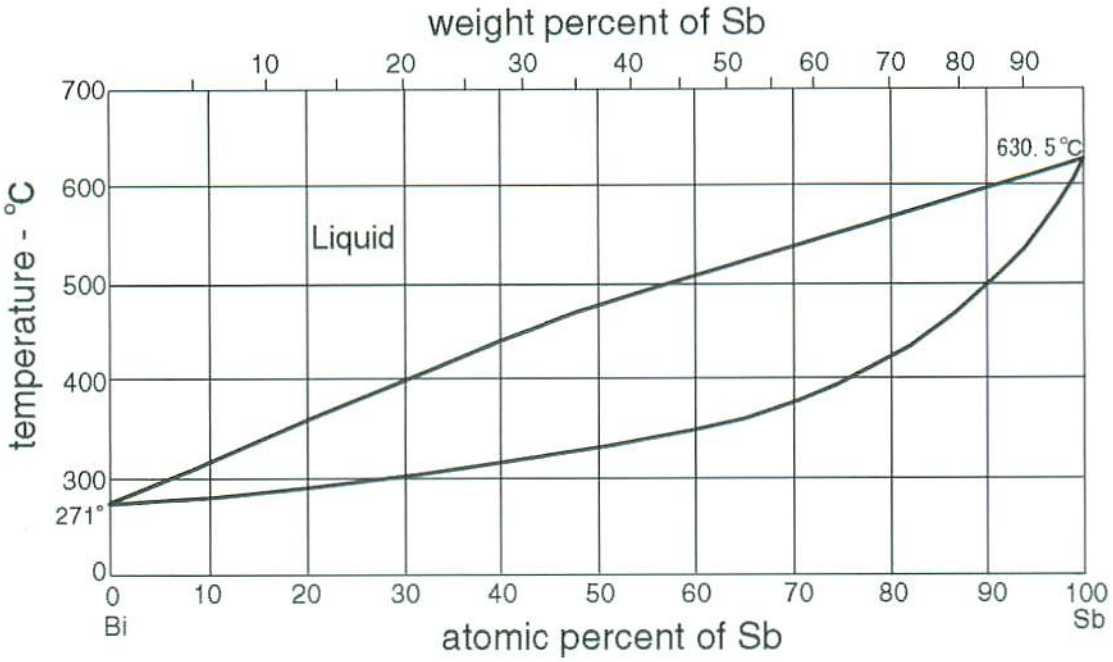

Phase Diagram of Bi-Sb system

[M. Hansen, K. Anderko; Constitution of Binary Alloys Second Edition, , 332-334(1985)]

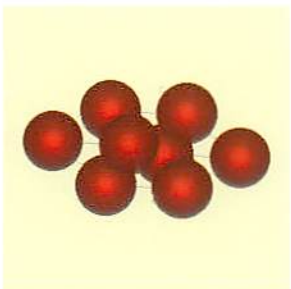

Trigonal/
Rhombohedral A7
(R-3m)

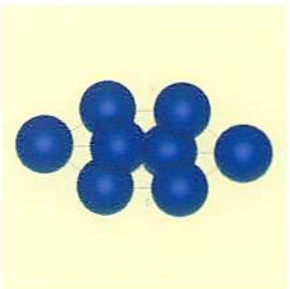

Bi:
a=0.47356 nm
α=57°14'
r=0.182 nm

Sb:
a=0.45064 nm
α=57°1'
r=0.161 nm

Crystal Structures of Bi-Sb system

Fig4-1. Phase diagram and crystal structure of Bi-Sb system

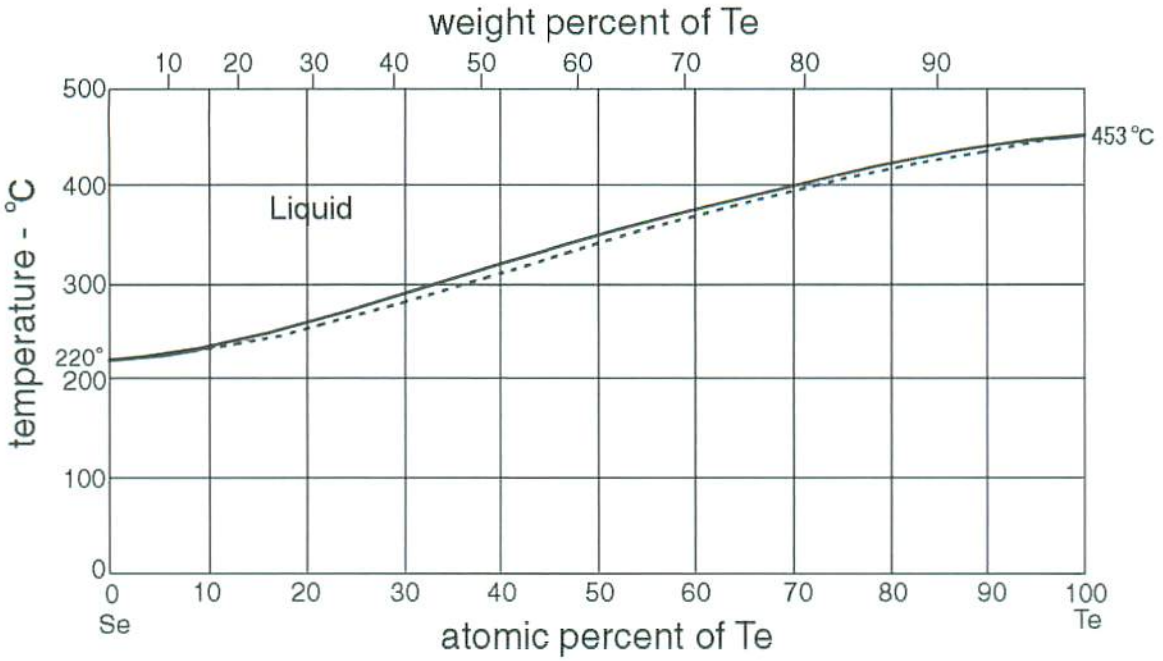

Phase Diagram of Se-Te system
[M. Hansen, K. Anderko; Constitution of Binary Alloys Second Edition, , 1188-1189(1985)]

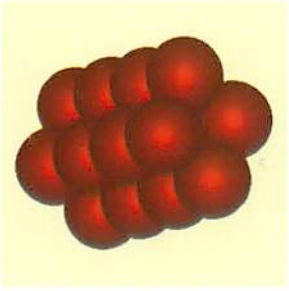

Trigonal/
Hexagonal A8
($P3_121$)

Se:
a=0.43640 nm
c=0.49594 nm
r=0.16 nm

Te:
a=0.44559 nm
c=0.59268 nm
r=0.17 nm

Crystal Structures of Se-Te system

Fig4-2. Phase diagram and crystal structure of Se-Te system

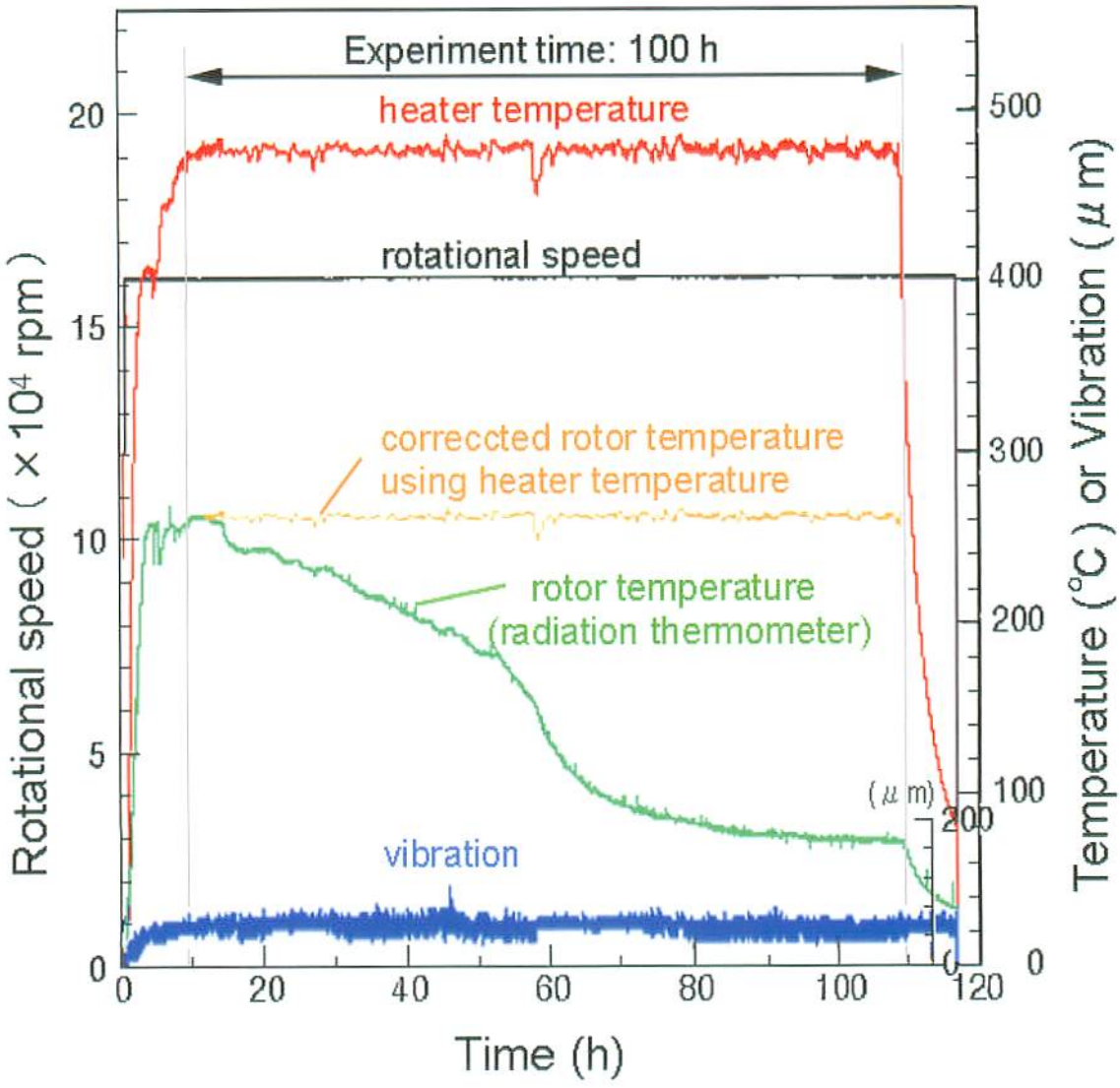

Fig.4-3 Record of ultracentrifuge experiment

(160,000rev.min^{-1} (maximum 1.02x10^{6}G), 260℃ , 100h)

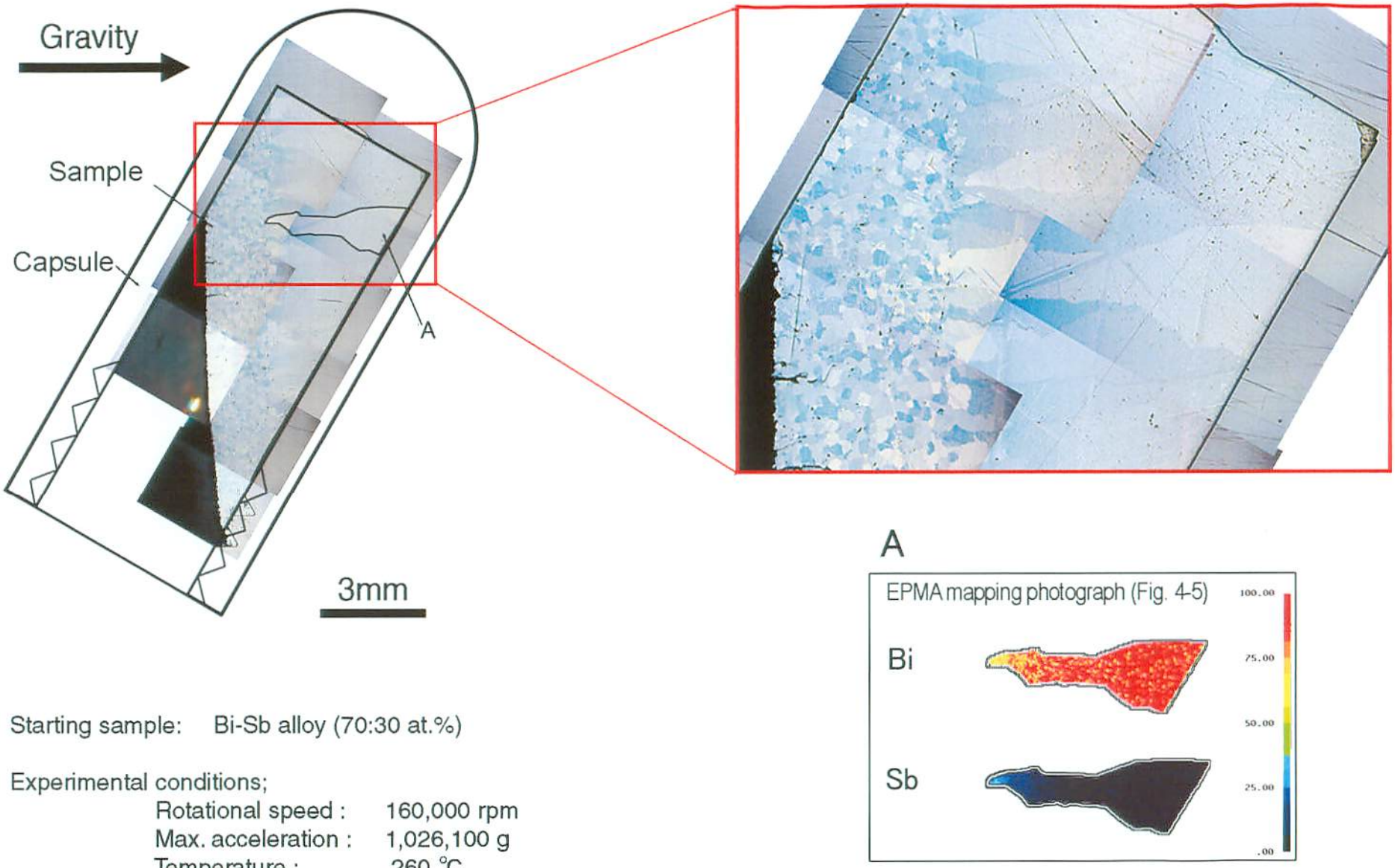

Starting sample: Bi-Sb alloy (70:30 at.%)

Experimental conditions;

Rotational speed :	160,000 rpm
Max. acceleration :	1,026,100 g
Temperature :	260 ℃
Time :	100 h

Fig. 4-4 The optical microphotograph of centrifuged Bi-Sb alloy.

a)

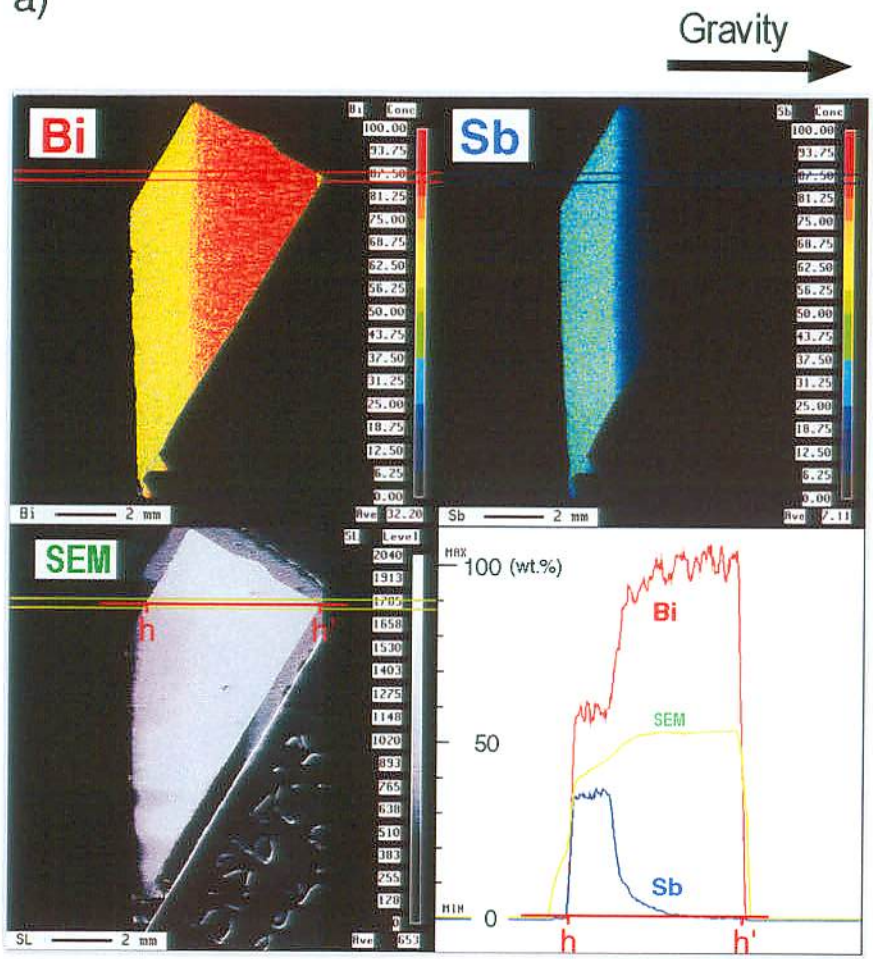

b)

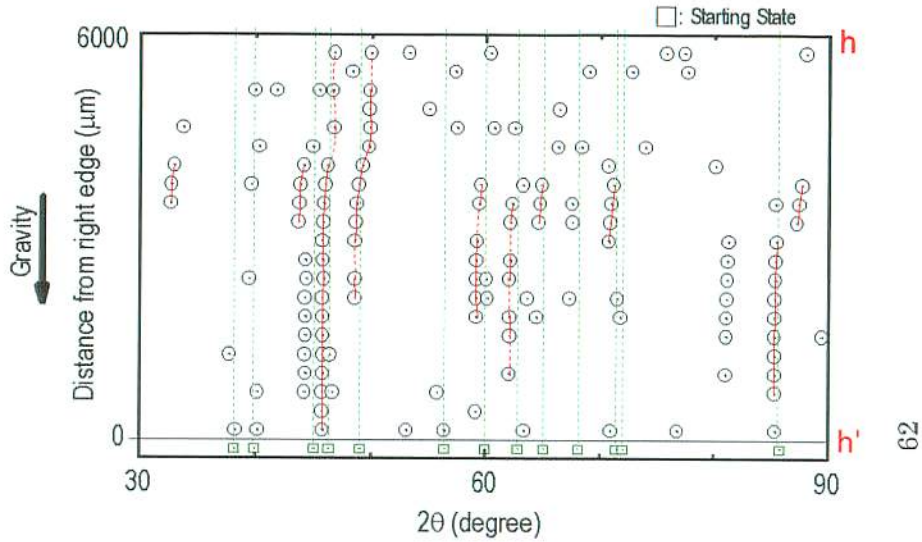

Starting sample: Bi-Sb alloy (70:30 at.%)

Experimental conditions;

rotational speed:	160,000 rpm
max. acceleration:	1,026,100 g
temperature:	260 ℃
time:	100 h

Fig. 4-5 a) EPMA mapping photograph and b) Peaks of micro area XRD pattern of centrifuged Bi-Sb alloy.

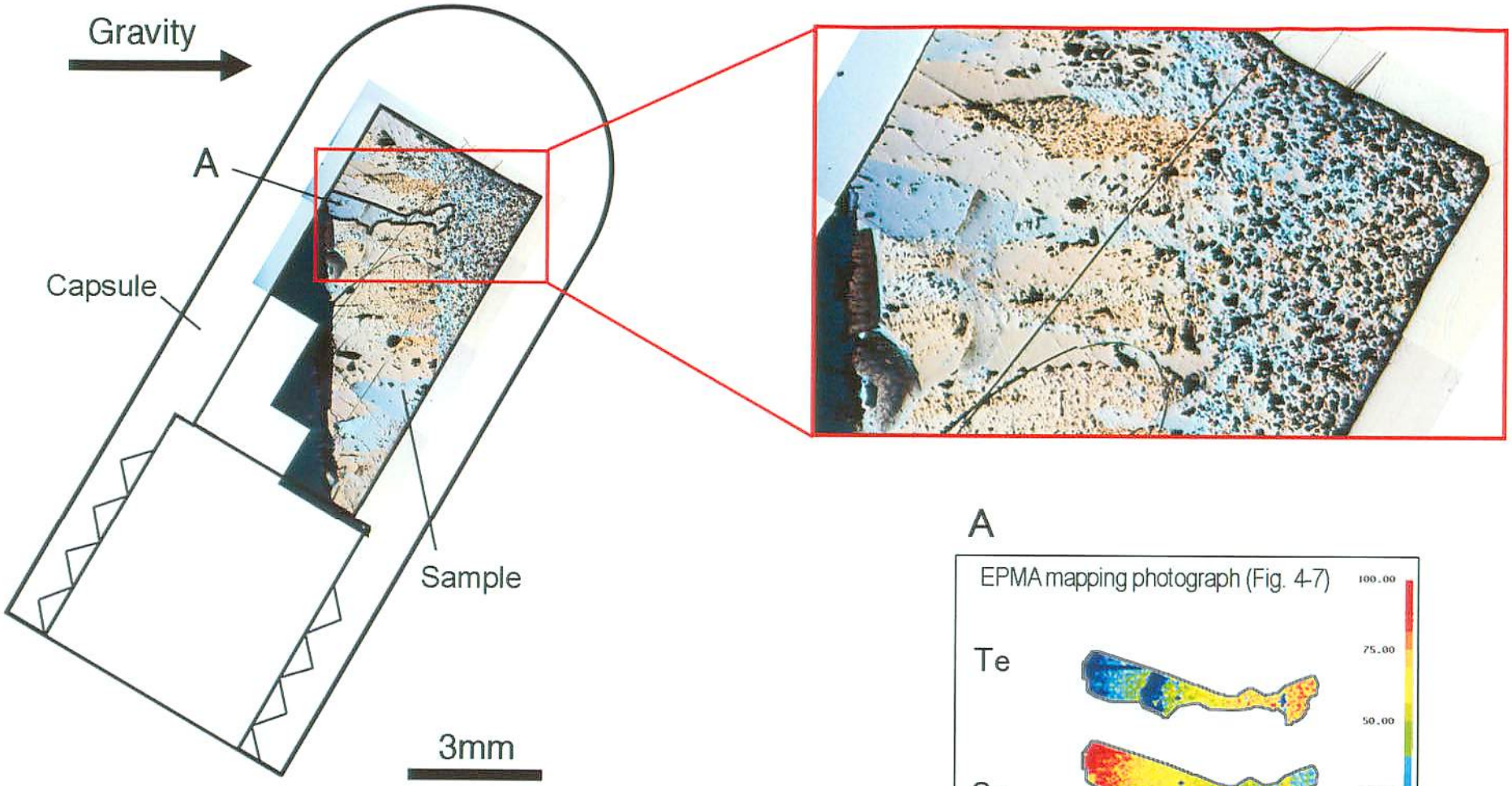

Starting sample: Se-Te alloy (70:30 at.%)
Experimental conditions;

Rotational speed :	160,000 rpm
Max. acceleration :	1,026,100 g
Temperature :	260 ℃
Time :	100 h

Fig. 4-6 The optical microphotograph of centrifuged Se-Te alloy.

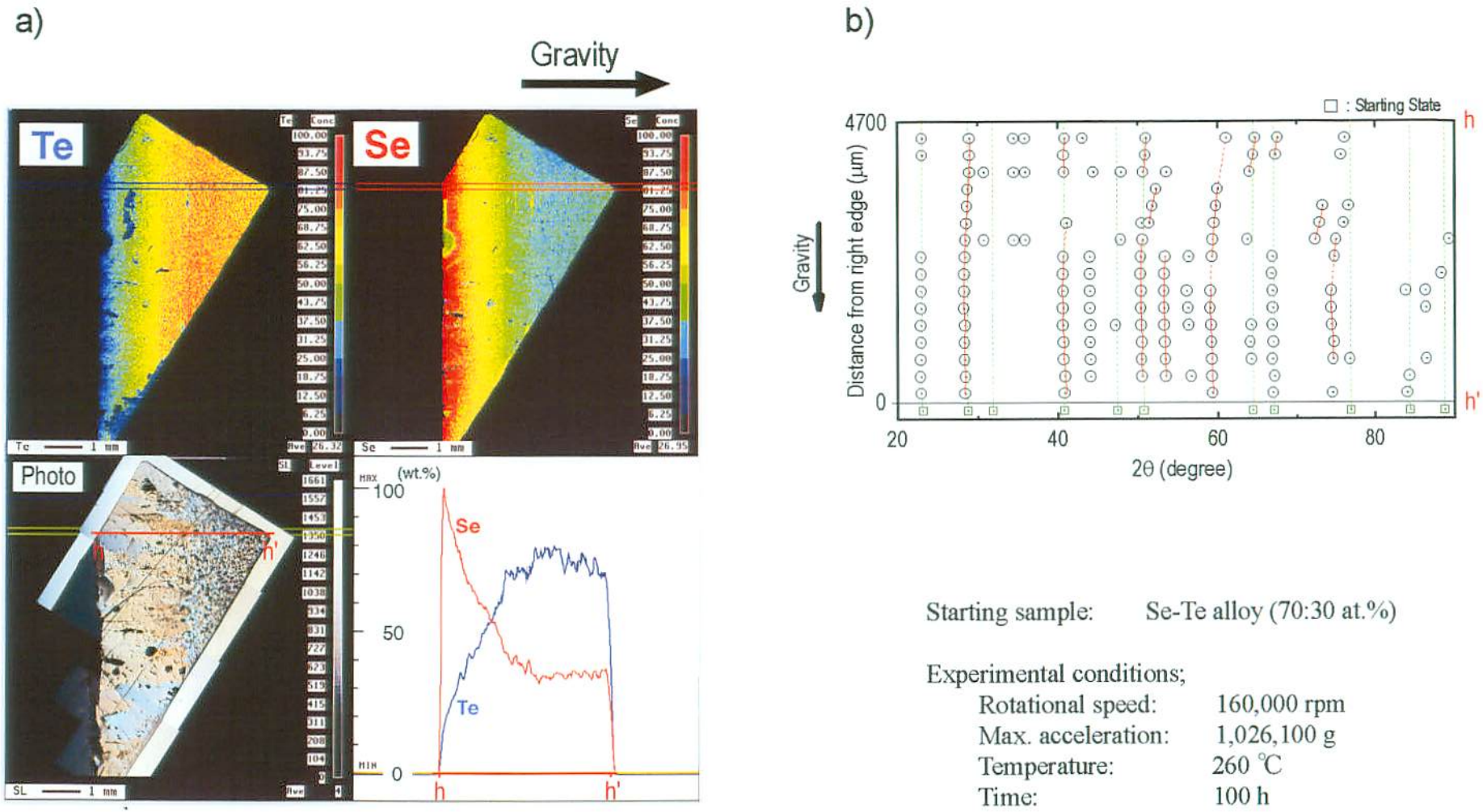

Starting sample: Se-Te alloy (70:30 at.%)

Experimental conditions;

Rotational speed:	160,000 rpm
Max. acceleration:	1,026,100 g
Temperature:	260 ℃
Time:	100 h

Fig. 4-7 a) EPMA mapping photograph and b) Peaks of micro area XRD pattern of centrifuged Se-Te alloy.

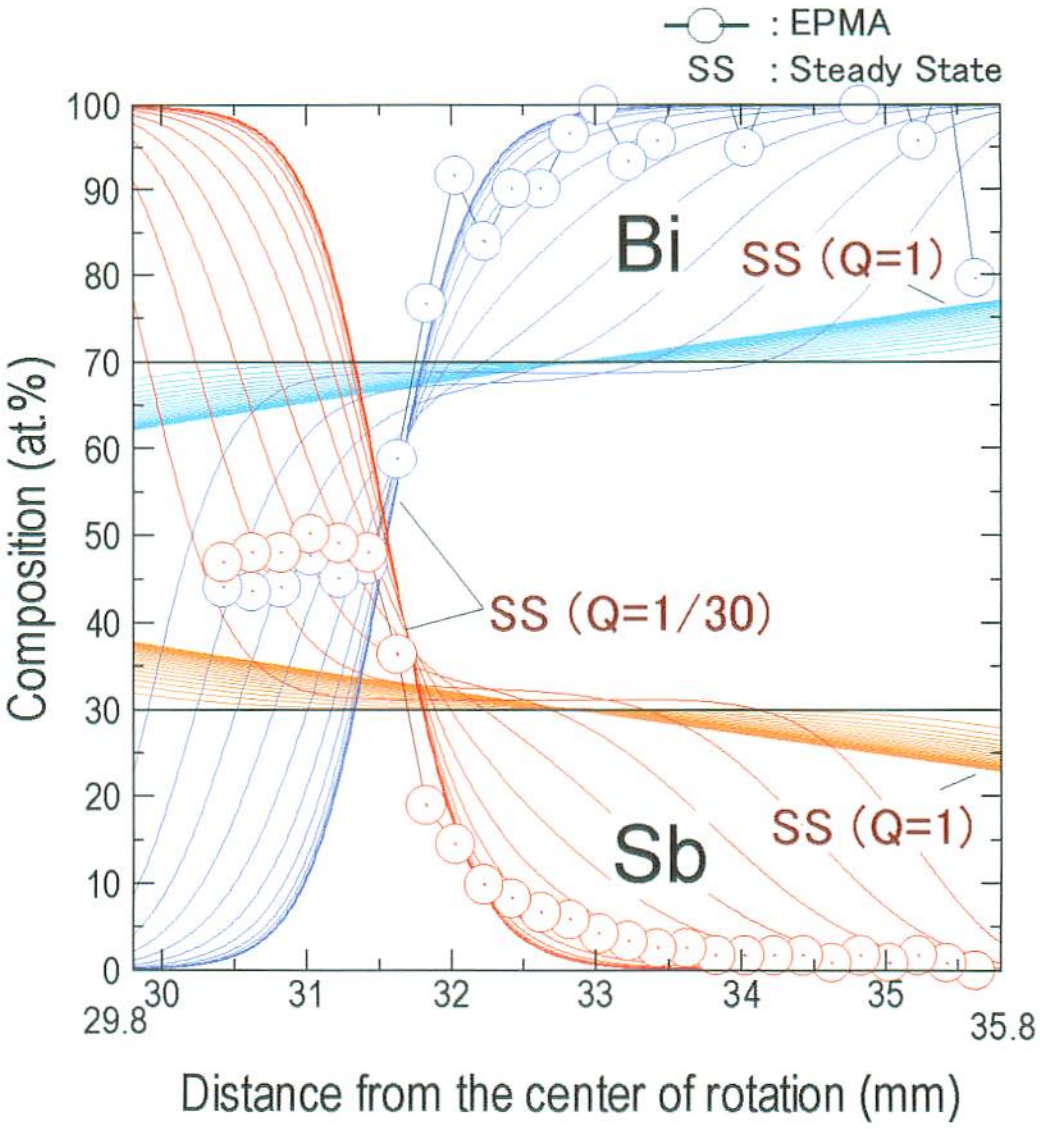

Fig. 4-8 Simulation result of the ssedimentation process in Bi:Sb=70:30 at.% system together with the experimental one.

simulation conditions;
radious: 29.8-35.8 mm
rotational speed: 160,000 rpm
max. acceleration: 1.02×10^6g
temperature: 260°C
Q=1, 1/30

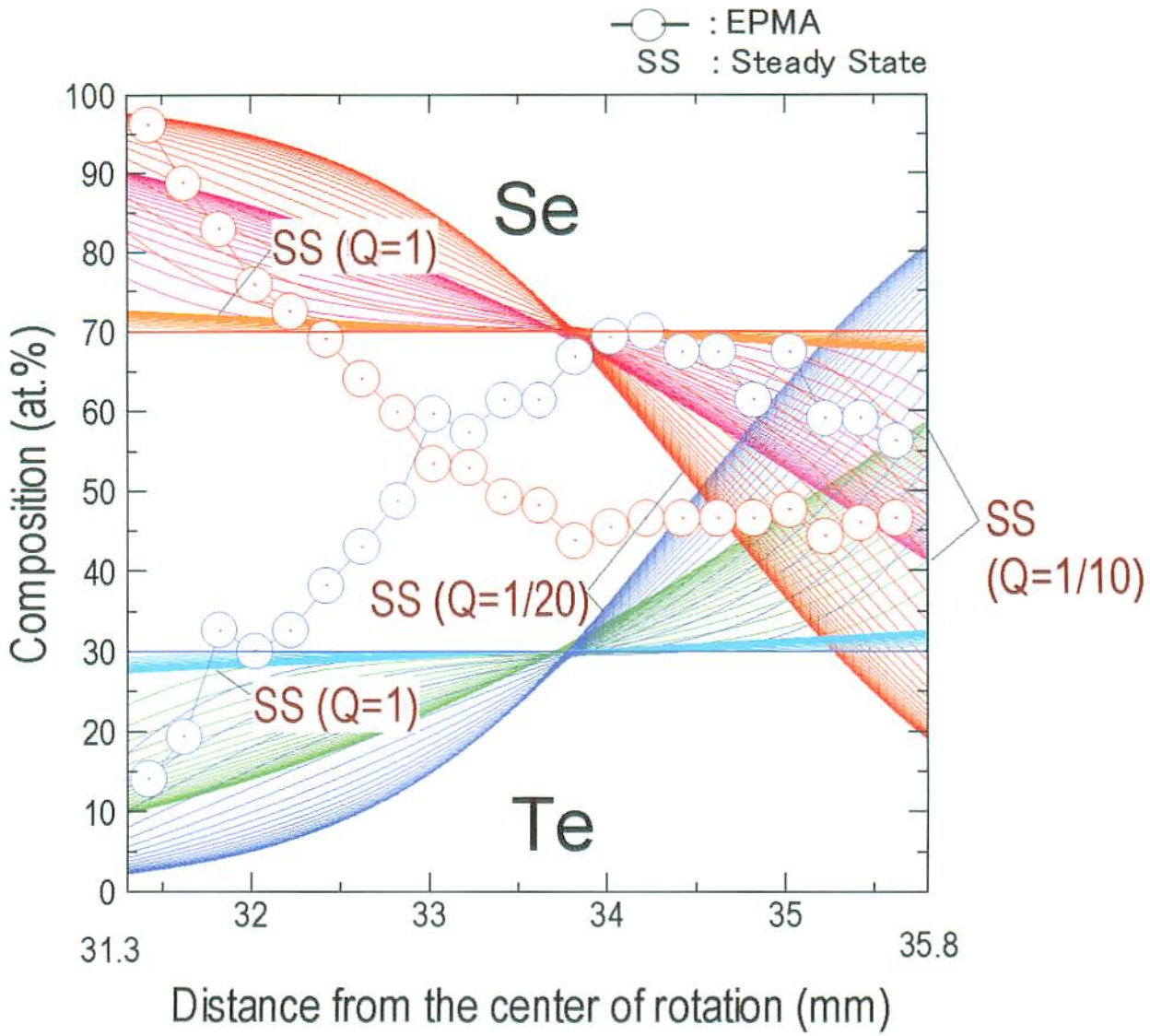

Fig. 4-9 Simulation result of the ssedimentation process in Se:Te=70:30 at.% system together with the experimental one.

simulation conditions;
radious: 31.3-35.8 mm
rotational speed: 160,000 rpm
max. acceleration: 1.02×10^6 g
temperature: 260°C
Q=1, 1/10, 1/20

CHAPTER 5

Sedimentation of atoms in miscible alloy that has several phases according to the composition ratio.

5-1. Briefing of the study

In this *Chapter 5*, we arrange and discuss the experimental results of ultracentrifuge experiment on miscible alloy that has several phases according to the composition rate. The In-Pb alloy was chosen for experiment because it has three phases according to the composition rate. The single phase sample of the intermediate α-phase (f.c.tetragonal) in In:Pb=80:20 at% was prepared to examine the phase transition with composition change by sedimentation of atoms. The experiments were performed in two conditions using ultracentrifuge of Kumamoto University one or *JAERI* one. Also we performed the simulation of the sedimentation process on this system to discuss the diffusion mechanism.

5-2. About the In-Pb system[1]:

The In-Pb alloy has three phases in solid state according to the composition rate. In-rich phase (tetragonal phase), intermediate α-phase (f.c.tetragonal phase) and Pb-rich phase (f.c.c phase) appear in the region of 0 to about 15 at%, 12 to 32 at% and 31 to 100 at% in Pb content, respectively, at the standard state. The phase diagram and the structures are shown in figure 5-1.

5-3. Experimental procedures

a) Starting sample:

If the phase transition due to shift the composition rate by sedimentation occurs on single phase starting sample during ultracentrifuge experiment, it should be considered the phenomenon as one of the proofs that "the sedimentation is in atomic scale". So,

we put the starting state α phase in the ratio In:Pb=80:20 at.%.

Starting sample for Experiment-1 (the experiment in Kumamoto University):

The starting sample was prepared by melting the In and Pb powder mixture in the Ti alloy capsule with a diameter of 3 mm and a depth of 13.5 mm at 223 C for 20 minutes under an Ar atmosphere. The powder mixture was prepared by milling to get the more uniform state after melting. The purity values of In and Pb powder were both 4N. You may well be wondered the temperature to melt the powder mixture seems not enough high for Pb. This is no problem because the powder mixture already alloyed into α phase by milling (Mechanically alloyed). Indeed, the X Ray Diffruction (XRD) pattern of the powder mixture shows f.c.tetragonal that of α phase. Also, the strained lattice state formed in milling process is released in the melting process.

The uniformity of the starting sample was confirmed by the EPMA, the X-ray diffraction method (XRD).

Starting sample for Experiment-2 (the experiment in JAERI):

The starting sample was prepared by melting the In and Pb shots in a Pyrex test tube at 500 C for 20 minutes under an Ar atmosphere. And it was annealed for 5 hours to get the more uniform state alloy. The purity values of In and Pb shots were both 5N. The lamp shaped sample was cut into column shaped pieces with a diameter of 5 mm, and it was set into titanium alloy capsules with an inner diameter of 5mm.

There is a difference in the alloying technique between ***Starting sample for Experiment-1 and for Experiment-2***, and the latter is little bit better state in purity, but both sample's states are good enough for experiment.

b) Equipments for the experiment:

The Experiment-1 was performed using the ultracentrifuge of Kumamoto University one. A rotor that has outer diameter of 46 mm was used for the experiment.

It was made of Ti alloy and the maximum radius of the sample is 18.6mm with the Ti alloy capsule that has a inner diameter of 3 mm and a depth of 13.5 mm. The specifications of the apparatus were introduced in the Introduction of *Chapter 3.*

The Experiment-2 was performed using the ultracentrifuge of *JAERI* one. A rotor that has outer diameter of 70 mm was used for the experiment. It was made of Ti alloy and the maximum radius of the sample is 30.5mm with the Ti alloy capsule.

The development and detailed specifications of the apparatus were introduced in *Chapter 3.*

d) Analysis and Observation:

The composition analysis was carried out using Electron Probe Micro Analyzer (EPMA, JXA-8900R, JEOL Ltd., Tokyo, Japan), and the Micro-area XRD analysis was carried out using the RINT2500VHF (Rigaku Ltd., Tokyo, Japan). The crystalline states were confirmed by the XRD patterns. After that, the lattice parameters were calculated in the respective crystalline state.

5-4. Ultracentrifuge experiments

5-4-1. Experimental conditions:

The ultracentrifuge experiment was performed under the condition that was shown in Table 5-1.

Table 5-1 Experimental conditions.

Experiments (Stating sample; In:Pb=80:20at%, intermediate α-phase)	Rotation rate (rev. min^{-1})	Maximum acceleration (g)	Temperature (℃)	Time (h)
Experiment-1 (at Kumamoto Univ.)	205,000-221,000	(0.87-1.02) $x10^6$	150-160	100
Experiment-2 (at *JAERI*)	155,000	$0.82x10^6$	150	100

The maxim acceleration Experimnt-2 was smaller than that of Experiment-1, but the generating energy was 1.5 times lager than it (refer Table. 3-1).

In the Experiment-1, it took 1 hour to reach aiming experimental conditions (temperature, rotation rate), and also it took 0.5 hour to cool down the sample temperature to 100 ℃ before release the gravity.

In the Experiment-2, it took 3 hours to reach aiming experimental conditions (temperature, rotation rate), and also it took 5 hour to cool down the sample temperature to 70 ℃ before release the gravity. These times were not counted in the both experiments. The operating record of the apparatus is the same shown in Figure 3-9.

5-4-2. Experimental results and discussions of Experiment-1

a) Microscope photograph

Figure 5-2 shows the microscope photograph at the polished surface cut at a plane containing the rotation axis of the centrifuged sample. The sketch in the left hand of the figure is the total view on the cut plane of the centrifuged sample in the Ti alloy capsule. The surface was finished with 1 μm diamond paste. Many small holes seen on the surface were not voids but the holes formed under polishing. A clear boundary was seen near the left side of the centrifuged sample. Also a very diffused boundary was visible in the right area of the sample.

b) EPMA analysis

Figure 5-3 shows the EPMA mapping photographs of the sample in the area shown in Fig. 5-2. The linear composition profiles were obtained along a straight line between h-h', and it showed almost linear changes in Pb and In contents. The Pb content continuously increased in the direction of gravity (arrow direction in the figure) from about 12 to 36 at%, and conversely, the In content decreased from about 88 to 64 at%. The slight jaggedness of the composition profiles was caused by the finishing touches of the surface. Figure 5-4 shows the micro-area EPMA mapping

photographs of the sample at 5 points (a, b, c, d, e) on the h-h' line shown in Fig. 5-3. Maps in upper, middle and bottom row of the Fig. 5-4 show the SEM image, In content and Pb content at the measurement points on the sample, respectively. The linear composition profiles of In and Pb were shown in the respective maps. It was confirmed that the composition rates were homogeneous in sub-micron scale.

c) Micro-area XRD measurement

The Micro-area XRD measurement was performed on the centrifuged sample along h-h' line (in Fig. 5-3) at the positions of every 380 μm distance from the right edge to the left for 3500 μm (13 points, diameter: 100 μm). Figure 5-5 shows the micro-area XRD patterns in the representative area A, B and C, together with that of the starting sample. These patterns showed that the crystal structures in the areas A, B and C were In-rich phase (tetragonal), intermediate α-phase (f.c.tetragonal) and Pb-rich phase (f.c.c.), respectively. This suggested that the tetragonal phase and the f.c.c phase appeared at a low- and high-gravity regions, respectively, from the starting state of f.c.tetragonal. These phase transitions clearly showed that the composition change was caused by the sedimentation of atoms.

Figure 5-6 shows the lattice parameters in the each phases obtained by the XRD patterns versus the distance from the right edge of the sample. In the Pb-rich phase and the α-phase, the lattice parameters tend to become large with the Pb content. The lattice parameters of α-phase varied from a=0.485 nm, c/a= 0.934 at a distance of 2500 μm to a=0.490 nm, c/a=0.931 at a distance of 1000 μm. And, the lattice parameters of the Pb-rich phase increased from a=0.481 nm at a distance of 1000 μm to a=0.483 nm at a distance of 100μm. The regular shifts of lattice parameter with composition rate showed that the graded structure was continuous in atomic scale.

It was found that left side area of the boundary mainly consisted of the In-rich phase and α-phase. In the area, the lattice parameters could not be determined, because the weak-intensity peaks for the two phases and the background peaks of such as SiC or diamond grains prevented us to get correct information. It was considered

that this area had melted under the ultracentrifuge experiment because the sample temperature reached the melting point due to the dropping of melting temperature caused by composition changes in the area and/or the ripple of temperature control (± 5℃).

5-4-3. Experimental results and discussions of Experiment-2

a) Microscope photograph

Figure 5-7-a) shows the microscope photograph at the polished surface cut at a plane containing the rotation axis of the centrifuged sample. The sketch in the left hand of the figure is the total view on the cut plane of the centrifuged sample in the Ti alloy capsule. The surface was finished with 1/4 μm diamond paste. Many small holes seen on the surface were not voids but the holes formed under polishing. The holes were much seen in the left hand of sample so it was considered that the left area rather soft. In the left hand of the sample surface, crystal grains are small. On the contrary, large crystal boundaries were seen in the right hand of the sample. The size of the crystal seen in the right area has about 2-3 hundreds μm in diameter.

In the sample, melted area was not seen. Because the new ultracentrifuge was well electrically controlled and the sample temperature was controlled in 150±1℃ of under the melting point of the In (156.63℃).

b) EPMA analysis

Figure 5-7-b) shows the EPMA mapping photographs of the sample in the area shown in a). The linear composition profiles were obtained along a straight line between h-h', and it showed almost linear changes in Pb and In contents (in c)). The Pb content continuously increased in the direction of gravity (arrow direction in the figure) from about 6 to 45 at%, and conversely, the In content decreased from about 95 to 55 at%. The slight jaggedness of the composition profiles was caused by the finishing touches of the surface.

c) Micro-area XRD measurement

The Micro-area XRD measurement was performed on the centrifuged sample along h-h' line (in b)) at the positions of every 200 μm distance from the right edge to the left for 4000 μm (24 points, diameter: 100 μm). Figure 5-8 shows the micro-area XRD patterns and the structures in the represent area A, B and C, together with that of the starting sample. The measurement was done twice: first, we measured the sample that was well finished with 1/4 μm diamond paste. But the obtained XRD patterns having steep peaks like single crystals. And the lattice parameter couldn't calculate. To calculate them, we performed the second measurement on the sample that was finished with #2000 sand paper. The patterns described in real line are the former and the patterns described in dotted line are the latter. Around the area A in figure is Pb phase (f.c.c) and large crystals that may be considered as single crystals are seen. Around B is á-phase (f.c.tetragonal) same as starting state, and around C is In phase (tetragonal). And, it was found that the peaks shift with composition in the almost all same crystal structures as it in case Expeiment-1. These phase transitions clearly showed that the composition change was caused by the sedimentation of atoms.

Figure 5-7-d) shows the lattice parameters in the each phases obtained by the XRD patterns versus the distance from the right edge of the sample. The a_0 and c_0 lattice parameters increased and decreased, respectively, with the increasing Pb composition in the In-rich phase. Both lattice parameters increased by >1 % with increasing Pb composition in the α-phase. The crystal grains of the FCC phase in the area A grew to several hundreds μm level. The EPMA and XRD results showed that the graded structure was in atomic scale, and as a result, was formed by the sedimentation of atoms.

The boundaries of the α-phase with the In-rich phase and Pb rich phase were situated at about 8.5-10.5 mol% and 30.3-35 mol% in Pb content, while the equilibrium phase boundaries were situated at 11.0-13.0 mol% and 31.0-32.0 mol%, respectively, at 150°C[1], as drawn in the figure. This result indicated that the super saturation of the α-phase occurred under a strong gravitational field.

5-5. Simulation of Sedimentation Process for Atoms

Also, we performed the simulation of sedimentation process for atoms in In-Pb system using self-consistent theory to discuss the sedimentation mechanism[2, 3]. We referred the simulation procedure presented in *chapter 2*. Performing this program, we can simulate the change of the composition rate to steady state for binary system under gravitational field, and also we can estimate the ratio of diffusion coefficient for sedimentation to that for usual diffusion by the internal chemical potential. The simulation conditions were summarized in Table 5-2.

Table 5-2 Simulation conditions.

Stating state	Rotation rate (rev. min^{-1})	Maximum acceleration (g)	Temperature (℃)	Q ($Q=D_1/D_2$)
In:Pb=80:20at%, uniform	210,000	0.92×10^6	155	1
	210,000	0.92×10^6	155	1/5

These conditions were almost the same as the experimental ones. Here, Q was the ratio of the diffusion coefficient for sedimentation (D_2) to that for usual diffusion by the internal chemical potential (D_1), and it was described as $Q=D_1/D_2=1+ln\ (\gamma)/\ ln(c)$ by using the following chemical potential representation: $\mu=\mu_0(T)+kTln(\gamma c)$, where γ was the activity coefficient[3, 4]. In addition, we assumed that the diffusion coefficients for the two components were equal and constant as the simulation parameter did not measured.

Figure 5-9 shows the simulation results of the In-Pb (80:20 at%) system together with the experimental result. Here, the plot in vertical axis was the composition rate, and the plot in horizontal axis was the distance from the center of rotation. The starting composition profiles were uniform in the ratio In:Pb=80:20 (at%). In the simulations, the calculated composition profiles gradually changed with time as shown by the slight lines in the figure, and the content of Pb increased gradually in the

direction of centrifugal force, and that of In increased to the opposite direction. This showed that the heavy Pb atoms moved in the direction of gravity, and the light In atoms moved to the opposite direction with time. The composition change of both elements was notable near edges of the sample, where atoms could not move more, and gradually accumulated there by the boundary condition that fluxes of atoms were zero at edges of the sample. Finally, the changes in composition profiles converged to the respective steady states. If we assumed that the experimental data was almost at steady state (100h), the simulation at $Q=1/5$ was rather comparable to the experimental result. It means that the diffusion coefficient for sedimentation was at least 5 times larger than that of usual diffusion.

It was found that the diffusion coefficient for sedimentation was much larger than that for usual diffusion. Under the strong gravitational field, the sample was also exposed to high pressure of around 0.1GPa. Under high pressure field, the number of vacancy decrease and the diffusion coefficient would become small. So, it was suggested that the diffusion mechanism of the sedimentation in this system was different from the vacancy mechanism.

5-6. Conclusions

In this study, we performed the ultracentrifuge experiments on the three-phase miscible alloy of In-Pb system using ultracentrifuges of Kumamoto University one or *JAERI* one (acceleration: 10^6 g level, starting state: uniform in 80:20 at%, intermediate α-phase).

The graded composition profiles was observed on the cut surface of the centrifuged samples. In the centrifuged sample of Experiment-1 performed in Kumamoto university, The Pb content continuously increased from about 12 to 36 at%, and conversely, the In content decreased from about 88 to 64 at% in the direction of gravity. And, In the centrifuged sample of Experiment-2 performed in *JAERI*, The Pb content continuously increased in the direction of gravity from about 6 to 45 at%, and

conversely, the In content decreased from about 95 to 55 at%. In the both samples, it was found that the Pb-rich phase and In-rich phase appeared at the strong- and weak-gravity field sides, respectively, from starting state of intermediate α-single phase. The continuous changes in lattice parameters were observed in each phases and the lattice parameters gradually changed with composition. These results showed that the obtained graded structure was continuous in atomic-scale, and was formed by the sedimentation of substitutional solute atoms.

We also performed the simulation of sedimentation process for Experiment-1 to discuss the diffusion mechanism. It was found that the diffusion coefficient for sedimentation was few times larger than that for usual diffusion. This indicated that the diffusion mechanism of the sedimentation in this system was different from the vacancy mechanism.

We are intending to study the sedimentation of atoms and the interaction with the phase equilibrium in binary alloys under strong gravitational field. At first, we have investigated the sedimentation for the all-proportional system of Bi-Sb system, and for the second, we did three-phase miscible alloy of the In-Pb system in this study. We are going to study on the other systems; partial miscible system, immiscible one, intermetallic compound, etc.

REFERENCES

[1] M. Hansen and K. Anderko: *Constitution of Binary Alloys*, 2nd ed., (Genium Publishing corporation, New York, 1991) p.854-855.

[2] T. Mashimo: Phys. Rev. A38 (1988) 4149-4154.

[3] T. Mashimo: Philos. Mag. A70 (1994) 739-760.

[4] M. Ono, T. Mashimo: Philos. Mag. A82 (2002) 591-600.

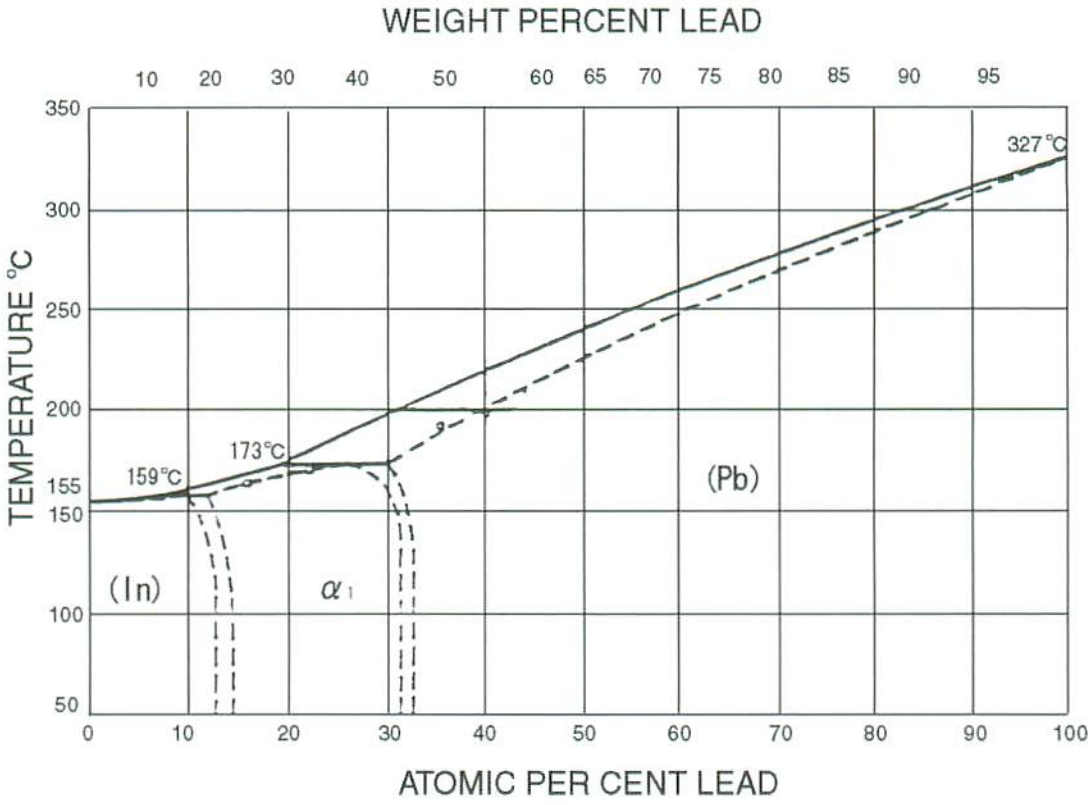

Phase Diagram of In-Pb system [1]

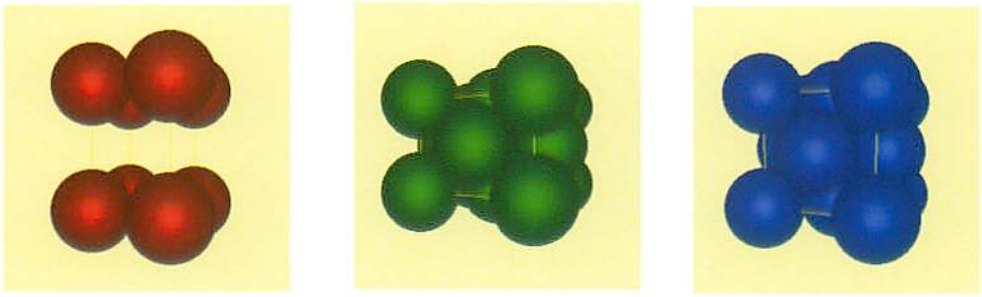

(In) phase: Tetragonal

(α) phase: F.C.Tetragonal

(Pb) phase: F.C.Cubic

Cristal Structures of In-Pb system

Fig. 5-1 Phase diagram and Cristal structure of In-Pb system

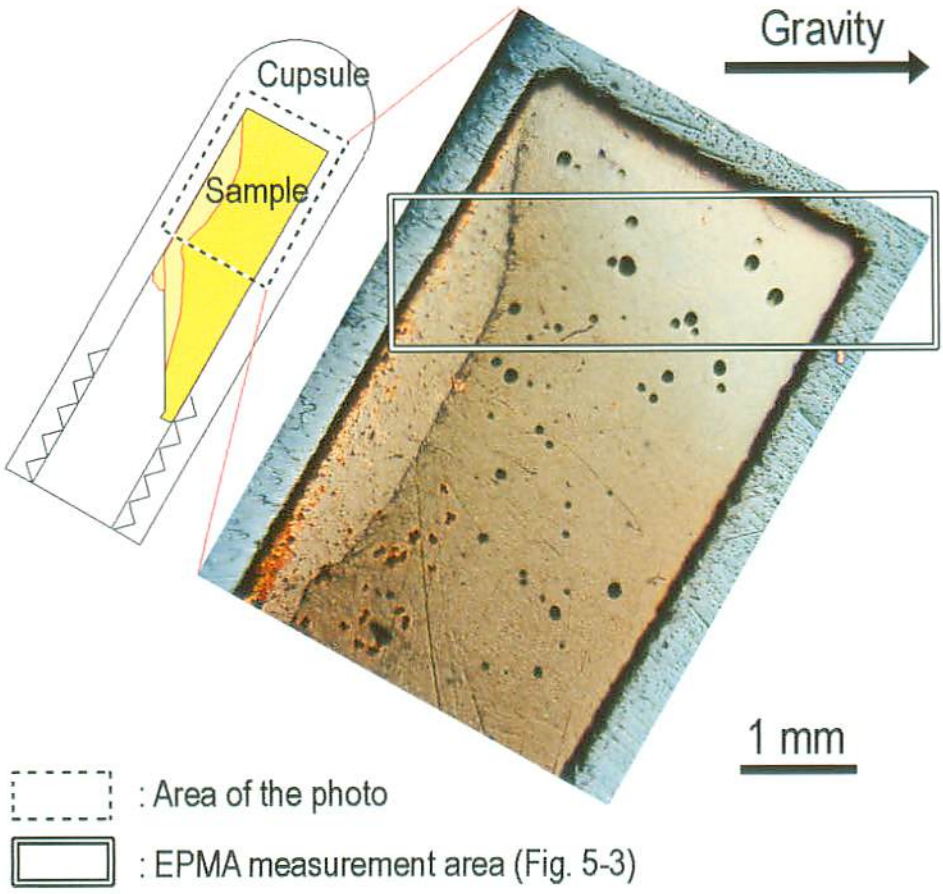

Starting material : In:Pb=80:20at.%
(After MA, Melt and cooled)

Experiment condition :

Rotation rate :	205,000 ~ 221,000 rpm
Acceleration :	870,000 ~ 1,020,000 g
Temperature :	150 ~ 160 ℃
Time :	100 hours

Fig.5-2 The optical microphotograph of centrifuged In-Pb alloy

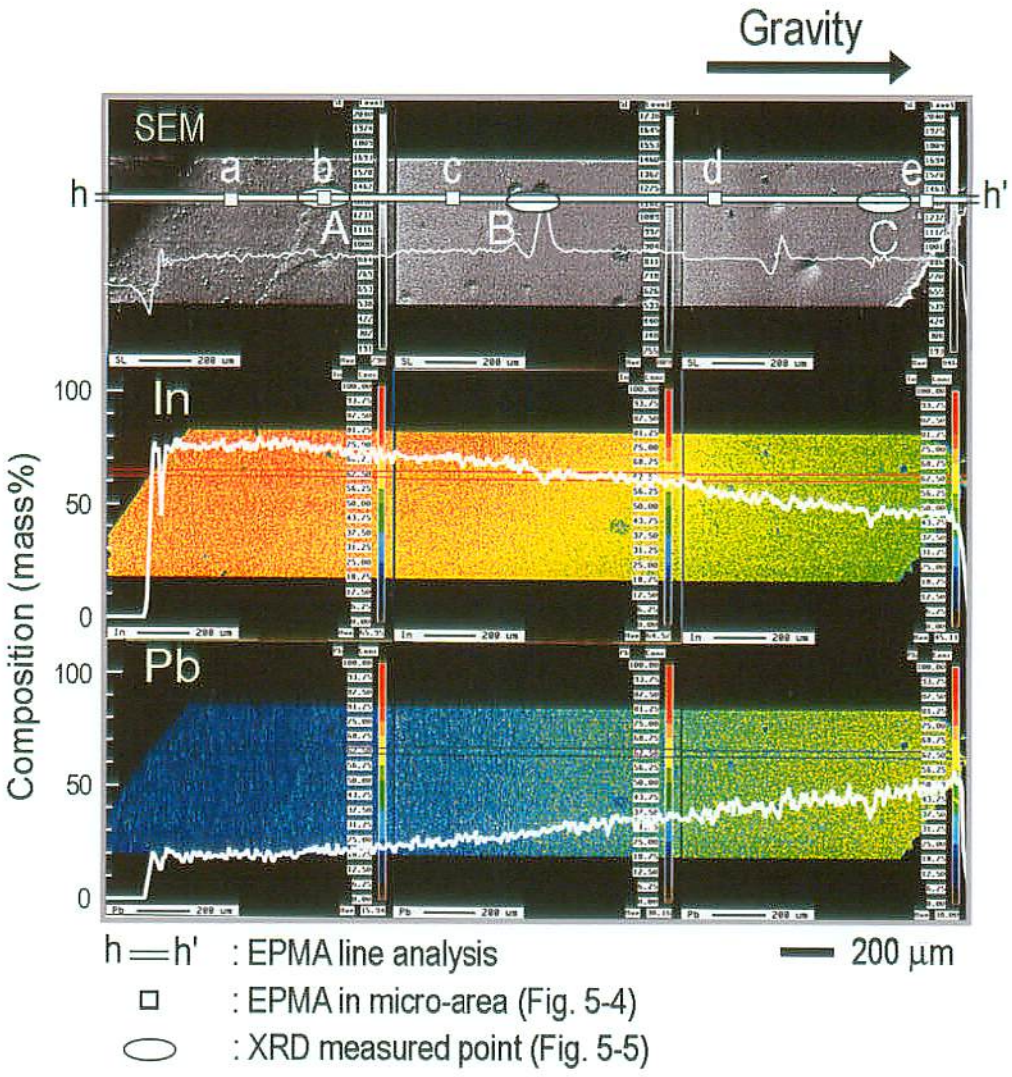

Fig. 5-3 EPMA mapping photographs with the linear composition profiles of In and Pb at the polished surface cut at a plane containing the rotation axis of the centrifuged sample.

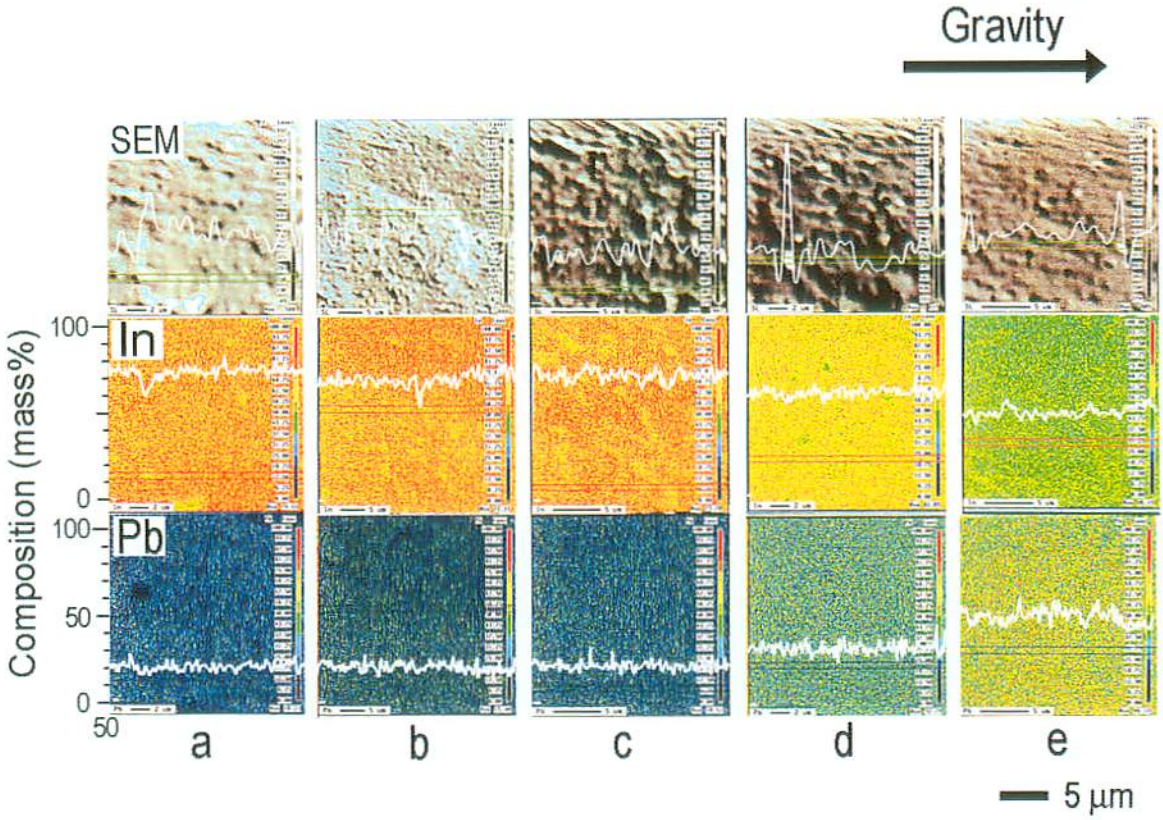

Starting material : In:Pb=80:20at.%

Experiment condition :

Rotation rate :	205,000 ~ 221,000 rpm
Acceleration :	870,000 ~ 1,020,000 g
Temperature :	150 ~ 160 ℃
Time :	100 hours

Fig. 5-4 Micro-area EPMA mapping photographs at 5 points (a, b, c, d, e) on the h-h' line of the centrifuged sample.

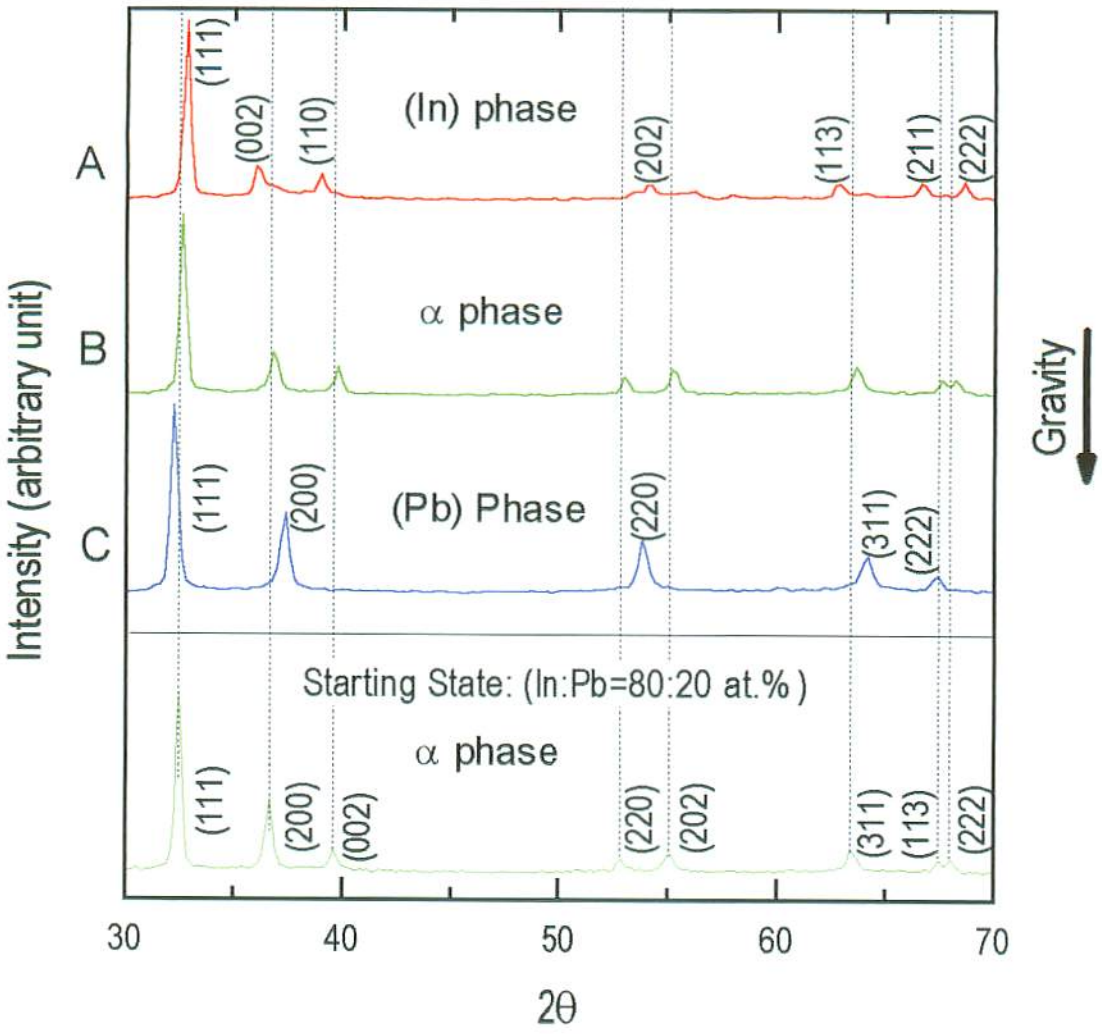

Fig.5-5 Micro-area XRD patterns of centrifuged sample in the representativearea A, B and C, together with that of the starting sample.

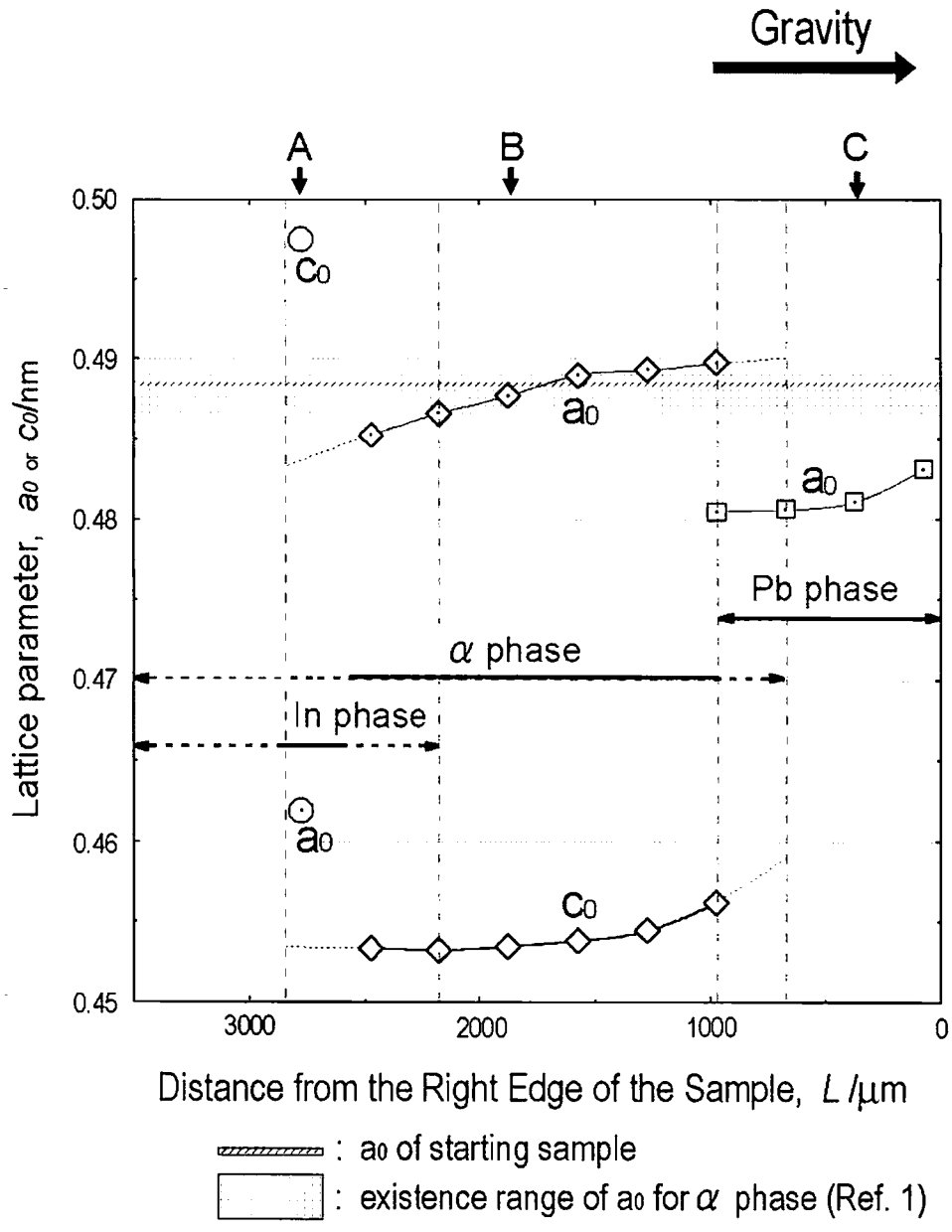

Fig. 5-6 Lattice parameters in each phases obtained by the XRD patterns versus the distance from the right edge of the centrifuged sample.

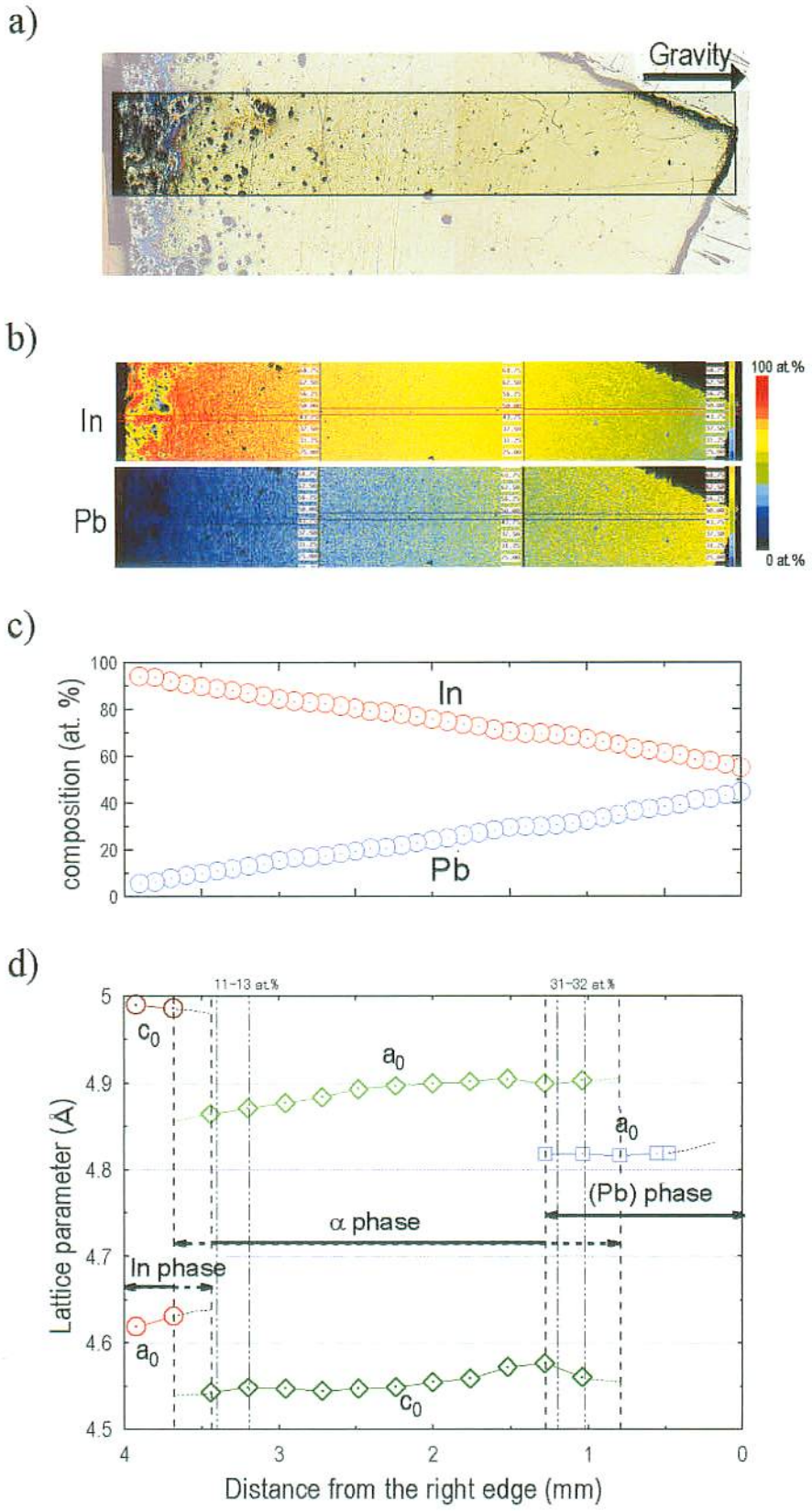

Fig.5-7 Experimental result of utracentrifuged In-Pb system alloy a) a photo around measurement area, b) EPMA color mapping, c) composition profile, d) Lattice parameter (In:Pb=80:20 at.%, 820,000 g, 100 h, 150 °C)

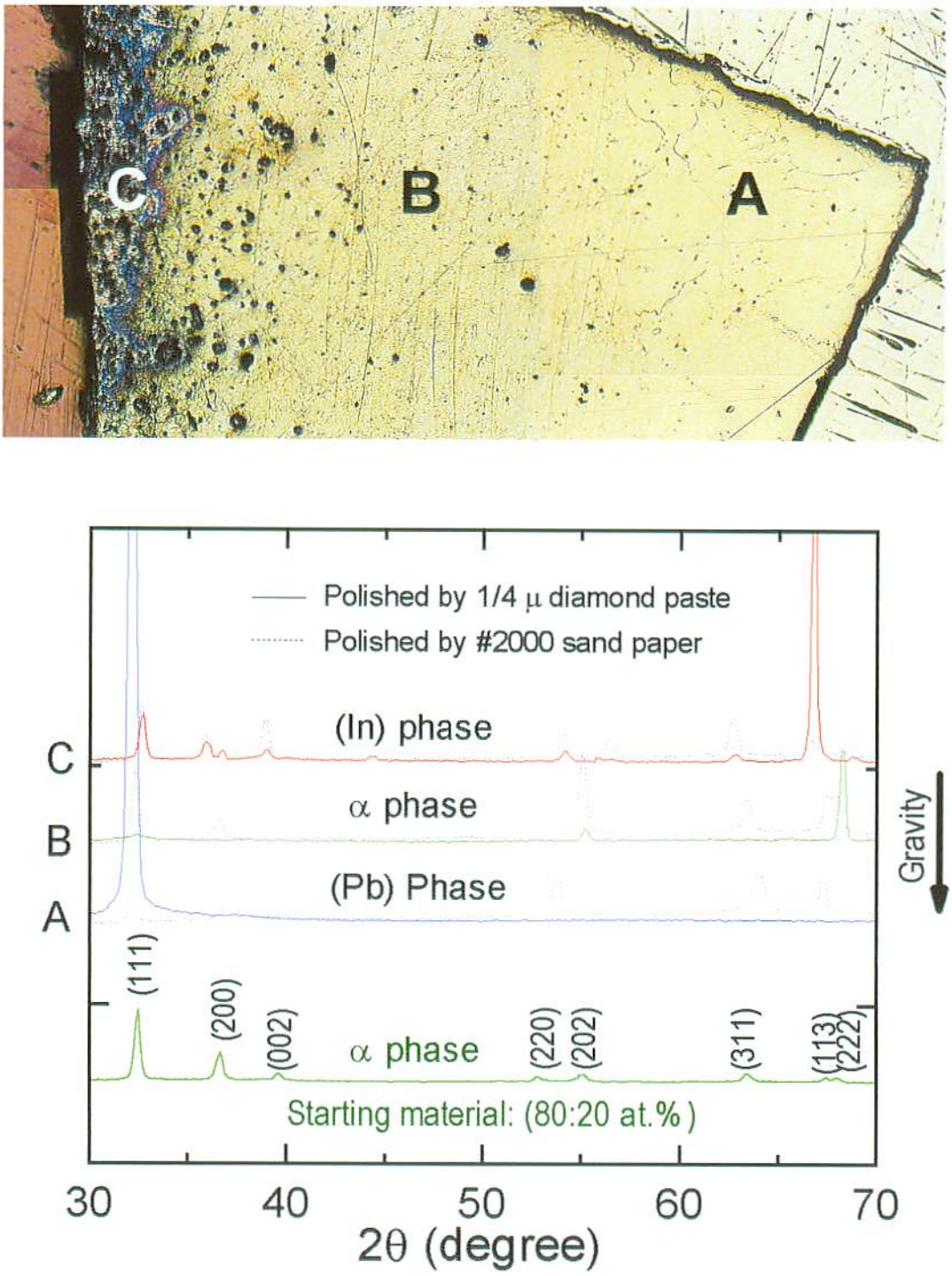

Fig.5-8 XRD pattarns of utracentrifuged In-Pb system alloy (In:Pb=80:20 at.%, 820,000 g, 100 h, 150 °C)

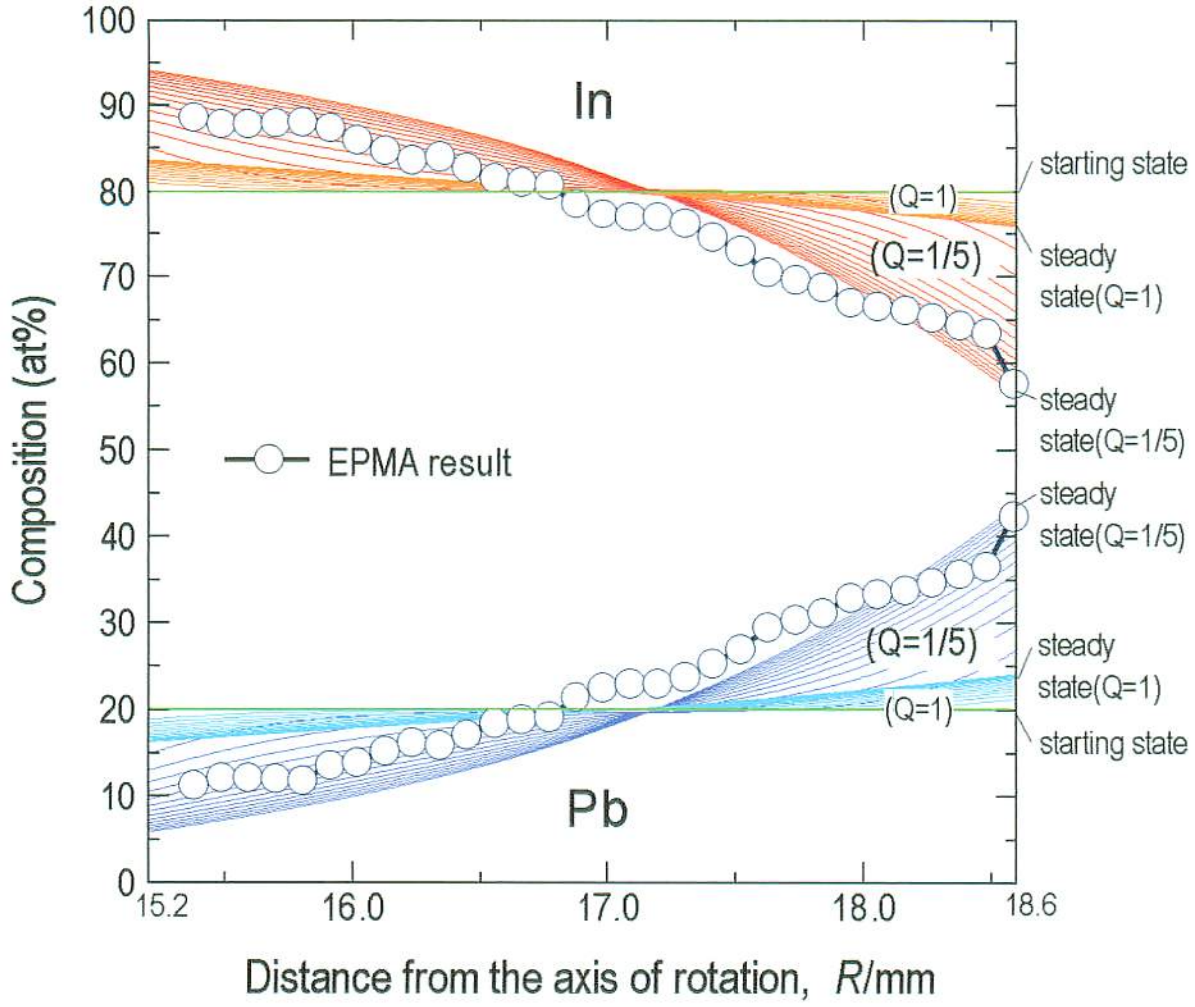

Fig.5-9 Simulation result of the sedimentation process in In:Pb=80:20 at.% system together with the experimental one.

Simulation conditions;

Radius:	15.2-18.6 mm
Rotational speed:	210,000 rev.min-1
Acceleration field:	0.92x106 g
Temperature:	155 ℃
Q:	1 and 1/5

CHAPTER 6

Sedimentation of atoms in the metallic compound under strong gravitational field.

6-1. Briefing of the study

We had realized the sedimentation of substitutional solute atoms in an all-proportional miscible system (Bi-Sb, Se-Te) and a three-phase miscible system (In-Pb). Our next interest is aimed at a compound material. For the first place, intermetallic compounds are chosen for the experiment to discuss the possibility of sedimentation of substitutional atoms. If the sedimentation of atoms occurs in the intermetallic compounds, the decomposition of the compound is expected. More over, if the intermetallic compound has solubility band, not only the decomposition but also the graded structure is expected.

In this *chapter 6*, we arrange and discuss the experimental results of ultracentrifuge experiment on an intermetallic compound of Bi-Pb system alloy (Bi_3Pb_7). The experiment was performed using ultracentrifuge of Kumamoto University one. The composition and crystalline state were analyzed by using the electron probe micro analyzer (EPMA) and the X-ray diffraction (XRD) method.

6-2. About the Bi-Pb system[1]:

The phase diagram and the structures are shown in figure 6-1. There is almost no miscible phase is seen in Bi-rich region because of the very small solid-solubility of Pb in Bi. On the contrary, this system has miscible phase in the Pb rich region as the solid-solubility of Bi in Pb is high and also the system has ε phase consisted of intermetallic compound. The intermetallic compound is Bi_3Pb_7, which has solubility band. The crystal structure of the Bi3Pb7 is H.C.P.. And the crystal structure of Bi is

Trigonal/Rhombohedral, and that of Pb phase is F.C.C.

6-3. Experimental Procedures

a) Stating sample:

The Bi_3Pb_7 lump shaped starting sample was prepared by melting the Bi and Pb powder mixture (composition: 30:70 mol%, atmosphere: Ar, impurity: 4N, temperature: 450 C), and by annealing it for 5 hours. The preparation was done under Ar atmosphere. It was found that the prepared sample was uniform in the ratio Bi:Pb=30:70% (Figure 6-2). And, also it was confirmed that the starting sample consisted of HCP phase (å-phase) that of Bi_3Pb_7 by the XRD method (Fig. 6-3). The sample was cut into column shaped pieces with a diameter of 3 mm, and was set into Ti alloy capsule with an inner diameter of 3 mm.

b) Equipments for the experiment:

The experiment was performed using the ultracentrifuge of Kumamoto University one. A rotor that has outer diameter of 46 mm was used for the experiment. It was made of Ti alloy and the maximum radius of the sample is 18.6mm with the Ti alloy capsule that has a inner diameter of 3 mm and a depth of 13.5 mm.

The specification of the apparatus was introduced in the Introduction of *Chapter 3.*

d) Analysis and Observation:

The composition analysis was carried out using Electron Probe Micro Analyzer (EPMA, JXA-8900R, JEOL Ltd., Tokyo, Japan), and the Micro-area XRD analysis was carried out using the RINT2500VHF (Rigaku Ltd., Tokyo, Japan). The crystalline states were confirmed by the XRD patterns.

6-4. Ultracentrifuge experiment

6-4-1. Experimental conditions:

The ultracentrifuge experiment was performed under the condition that was shown in Table 6-1.

Table 6-1 Experimental conditions.

Experiments (Stating sample; Bi_3Pb_7, intermetallic compound)	Rotation rate (rev. min^{-1})	Maximum acceleration (g)	Temperature (°C)	Time (h)
Experiment-90h (at Kumamoto Univ.)	197,000-207,000	(0.81-0.89) $x10^6$	137.0-144.7	90
Experiment-150h (at Kumamoto Univ.)	197,000-207,000	(0.81-0.89) $x10^6$	138.9-147.6	150

In all experiments, it took 1 hour to reach aiming experimental conditions (temperature, rotation rate), and also it took 0.5 hour to cool down the sample temperature to 100 °C before release the gravity. These times were not counted in the experiments. We are going to discuss the experimental result using Experiment-90h.

6-4-2. Results and Discussions:

a) Microscope photograph

Figure 6-4 shows the microscope photograph at the polished surface cut at a plane containing the rotation axis of the centrifuged sample (Experiment-90h). The sketch in the left hand of the figure is the total view on the cut plane of the centrifuged sample in the Ti alloy capsule. The surface was finished with 1 μm diamond paste. It was considered that the centrifuged sample has 3 areas because two clear boundaries were seen on the sample. For simple, we are going to discuss the experimental result dividing the area into X, Y and Z as shown in the sketch. In the Y, there are many black dots can be seen. These are the SiC grains that were buried when cutting and polishing the sample. This is because this area may be soft.

b) EPMA analysis

Figure 6-5 shows an EPMA mapping photograph of Bi and Pb at the polished surface cut at a plane containing the rotation axis of the centrifuged sample. The composition profiles had changed in the area Y and Z of the sample as shown in Fig. 6-4, in which the graded structure was seen. These areas located in weak-gravity side. In the area Y, the composition ratio of Pb increased from starting state, and that of Bi decreased 30 to 20 wt.%. Conversely, in the area Z, the composition ratio ofPb decreased from starting state, and that of Bi increased. It was assumed that the composition changes in the area of Y and Z were caused by the sedimentation of Bi and Pb atoms to opposite direction each other. In the area X located in strong-gravity side, the composition ratio was same as starting sample. And, it is considered that the composition change was very small or non in the area. The composition change was remarkable around the weak-gravity side, which probably because the diffusion coefficients of Bi and Pb varied with the composition.

Fig. 6-6 is the EPMA mapping photographs of centrifuged sample in the micro areas. The measurement areas are shown in the sketch below. In the area X, measured a,b,c were the same state as b shown in figure, and the composition ratio were the same state as starting sample. In the area Y, all condition were the same state as d shown in figure, the composition of Pb increased from starting state, and high concentration Pb area were seen in the measured area. In the area Z, around g near Y area, the composition of Pb decreased from starting state, and that of Bi increased, and the appearance of the cluster should be considered as Bi became to see. And, the near area i, the more cluster increased. Form the measurements of ghi area, it is considered that these graded structure were consisted of Bi_3Pb_7 and Bi clusters.

c) Micro-area XRD measurement

Figure 6-7 shows the micro-area XRD patterns at three representative points (diameter: 100 ì m) in the areas X, Y, Z of the centrifuged sample, together with that of the starting sample. At the area X, the pattern shows this area is whole Bi_3Pb_7. As no

composition change was observed by EPMA at this area, it is considered that the area X almost remained to be starting sample. In the Area Y, the pattern shows this area is consisted of Bi_3Pb_7 and (Pb) phase that was seen in EPMA result as Pb enriched state. And, the area Z, as we expected observing EPMA result, consisted of Bi and Bi_3Pb_7 mixed phase. The appearance of Bi and Pb phases accompany with composition change from Bi_3Pb_7 (decomposition) clearly showed that the sedimentation of substitutional solute atoms occurred.

By the way, for 90h experimented sample (Experiment-90h), the concentration change in the X area could not confirmed. Fig.6-8 and Fig.6-9 are the experimental result of the 150h experimented sample (Experiment-150h), which experiment was performed with time extent to 150 h. In this time extended sample, the graded structure was observed in the area X. And, it is considered that the composition change occurred in area X same as in area Y and Z, however the change was slow.

6-5. Conclusion

In this study, we performed the mega-gravity field experiment on an intermetallic compound of Bi-Pb system alloy (Bi_3Pb_7), and the composition and crystalline states were studied. It was found that the composition profiles changed, and the decomposition occurred. The present result showed that the sedimentation of Bi and Pb atoms occurred in the intermetallic compound of Bi_3Pb_7. It is expected that the sedimentation of substitutional solute atoms can be realized in other compounds.

REFERENCES

[1] M. Hansen and K. Anderko: *Constitution of Binary Alloys*, 2nd ed., (Genium Publishing corporation, New York, 1991) p.324-327.

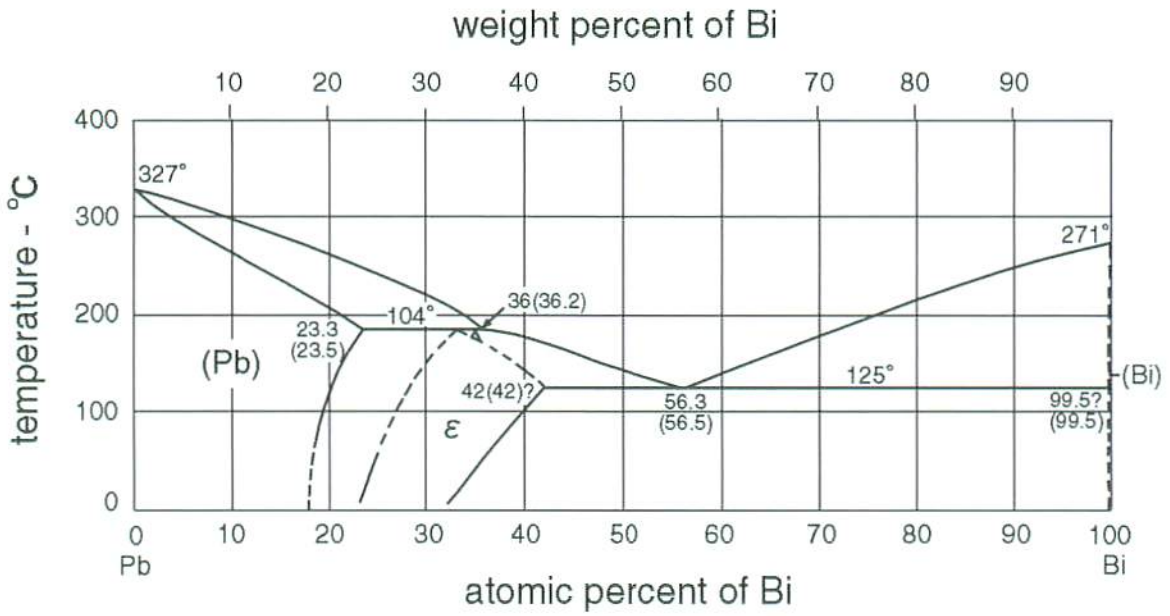

Phase Diagram of Bi-Pb system [1]

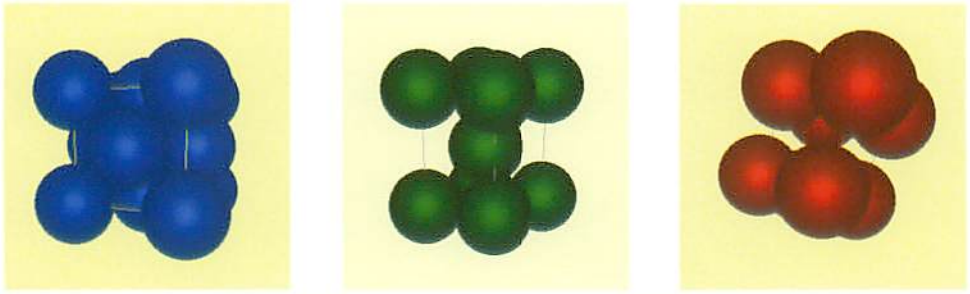

(Pb) phase: F.C.Cubic

(ε) phase: H.C.P

(Bi) phase: Rhombohedral

Crystal Structures of Bi-Pb system

Fig.6-1 Phase diagram and crystal structure of Bi-Pb system

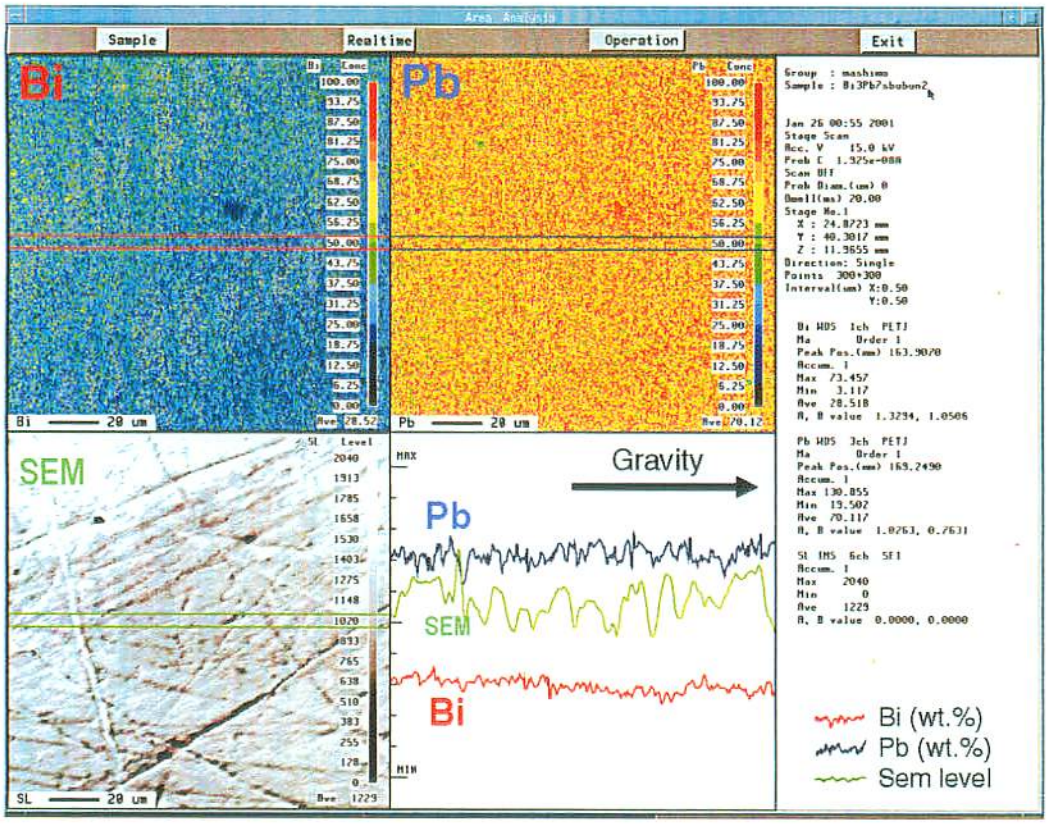

Mixing condition:

Elements: Bi, Pb (total 20.0g)
Composition: 30:70 at.%
Atmosphere: Argon

Annealing:

Atmosphere: Argon
Time: 5 h

Fig.6-2 EPMA mapping photograph of Bi_3Pb_7 strating sample.

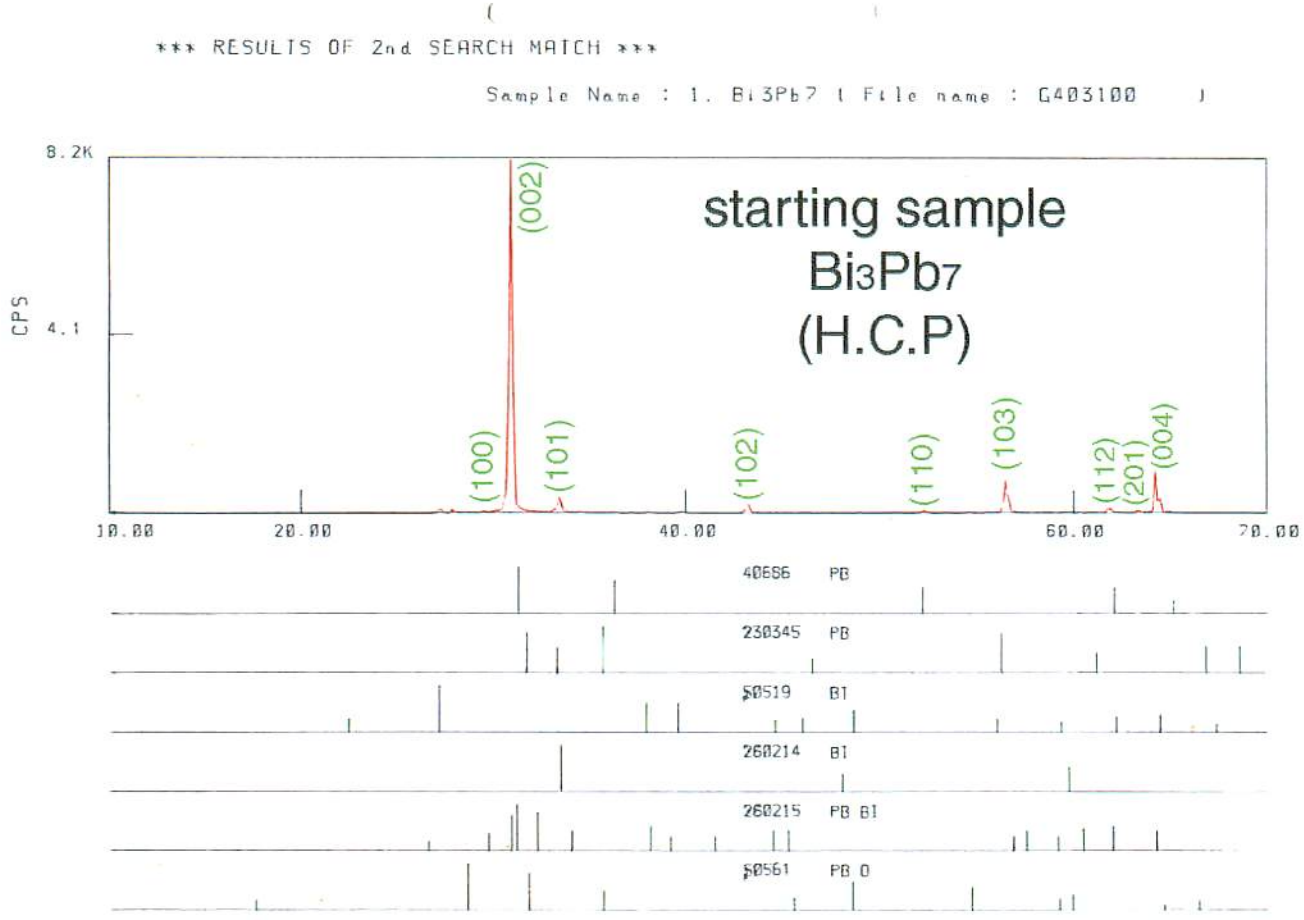

Mixing condition:

Elements: Bi, Pb (total 20.0g)
Composition: 30:70 at.%
Atmosphere: Argon

Annealing:

Atmosphere: Argon
Time: 5 h

Fig.6-3 XRD pattern of Bi_3Pb_7 starting sample

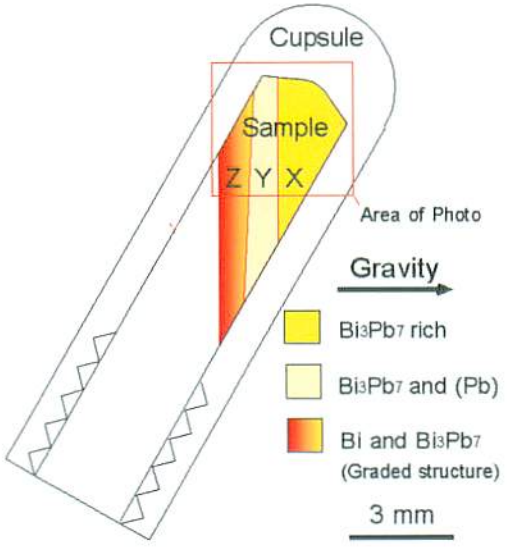

Bi3Pb7 (90h), after experiment

Starting Material : Bi3Pb7 (5h annealed)

Experimental Conditions :

Rotation rate :	197,000 ~ 214,000 rpm
Acceleration :	805,000 ~ 956,000 g
Temperature :	137.0 ~ 144.7 °C
Time :	90 hours

Fig.6-4 Optical micro photogaph of centrifuged Bi3Pb7 (90h)

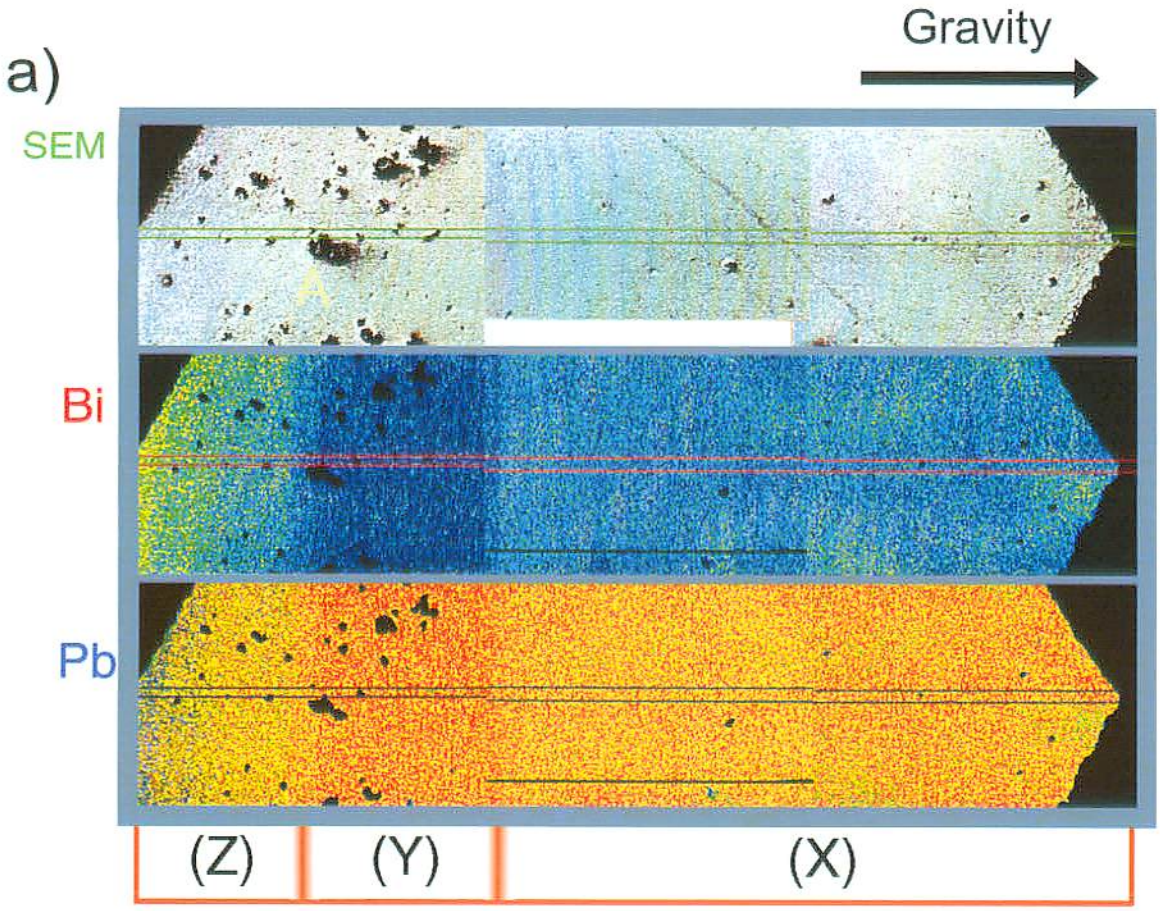

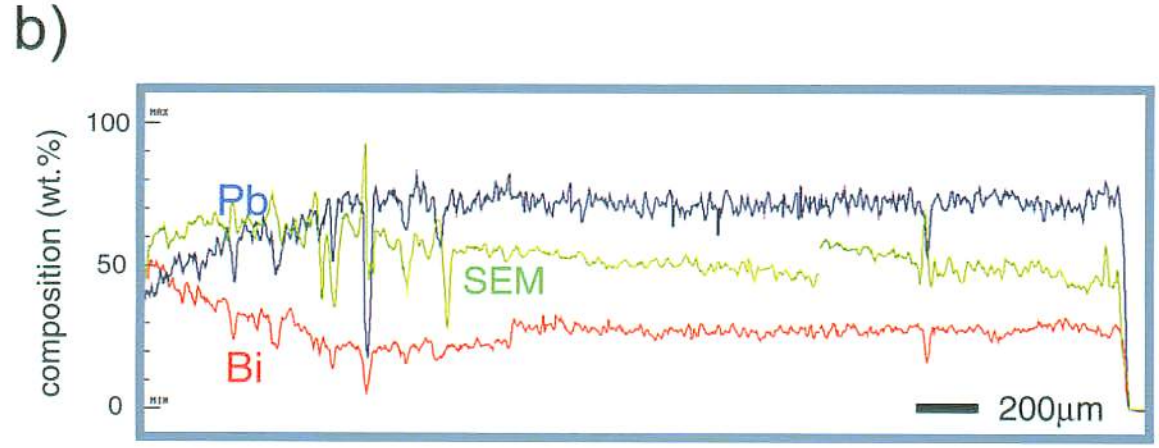

Starting material : Bi_3Pb_7 (≒ 30:70 wt.%)
(anealed)

Experimental conditions :

Rotation rate :	197,000 ～ 214,000 rpm
Acceleration :	805,000 ～ 956,000 g
Temperature :	137.0 ～ 144.7 ℃
Time :	90 hours

Fig.6-5 Composition profiles of the centrifuged Bi_3Pb_7 sample measured by EPMA.

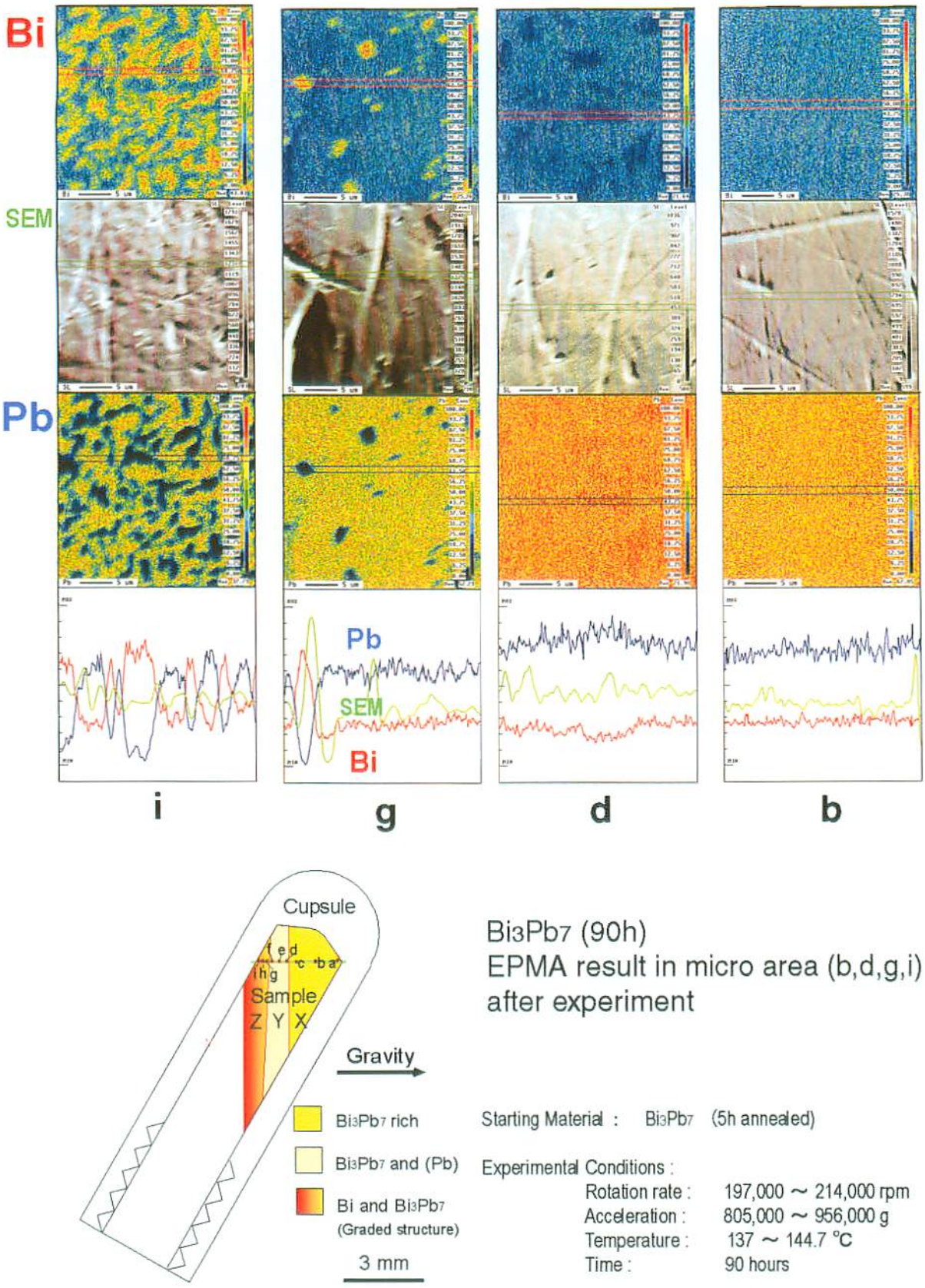

Fig.6-6 Composition profiles of the centrifuged Bi_3Pb_7 (90h) sample measured by EPMA in micro-area.

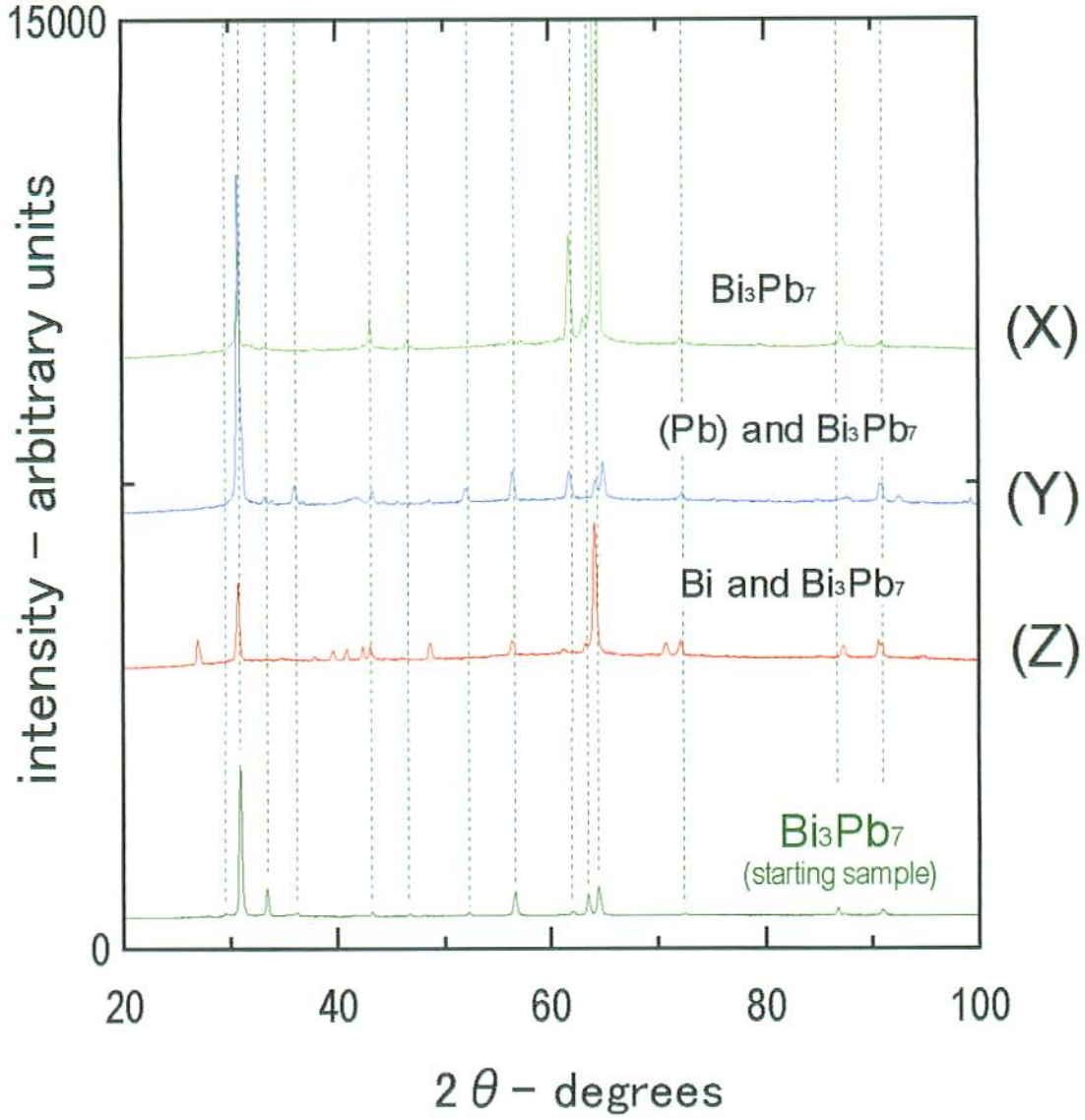

Starting material: Bi_3Pb_7 (≒30:70 wt.%)
(anealed)

Experimental conditions :

Rotation rate :	197,000–214,000 rpm
Acceleration:	805,000–956,000 g
Temperature:	137.0–144.7 ℃
Time:	90 hours

Fig. 6-7 XRD patterns of the centrifuged Bi_3Pb_7

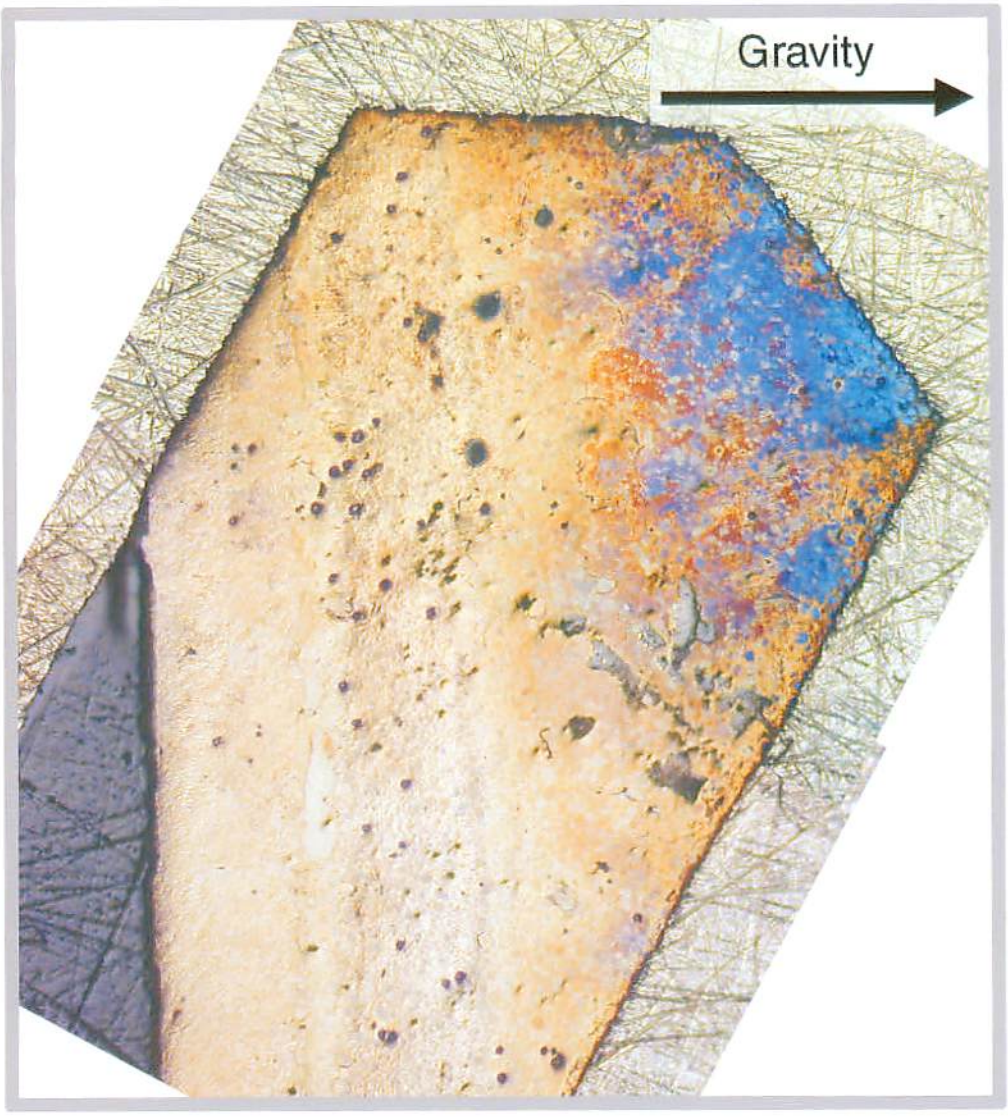

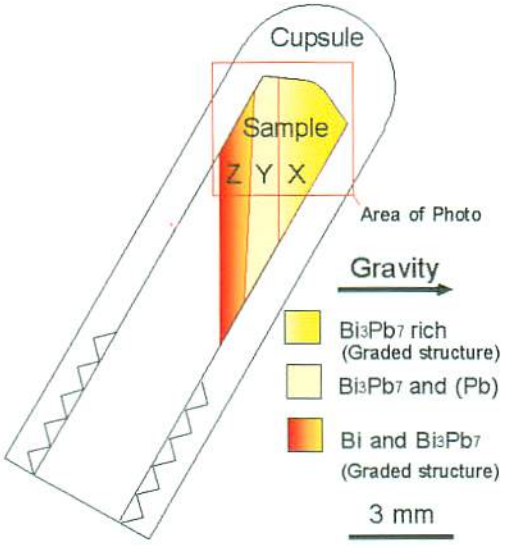

Bi3Pb7 (150h), after experiment

Starting Material : Bi3Pb7 (5h annealed)

Experimental Conditions :

Rotation rate :	197,000 ~ 214,000 rpm
Acceleration :	805,000 ~ 956,000 g
Temperature :	137.0 ~ 144.7 °C
Time :	150 hours

Fig.6-8 Optical micro photogaph of centrifuged Bi3Pb7 (150h)

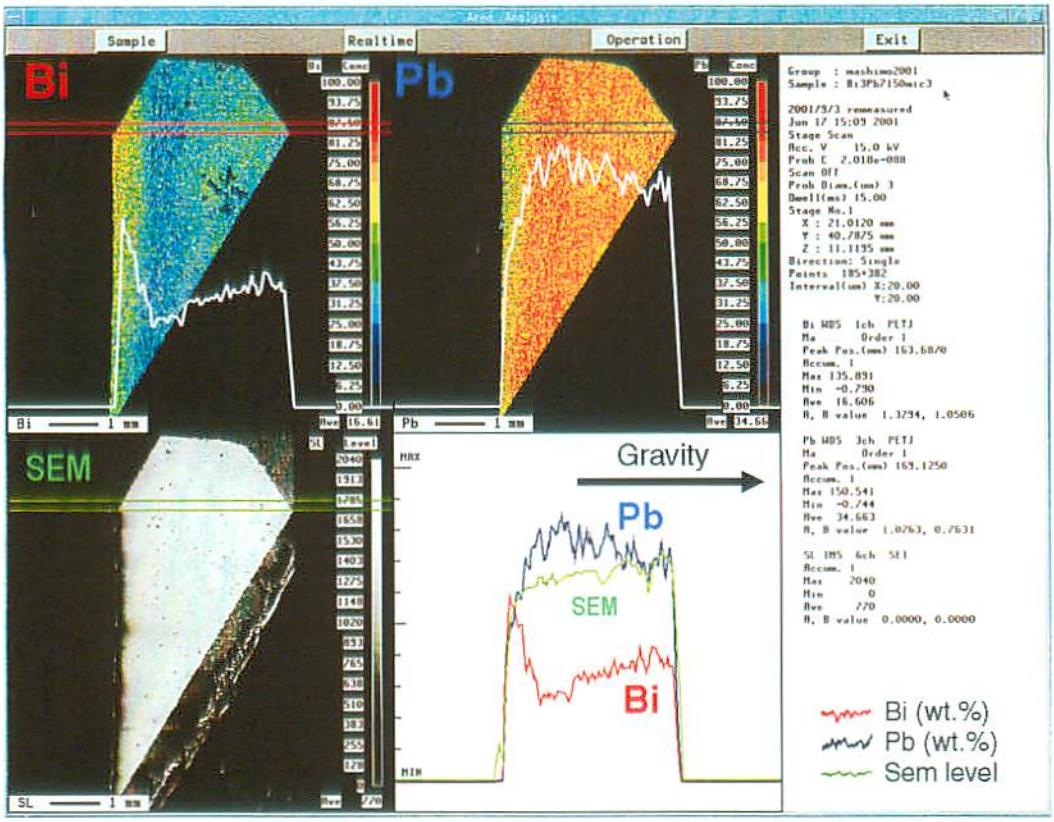

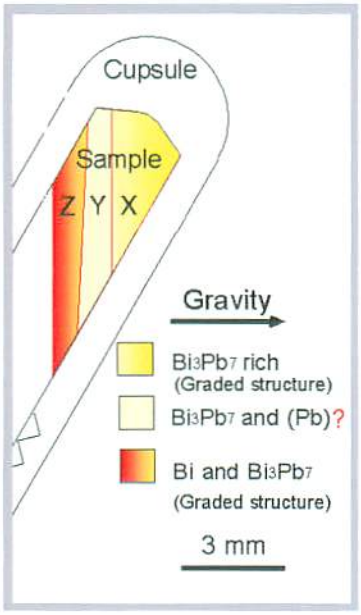

Starting material : Bi_3Pb_7 (30:70 wt.%)
(anealed)

Experiment condition :

Rotation rate :	197,000 ~ 214,000 rpm
Acceleration :	805,000 ~ 956,000 g
Temperature :	137.0 ~ 144.7 °C
Time :	150 hours

Fig.6-9 EPMA mapping photograph of the centrifuged Bi_3Pb_7 sample (150h)

CHAPTER 7
General conclusions

In this study, we studied the sedimentation of atoms and the interaction with the phase equilibrium mainly in binary alloys under strong gravitational field using the ultracentrifuge of Kumamoto University and of *JAERI*. And, in some of alloys, the sedimentation process was mostly cleared by investigating the centrifuged sample and comparing the experimental results with simulation ones, although the mechanism was not cleared.

In the *Chapter 1*, we introduced ultra-centrifugal field and the expected effect on materials.

In the *Chapter 2*, we introduceed the self-consistent equations for the sedimentation of atoms in a multi-component condensed system and simulation procedure of the sedimentation process for atoms, and we performed the simulation for Bi-Sb alloy. And, it was concluded that the diffusion rates for sedimentation are much faster than conventional value, even though substitutional solutes act in this system.

In the *Chapter 3*, we introduced the development of the new ultracentrifuge and arranged the specification of the two different type ultracentrifuge used for the experiment. It is expected that the investigation materials and phenomena under an ultra-strong gravitational field will be expanded much by using the present apparatus.

In the *Chapter 4*, we performed the ultracentrifuge experiment on the Bi-Sb and Se-Te system alloy using new ultracentrifuge of *JAERI* one. We just have composition analysis on the both centrifuged sample, and discuss the sedimentation process and mechanism comparing with simulation, as it is convenient to examine the sedimentation process and mechanism comparing with the simulation on the all-proportional miscible

system. In the centrifuged Bi-Sb alloy, the Bi content continuously increased in the direction of gravity (arrow direction in the figure) from about 60 to 100 wt.%, and conversely, the Sb content greatly decreased from about 45 to almost 0 wt.%, even in crystal grains. In the centrifuged Se-Te alloy, the Te content continuously increased in the direction of gravity (arrow direction in the figure) from almost 0 to 70 wt.% through the maximal of 75 wt.%, and conversely, the Se content greatly decreased from almost 100 to about 35 wt.% also having minimal of 30 wt.%. In the both alloys, the large composition gradients observed even in single-crystal particles. This showed that the graded structure was continuous in atomic scale in both alloys and the obtained graded structures were formed by the sedimentation of substitutional solute atoms. Also it was found that the diffusion coefficients for sedimentation in the two alloys (Bi-Sb, Se-Te alloy) were much larger than that for usual diffusion by simulations. This simulation results indicated that the diffusion mechanism of the sedimentation in this system was different from the vacancy mechanism.

In the *Chapter 5*, we performed the ultracentrifuge experiments on the three-phase miscible alloy of In-Pb system using ultracentrifuges of Kumamoto University one or *JAERI* one (acceleration: 10^6 g level, starting state: uniform in 80:20 at%, intermediate α-phase). The graded composition profiles was observed on the cut surface of the centrifuged samples. In the centrifuged sample of Experiment-1 performed in Kumamoto university, the Pb content continuously increased from about 12 to 36 at%, and conversely, the In content decreased from about 88 to 64 at% in the direction of gravity. And, In the centrifuged sample of Experiment-2 performed in *JAERI*, the Pb content continuously increased in the direction of gravity from about 6 to 45 at%, and conversely, the In content decreased from about 95 to 55 at%. In the both samples, it was found that the Pb-rich phase and In-rich phase appeared at the strong- and weak-gravity field sides, respectively, from starting state of intermediate α-single phase. The continuous changes in lattice parameters were observed in each phases and the lattice parameters gradually changed with composition. These results showed that

the obtained graded structure was continuous in atomic-scale, and was formed by the sedimentation of substitutional solute atoms. We also performed the simulation of sedimentation process for Experiment-1 to discuss the diffusion mechanism. It was found that the diffusion coefficient for sedimentation was few times larger than that for usual diffusion. This indicated that the diffusion mechanism of the sedimentation in this system was different from the vacancy mechanism.

In the *Chapter 6*, we performed the mega-gravity field experiment on an intermetallic compound of Bi-Pb system alloy (Bi_3Pb_7), and the composition and crystalline states were studied. It was found that the composition profiles changed, and the decomposition occurred. The present result showed that the sedimentation of Bi and Pb atoms occurred in the intermetallic compound of Bi_3Pb_7. It is expected that the sedimentation of substitutional solute atoms can be realized in other compounds.

ACKNOWLEDGEMENTS

The author would like to be grateful to Prof. Mashimo of Kumamoto University for his guidance, support, and encouragements consistently in carrying out this doctorial dissertation.

The author would like to be grateful to Dr. T Osakabe, Dr. X. Huang and Dr. V. Lue of Advanced Science Research Center, Japan Atomic Energy Research Institute for their help in the ultracentrifuge experiments. The author would like to be grateful to Mr. Y. Ogawa, Mr. K. Kamada, Mr. Hirota and Dr. M. Koinuma for their supporting in X-ray diffraction analyses. The author would like to be grateful to Mr. T. Udou for his supporting in vaporizations of samples.

The author would like to be grateful to Prof. S. Satonaka, Prof. A. Chiba, Prof. M. Nishida, Prof. I. Oda and Prof. H. Ihara for their usual advice in accomplishing this work.

The author would like to thank Mr. T. Kinoshita, Mr. H. Ueno, Mr. H. Kanagae, Mr. M. Ichikawa, Mr. H. Mori, Mr. N. Monji of the member of the Mega-Gravity experiment team of Mashimo Lab. And also the author would like to thank Mr. N. Nishihara, Mrs. R. Nishimura, Mr. K. Teramoto, Mr. T. Itai and Mr. Miyamoto of the member of the Mega-Gravity experiment team of Ihara Labo.

The author would like to thank Mr. X. Fan, Mr. Y. Zhang, Mr. H. Iwashita, Mr. Y. Ikeda the member of the Mashimo labo. 2002.

Also, the author would like to thank Dr. M. Uchino, Dr. V. Dominique, Mr. M. Nakamura, Mr. M. Kaetsu, Mr. H. Ikeda, Mr. J. Sakata, Mr. K. Tsumoto, Mr. Andou, Mr. Nagakui, Mr. K. Kuramoto, Mr. K. Nakamura, Mr. T. Araki, Mr. S. Fujiwara and Mr. K. Sakurai, who had been in Mashimo Lab., for their encouragement in usual life.

The author would like to be grateful to Prof. Mr. S. itoh, Prof. K. Hokamoto, Mr. S. Nagano and Mr. S. Akimaru and other colleagues in Itoh Lab. and Hokamoto Lab. for their encouragements.

This work was supported by grant Aid for Scientific Research from Japan Ministry of Education, Science, and Culture.

Main papers of the present study

Chapter 2

*1 Masao Ono and Tsutomu Mashimo; "Sedimentation process for atoms in a Bi-Sb system alloy under strong gravitational field: a new type of diffusion of substitutional solutes", Philosophical Magazine A, 2002, Vol. 82, No. 3, 591-600

*2 Masao Ono and Tsutomu Mashimo; "Simulation of sedimentation of atoms in a binary alloy in strong gravity", Processing by Centrifugation, 2001, 149-153

Chapter 3

*3 "Advanced high-temperature ultracentrifuge apparatus for mega-gravity materials science",
Review of Scientific Instruments, January 2003, Vol. 74, No. 1, 160-163

Chapter 5

*4 Tsutomu Mashimo and Masao Ono; "Mega-Gravity experiment on In-Pb alloy", Processing by Centrifugation, 2001, 155-158

Other papers related to the present study

*1 X. S. Huang, T. Mashimo, M. Ono, T. Tomita, T. Sawai, T. Osakabe, and N. Mori; "Observation of crystalline state of the graded structure Bi-Sb alloy prepared under a strong gravitational field of around 1 million G"
Advances in Space Research, to be submitted.